I think it is the general rule that the originator of a new idea is not the most suitable person to develop it, because his fears of something going wrong are really too strong. (Paul Dirac)
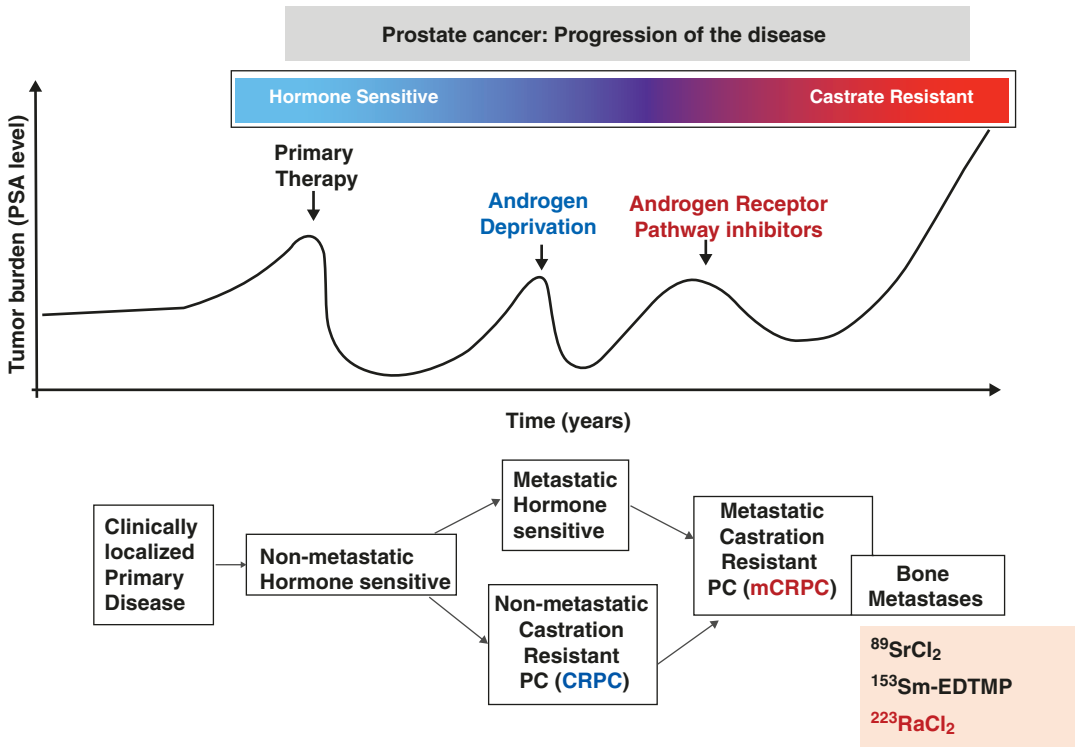
22.1 Prostate Cancer

Prostate cancer, adenocarcinoma in the prostate gland, is the second most common cancer, and the fifth leading cause of cancer-related death among men worldwide. The American Cancer Society's estimated that the number of new cases of prostate cancer, in the Unites States, was 248,530 in 2021. and the estimated deaths were 34,130 [1]. For patients diagnosed with primary prostate cancer, 5-year survival rates exceed 90%. However, for patients with advanced prostate cancer with tumor cells present at distant sites outside of the prostate there are severe impacts on quality of life and a low (<30%) 5-year survival rate. Upon metastasis to the bone, the 5-year survival rate falls to a dismal 3–5%, making the disease essentially incurable [2, 3].

The androgen receptor (AR), an intracellular DNA-binding, hormone-responsive transcription factor, is the key molecular driver for male organ development and is the oncological driver of prostate cancer. Following binding of androgens, such as testosterone, in the cytoplasm, the AR is activated and then translocates to the nucleus and stimulates the expression of genes involved in differentiation and proliferation [4, 5].

22.1.1 Screening and Diagnosis

The initial screening in men of 45–50 years is based on the serum prostate-specific antigen (PSA) test and digital rectal examination (DRE). The disease progression (Fig. 22.1) from the primary disease in the prostate gland to the metastatic castrate-resistant prostate cancer (mCRPC) is monitored, generally, based on serum PSA levels. The diagnosis of prostate cancer is based on the microscopic evaluation of prostate tissue obtained via needle biopsy. If the PSA level is ≥3 ng/mL, a biopsy of the prostate, under the guidance of transrectal ultrasonography (TRUS), or MRI, is recommended to obtain 10–12 tissue samples in a grid-like pattern. A pathologist examines these samples and issues a primary *Gleason grade* for the predominant histological pattern and a secondary grade for the highest pattern, both on a scale of 1–5 based on the microscopic architecture, and appearance of the cells. As shown in Table 22.1, based on the sum of Gleason scores, PSA level, and clinical stage, the clinicians stratify the diagnosis of prostate cancer into low, intermediate, and high-risk categories [7].

Fig. 22.1 A schematic showing the disease progression in patients with prostate cancer. At this time, the radiopharmaceuticals in clinical use are only for the treatment of bone pain palliation or alpha therapy of bone metastases in mCRPC. (The figure modified from Abou et al. [6])

Table 22.1 Prostate cancer risk stratification

Risk stratification[a]	Clinical status	PSA level (ng/mL)	Gleason score (GS)	Comment
Very low risk	T1c	<10	6 or less	With <3 biopsy cores with cancer
		0.15 ng/mL/g		Presence of 50% or less in each core
Low risk	T1–T2a	<10	6 or less	
Intermediate risk	T2b–T2c	10–20	7	
High risk	T3a	>20	8	
Very high risk	T3b–T4	>20	8–10	Primary Gleason pattern 5, or >4 biopsy cores with GS of 8–10

[a] National Comprehensive Cancer Network Risk Stratification from Litwin and Tan [7]

22.1.2 Treatment for Localized Prostate Cancer

For many low-risk patients with clinically localized primary disease, "watchful waiting" and "active surveillance" to monitor indolent disease by serial biopsy and prostate-specific antigen (PSA) measures is an appropriate option. If treatment is desired for primary prostate cancer, standards of care may involve surgical resection (radical prostatectomy), external beam or proton radiotherapy, and brachytherapy [6, 7]. These

treatment options are often curative. In the case of recurrent disease or advanced-stage prostate cancer, the main therapy is androgen ablation using luteinizing hormone releasing hormone (LHRH) agonists and antagonists and/or anti-AR drugs [8]. Although localized prostate cancer can be treated effectively by these therapies, almost all patients ultimately progress to mCRPC. Most patients with metastatic disease initially respond to androgen deprivation therapy, taxane-based chemotherapies, immunotherapy, or radium-223 but, each of these regimens provides only limited 2–4 months median survival benefit [9, 10]. The median survival for men with mCRPC ranges from 13 to 32 months with a 15%, 5-year survival rate. Most deaths from prostate cancer, however, are attributed to the incurable, late-stage cancer form [3, 11].
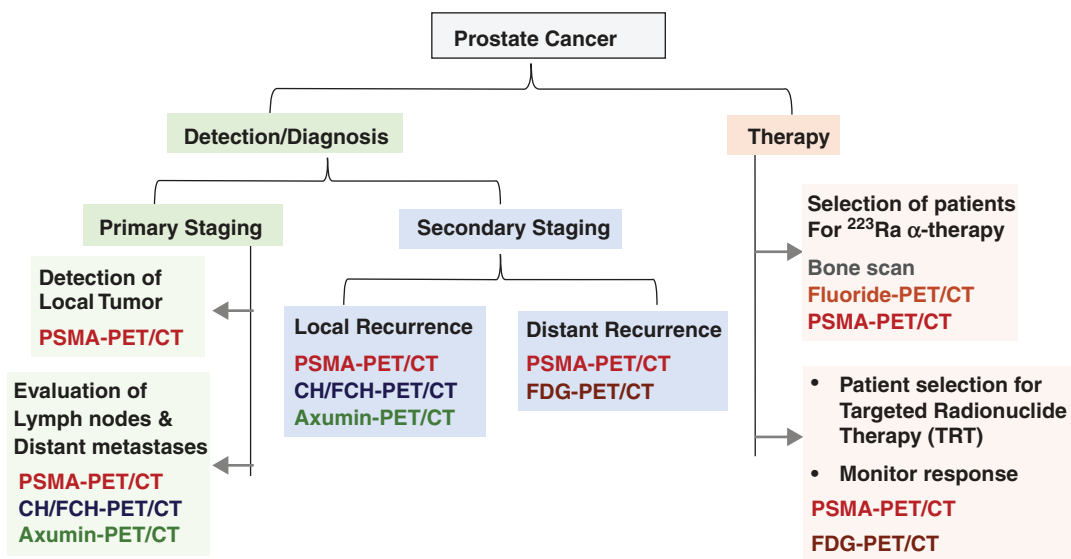
22.1.3 Role of Imaging in Prostate Cancer

Currently, imaging plays a key role in many aspects of prostate cancer but, its role is evolving to accurately answer key clinical questions at various phases of the disease in a cost-effective manner. The implementation of theranostic approaches to characterize and personalize patient management is beginning to be realized for prostate cancer patients. These clinical decision-making landmarks include:

- Accurate primary diagnosis,
- Characterization and staging of cancer at the time of initial presentation,
- Determination of local recurrence or distant disease at the time of biochemical recurrence of prostate cancer to select the most appropriate therapy,
- Accurate assessment of therapy response to various treatment regimen under the new practice paradigm,

- Prediction of patient outcomes such as time-to-event endpoints (for example, time to hormone refractoriness in castrate-sensitive disease, time to progression, and overall survival).

The imaging techniques in prostate cancer can be classified into two different methods: structural imaging and molecular imaging. The structural imaging (TRUS, CT, MRI, and multiparametric MRI) provides details about the anatomy and anatomical relations such as size, local invasions, tumor borders, and anatomical distortions. In contrast, molecular imaging shows molecular content, biochemistry, physiological dynamics, and the biology of the tumor tissue, noninvasively. To make medicine "personalized," the clinicians need to know both structural and molecular information about the tumor.

Theranostics refers to a combination of a predictive PET/SPECT biomarker with a therapeutic radiopharmaceutical with similar PK and biodistribution as that of imaging biomarker. The identification of potential biological targets in advanced prostate cancer and androgen-independent disease is critical for improving the detection of metastatic tumor burden based on PET, and SPECT molecular imaging studies, and for the development of targeted radionuclide therapy. Ideally these targets are exclusively expressed in normal prostate tissue but, which are highly expressed in metastatic disease. Several cell surface proteins, glycoproteins, receptors, enzymes, and peptides have been tested as targets for molecular imaging and targeted radionuclide therapy of prostate cancer. In recent years, significant advancements in the diagnostic molecular imaging studies and targeted radionuclide therapeutic modalities for metastatic prostate cancer have revolutionized its management in daily practice [6, 12]. As shown in Fig. 22.2, the role of molecular imaging may play a significant role in primary staging, secondary staging and, finally, in TRT.

Fig. 22.2 Role of PET radiopharmaceuticals for molecular imaging studies in prostate cancer

22.2   Biological Targets in mCRPC

Prostate cancer starts as localized prostate cancer when it is only found in the prostate gland and surgery, or radiation can be used to treat the cancer. As it advances, there may be a biochemical recurrence, which means a rise in the PSA level. It might also progress to become nonmetastatic castration-resistant prostate cancer (mCRPC), a form of advanced prostate cancer when the localized prostate cancer no longer completely responds to treatments that lower testosterone. Metastatic hormone-sensitive prostate cancer (mHSPC) and metastatic castration-resistant prostate cancer (mCRPC) are advanced forms of the condition that do not respond to initial treatments and have started to spread beyond the prostate, such as the lymph nodes, bones, liver, or lungs. Both mHSPC and mCRPC refer to cases where the cancer cells have started to spread to other parts of the body. While mHSPC still responds to ADT, mCRPC does not respond to ADT and leads to very poor prognosis.

Several important biological targets (such as bone matrix, PSMA, and GRPR) have been identified to develop targeted radiopharmaceuticals for

molecular imaging and therapy of mCRPC. Tables 22.2 and 22.3 show both FDA-approved and investigational radiopharmaceuticals for imaging and therapy [13–18].

22.2.1 Bone Matrix

Bone is composed of three parts: compact bone, trabecular bone, and bone marrow. Compact bone is a hard, solid bone tissue and forms the outside layer of bone. Trabecular bone (or spongy bone) and bone marrow are found in the inside of bone. New bone is constantly being produced while old bone is broken down. The bone marrow is composed of two distinct stem cell lineages, cells of hematopoietic origin and those of mesenchymal origin. Hematopoietic stem cells (HSCs) give rise to all blood cell types, including macrophages that differentiate into osteoclasts, while mesenchymal stem cells (MSCs) are responsible for the generation of stromal cells, osteoblasts, and osteocytes. Bone is made up of an extracellular matrix (ECM) surrounding osteoclasts, osteoblasts, osteocytes, and bone marrow stromal cells (BMSC). The ECM contains both, an organic

Table 22.2 Radiopharmaceuticals for molecular imaging of prostate cancer

	Biochemical target/mechanism	Radiopharmaceutical	FDA
1	Bone matrix	^{99m}Tc-MDP and ^{99m}Tc-HDP	Approved
	Bisphosphonate analogs: Binding to hydroxyapatite	^{111}In-DOTA^{Zol}	IND
		^{68}Ga-DOTA^{Zol}	
	Bone matrix	^{18}F sodium fluoride	Approved 1972
2	Glucose metabolism	[^{18}F]Fluorodeoxyglucose (FDG)	Approved
	FDG is a substrate for the enzyme *hexokinase*		
3	Lipid metabolism	[^{11}C]Choline (CH)	Approved 2012
		[^{18}F]Fluorocholine (FCH)	IND
		[^{18}F]Fluoroethyl choline (FeCH)	IND
4	Amino acid transport	[^{18}F]FACBC ([^{18}F]Fluciclovine or Axumin®)	Approved 2016
5	Androgen receptor (AR)	[^{18}F]FDHT	IND
		[^{18}F]Enzalutamide (FEZT)	IND
6	Anti-PSMA (*prostate specific membrane antigen*) mAbs	^{111}In-capromab pendetide (ProstaScint™)	Approved 10/1996
		^{111}In-DOTA-J591 mAb	IND
		^{177}Lu-DOTA-J591 mAb	IND
		^{89}Zr-DFO-J591 mAb	IND
		^{89}Zr-DF-IAB2M (J591 minibody)	IND
7	PSMA: Small-molecule PSMA inhibitors	^{68}Ga-PSMA-HBED-CC (PSMA-11) (gozetotide)	Approved 12/2020
		[^{18}F]AlF-PSMA-11	IND
		^{18}F-DCFPyL (piflufolastat F 18) Pylarify®	Approved 5/2021
		[^{18}F]DCFBC	IND
		[^{18}F]PSMA-1007	IND
		[^{18}F]-rhPSMA-7.3	IND
		[^{18}F]JK-PSMA-7	IND
		[^{18}F]CTT1057	IND
		^{68}Ga-rhPSMA-7.3	IND
		^{68}Ga-PSMA-I&T	IND
		^{68}Ga-PSMA-617	IND
		^{152}Tb-PSMA-617	IND
		^{99m}Tc-MIP-1404 (Trofolastat™)	IND
		$^{123/124}$I-MIP-1095	IND
8	Gastrin-releasing Peptide receptor (GRPR) antagonists	^{68}Ga- BAY86-7548 (^{68}Ga-RM2)	IND
		^{68}Ga-SB3; ^{111}In/^{177}Lu-SB3	IND
		^{68}Ga-JMV4168; ^{177}Lu-JMV4168	IND
		^{68}Ga-NeoBOMB1; ^{177}Lu-NeoBOMB1	IND
		[^{66}Ga]Ga-NOTA-PEG2-RM26	IND
		^{64}Cu-CB-TE2A-AR06	IND
9	Poly (ADP-ribose) Polymerase-1 (PARP-1)	^{18}F-Olaparib	IND
		^{18}F-WC-DW-F	

component, formed by type I collagen, proteoglycans and glycoproteins, and inorganic ions (calcium and phosphate) organized in hydroxyapatite crystals, a naturally occurring mineral form of calcium apatite, $Ca_5(PO_4)_3(OH)$.

In prostate cancer, bone is the most common and preferred site for metastatic involvement of cancer. The presence of bone metastases implies poorer prognosis, shortens survival, and is associated with a multitude of complications, including

Table 22.3 Radiopharmaceuticals for the targeted therapy of prostate cancer

	Biochemical target/mechanism	Radiopharmaceutical	Indication	FDA
1	Bone matrix *(binding to hydroxyapatite)*	^{89}Sr dichloride	Bone pain palliation	Approved 1993
		^{153}Sm-EDTMP (lexidronam)		Approved 1997
		^{177}Lu-EDTMP or DOTMP		
		^{166}Ho-DOTMP or EDTMP		
		^{177}Lu-DOTA^{Zol}		
2	Bone matrix *(binding to hydroxyapatite)*	^{223}Ra chloride	Therapy of mCRPC of bone	Approved 2013
3	Anti-PSMA *(prostate-specific membrane antigen)* mAbs	^{90}Y-DOTA-huJ591 mAb	Therapy of mCRPC	IND
		^{177}Lu-DOTA-huJ591 mAb		IND
		^{225}Ac-DOTA-huJ591 mAb		IND
		^{177}Lu-rosopatamab (TLX591, aka ^{177}Lu-J591)		IND
		^{227}Th-PSMA-TTC (BAY 2315497)		IND
4	Small-molecule PSMA inhibitors	^{177}Lu-PSMA-617 Vipivotide tetraxetan (Pluvicto)	Therapy of mCRPC	Approved 03/2022
		^{225}Ac-PSMA-617		IND
		^{149}Tb-PSMA-617		IND
		^{177}Lu-PSMA-I&T		IND
5	GRPR antagonists	^{177}Lu-RM2		IND

severe bone pain, pathological fracture, spinal cord compression, and hypercalcemia [19]. When tumor cells invade the bone, the cancer cells can stimulate osteoblasts and osteoclasts [20]. The activated osteoblasts stimulate bone formation, hardening the bone (osteoblastic or sclerotic process), while the activated osteoclasts then dissolve the bone, weakening the bone (osteolytic phenomenon). Bone metastases in prostate cancers are, typically characterized by an osteoblastic picture due to excess bone deposition [19]. Bisphosphonates inhibit osteoclast-mediated bone resorption by binding to bone mineral, interfering with osteoclast activation. These agents also promote repair by stimulating osteoblast differentiation and bone formation. Also, phosphate and diphosphonate molecules preferentially bind to calcium ions in the hydroxyapatite and accumulate to a high concentration only in bones. As a result, these agents play an increasing role in the treatment of painful bone metastases.

While Fluoride ion (^{18}F$^-$) can replace the hydroxy group (OH$^-$) in the hydroxyapatite, the divalent calcium analogs such as ^{89}Sr and ^{223}Ra substitute calcium or bind to hydroxyapatite in bones and deliver ionizing radiation to areas with increased osteoblastic activity [21]. Radiolabeled bisphosphonate analogs (Fig. 22.3) were developed for imaging studies to detect metastatic foci in bone and for the palliation of bone pain from osseous metastases.

22.2.2 Androgen Receptor (AR)

AR plays pivotal roles in prostate cancer, CRPC. The AR is the key driver of prostate differentiation and PC progression. AR is a steroid receptor transcriptional factor consisting of four main domains, an N-terminal domain (NTD), a DNA-binding domain (DBD), a hinge region (HR), and a ligand-binding domain (LBD) that binds androgens, including testosterone (T) and dihydrotestosterone (DHT) (Fig. 22.4). Upon steroid binding, the AR is activated and undergoes a conformational change and releases heat-shock proteins (hsps). The AR translocates to the nucleus where dimerization, DNA binding and the recruitment of coactivators occur. Target genes are transcribed (mRNA) and translated into proteins [22].

Fig. 22.3 Bisphosphonate analogs as radiopharmaceuticals for imaging and therapy of prostate cancer bone metastases

Fig. 22.4 PET radiopharmaceuticals for molecular imaging studies of androgen receptor (AR) in prostate cancer

Prostate cancer growth and progression is stimulated by androgens (testosterone), acting through the nuclear AR, which is a ligand-dependent transcription activator involved in cellular proliferation and differentiation, and is present in all histologic types of prostate tumors, in recurrent carcinoma, and in tumor metastases [4, 23].

The effectiveness of repressing or inhibiting this central AR signaling by androgen deprivation therapy (ADT) is the cornerstone of advanced PC treatment. In PCa, AR signaling is perturbed by excessive androgen synthesis, AR amplification, mutation, or the formation of AR alternatively spliced variants (AR-V) that lack the LBD. Current therapies for advanced PCa include androgen synthesis inhibitors that suppress T and/or DHT synthesis, and AR inhibitors that prevent ligand binding at the LBD. AR expression can be heterogeneous within and between lesions, and can change over time, either spontaneously or as a result of treatment; whole-body information about the AR status of all lesions in a patient would be advantageous for clinical management. Thus, imaging the expression levels of AR is a viable strategy to measure AR receptor density and the pharmacological response to antiandrogen therapies (such as abiraterone acetate and enzalutamide), designed to block the AR signaling axis [24]. [^{18}F]Fluoro-16β-5α-dihydrotestosterone ([^{18}F]FDHT), a ligand that targets the LBD of AR, was originally developed to assess AR occupancy [25–28]

### 22.2.3 Prostate-Specific Membrane Antigen (PSMA)

In 1987, PSMA was discovered as a novel antigenic marker in prostate cancer cells and in the serum of prostate cancer patients. PSMA, also known as glutamate carboxypeptidase II (GCPII), *N*-acetyl-ʟ-aspartyl-ʟ-glutamate peptidase I (*NAALADase I*) or *N*-acetyl-aspartyl-glutamate (*NAAG) peptidase*, is an enzyme that is encoded by the *folate hydrolase* (FOLH1) gene in humans [29]. PSMA/GCPII plays separate roles in different tissues, such as the prostate, kidney, small intestine, central and peripheral nervous system and, thus, is recognized by different names. In the

last two decades, PSMA has emerged as the pre-eminent prostate cancer target for developing both diagnostic and therapeutic agents in prostate cancer [30].

PSMA/GCPII was first characterized by the murine mAb 7E11, derived from mice immunized with partially purified, cell membrane fractions, isolated from the human prostate adenocarcinoma (LNCap) cell line. Immunohistochemical analysis revealed high expression of PSMA/GCPII in the epithelial cells of the prostate with an intense over-expression in the cancer tissue, compared with normal or hyperplastic prostates. Other tissues have also shown to express lower amounts of PSMA/GCPII, for example epithelia of small bowel and the proximal tubules of the kidney [30].

PSMA is a class II transmembrane glycoprotein with a unique 3-part structure (Fig. 22.5a): a short N-terminal cytoplasmic tail of 1–18 AA, a single membrane-spanning helix of 19–43 AA, and an extracellular part, consisting of 44–750 AA with an approximate molecular weight of 84 kDa [30]. The bulk of PSMA protein is the extracellular part, which is further divided into three domains, namely, the protease (57–116 aa and 352–590 aa), apical (117–351 aa), and the C-terminal domain or the dimerization domain (591–750 aa) and collectively performs the substrate/ligand recognition role [31]. In PCa, the expression of PSMA/GCPII is negatively regulated by androgens [32]. PSMA expression on the cell surface increases with AR inhibition [33, 34] and is favored by other growth factors, such as basic fibroblast growth factor, TGF, and EGF. Also, the degree of PSMA/GCPII expression is positively correlated with the Gleason score and disease progression.

PSMA is considered to be the most well-established target antigen in prostate cancer, since it is highly and specifically expressed at all tumor stages on the surface of prostate tumor cells [35, 36]. PSMA switches from a cytosolically located protein in the normal prostate to a membrane-bound protein in prostatic carcinoma. The majority of PSMA expression appears to be restricted to the prostate and the level of PSMA expression is increased with increased tumor dedifferentiation, and in metastatic and hormone-
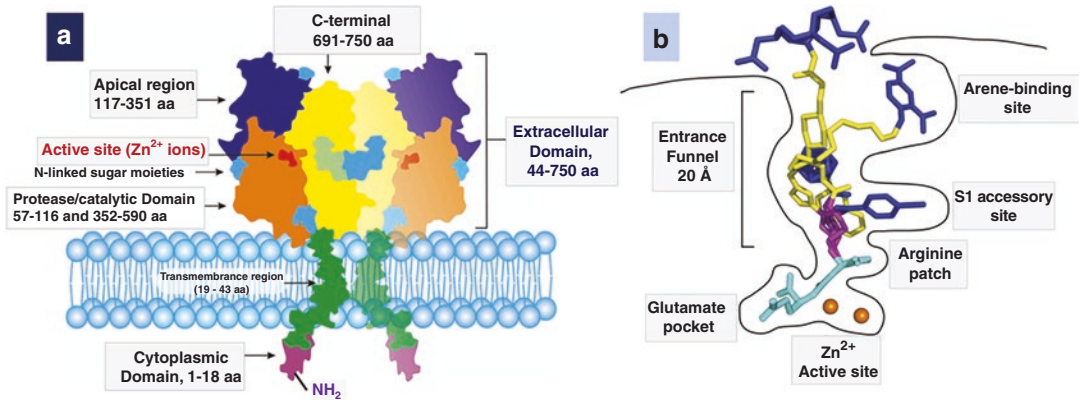
Fig. 22.5 Schematic representation of PSMA/GCPII (also termed as NAAG hydrolase) transmembrane protein homodimer (**a**) (From Evans et al. [30]). Schematic representation of the PSMA-binding cavity (**b**). Glu-Urea-based PSMA inhibitors should contain several structures for interaction between the ligand and the binding site. The pharmacophore (cyan) interacts with the arginine patch, glutamate pocket, and zinc active site, the linker (yellow) is positioned in the entrance funnel, the effector moiety (blue) interacts with the S1 accessory site and arene-binding site on the interior of the funnel. The orange spheres represent Zinc ions. (From Bařinka et al. [31])
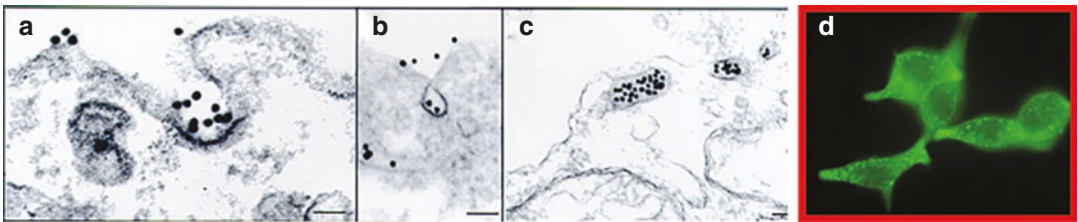
Fig. 22.6 Immunoelectron microscopy of internalized J591 mAb in LNCaP cells. Accumulation of gold particles in clathrin-coated vesicles (**a**, **b**), and in vesicles proximal to the plasma membrane (**c**). Confocal microscopy revealing internalization of J591 mAb (**d**). (From Lu et al. [40])

refractory cancers [37, 38]. In addition to expression by prostate cells, it can be expressed also by nonprostate tissues, such as small intestine, proximal renal tubules, and salivary glands albeit at levels 100- to 1000-fold less than in prostate tissue. PSMA expression was also found on the vascular endothelium of solid tumors and sarcomas but, not in normal tissues [30]. The rapid internalization and recycling of PSMA means that high concentrations of a targeted drug can be accumulated in PSMA/GCPII positive cells.

22.2.3.1 Anti-PSMA mAbs

As mentioned earlier, 7E11-C5.3 was the first anti-PSMA mAb originally developed in 1987. It recognizes and binds to an intracellular or cytoplasmic epitope of PSMA in the fixed cells and necrotic cells but, not the intact viable cells [39]. The 7E11-C5.3 antibody is of the IgG1, kappa subclass (IgG1κ) murine mAb. This antibody was radiolabeled with ^{111}In and was commercialized as an imaging agent, known as ^{111}In-capromab pendetide (ProstaScint™).

In 1997, Dr. Bander and his colleagues at Weill Cornell Medicine in New York reported the development of four mAbs (J591, J415, J533, and E99) to the extracellular domain of PSMA on viable tumor cells and demonstrated antibody induced internalization of PSMA (Fig. 22.6) [40, 41]. Based on preclinical studies, J591 mAb was selected for the development of targeted radiopharmaceuticals for imaging and therapy [42].

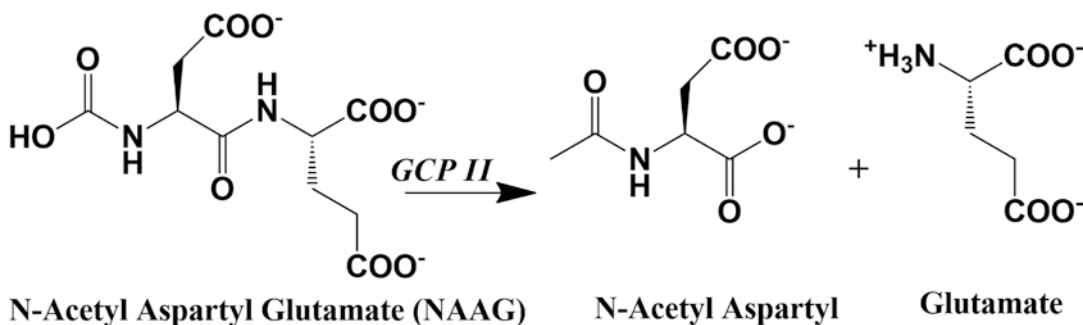### 22.2.3.2 Small-Molecule PSMA Inhibitors

The two distinct enzyme activities of PSMA include *folate hydrolase* and *NAALADase 1*. The role of these two enzymes is to release the terminal glutamate residue from the substrate molecule. In the intestine, PSMA binds with folate(poly)gamma glutamate in the intestine and releases the glutamate and folic acid. In the brain, PSMA hydrolyzes the *N*-acetyl-L-aspartyl-L-glutamate (NAAG) substrate to yield aspartate and glutamate (Fig. 22.7). *NAALADase* enzyme activity of PSMA has been explored for the development of radiopharmaceuticals. Studies of the *NAALADase* enzyme structure have revealed an ~20 Å deep tunnel leading from the surface of the enzyme to the active site containing two zinc cations (Zn^{++}) participating in the NAAG binding, called the "*NAAG binding pocket*" (Fig. 22.5b), which is also the site for the binding of PSMA inhibitors [31].

PSMA or *NAALADase* enzyme inhibitors mimic the structure of the substrate (NAAG), bind to PSMA, and reduce the ability of the enzyme to convert the substrate NAAG into aspartate and glutamate. The enzyme inhibition capacity (IC_{50}) is expressed in nanomoles (nM). The lower the IC_{50} value is, the greater the ability of the inhibitor to block the enzyme reaction. Since the 1990s, three different families of PSMA inhibitors have been developed [13, 43]. The chemical structures of different families of small-molecule PSMA inhibitors are shown in Fig. 22.8.

(a) Phospho(i)nate and thiol-based analogs: Among these compounds, 2-Phosphonomethyl pentanedioic acid (2-PMPA) has the most potent enzymatic activity ($EC_{50} = 0.3$ nM).
(b) Glutamate-phosphoramidate analogs.
(c) Glutamate-Ureido-based inhibitors.

The clinical success of radiolabeled PSMA inhibitors is based on a small motif binding to the catalytic NAAG hydrolyzing site in the PSMA molecule. This 2-[3-(1,3-dicarboxypropyl)-ureido] pentanedioic acid (DUPA) motif was first described by Kozikowski et al. [44]. This class of inhibitors contain a urea bond (–NH–CO–NH–) formed by the conjugation of two amino acids (Glu and Asp). In 2002, Pomper et al. at John Hopkins School of Medicine in the USA reported the synthesis of the first radiolabeled PSMA inhibitor, [^{11}C]DCMC, one of the potent urea-based PSMA inhibitors synthesized ($IC_{50} = 1.4$ nM). Extensive structure–activity studies suggested that the L-glutamic acid must remain intact without structural modification to maintain the desired biological function. Hence, a variety of PSMA inhibitors have been synthesized based on DUPA motif (Fig. 22.8) and modification at the aspartate end by replacing aspartic acid with other amino acids, such as lysine, glutamic acid, or their derivatives [43].

Fig. 22.7 In the brain, PSMA or the *NAALADase* enzyme converts the substrate NAAG into aspartate and glutamate
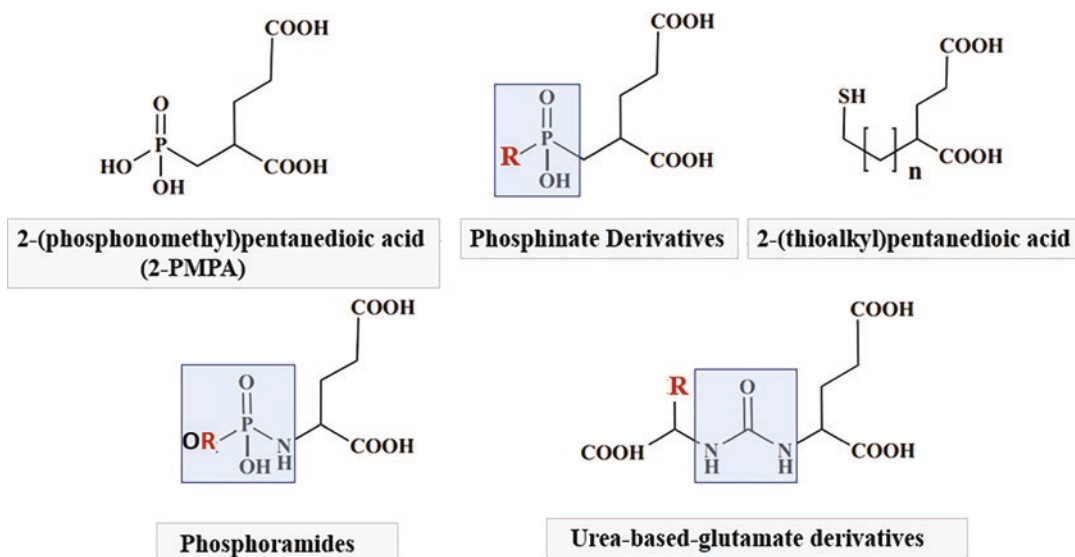
Fig. 22.8 Different families of small-molecule PSMA inhibitors. Phosphinate derivative 2-PMPA is one of the most potent PSMA inhibitors. Most of the radiolabeled PSMA inhibitors for imaging and therapy are urea-based glutamate derivatives containing two amino acids

22.2.4 Gastrin Releasing Peptide Receptor (GRPR)

GRPRs are G-protein coupled receptors of the bombesin family and are overexpressed in a majority of primary prostate cancers and more than 50% of lymph and bone metastases [45]. However, the expression of GRPR in prostate cancer is heterogeneous, dynamic, and dependent on the stage of the disease [46]. Overexpression of GRPR and GPRR-mediated signaling can stimulate the growth of both androgen-dependent, and androgen-independent prostate cancer cells [47], and indirectly promotes angiogenesis, and increase the invasive potential of prostate cancer [48]. Overexpression of the GRPR in prostate cancer but, not in the hyperplastic prostate, provides a promising target for staging and monitoring of prostate cancer.

Gastrin-releasing peptide (GRP), a neuropeptide, is a regulatory molecule that has been implicated in several physiological and pathophysiological processes. Bombesin (BBN) (Fig. 22.9) is a 14-amino acid analog (isolated from the European frog *Bombina bombina)* of the human GRP that binds to the GRPR (also known as BB2R). A variety of radiolabeled GRPR agonists and antagonists have been developed for targeting GRPR-positive tumors, and were evaluated in preclinical and clinical studies [49, 50]. Recent reports have shown that GRPR antagonists show properties superior to GRPR agonists, affording higher tumor uptake and lower accumulation in physiologic GRPR-positive nontarget tissues. GRPR agonists activate the receptor and induce side effects. GRPR antagonists, however, are expected to have no adverse effects [49].

Bombesin: Pyr-Gln-Arg-Leu-Gly-Asn-Gln-Trp-Ala-Val-Gly-His-Leu-Met-NH$_2$

^{68}Ga-RM2: ^{68}Ga-DOTA-4-amino-1-carboxymethylpiperidine-
(BAY86-7548)   D-Phe-Gln-Trp- Ala-Val-Gly-His-Sta-Leu-NH$_2$

^{68}Ga-RM26: ^{68}Ga-1,4,7-triazacyclononane-N,N9,N\$-triacetic acid-
                                            D-Phe-Gln-Trp-Ala-Val-Gly-His-Sta-Leu-NH$_2$

^{68}Ga-SB3: ^{68}Ga-DOTA-*p*-aminomethylaniline-diglycolic acid-
                                        D-Phe-Gln-Trp-Ala-Val-Gly-His-Leu-NHEt

Fig. 22.9 Bombesin and radiolabeled analogs for theranostics of gastrin-releasing peptide receptor (GRPR) in prostate cancer

22.3   Radionuclides for Imaging and Therapy

Radionuclides useful for molecular imaging studies based on PET or SPECT decay either by positron (β^+) emission, electron capture (*EC*), or isomeric transition (IT). The radionuclides that are used for therapy decay by emitting either β^- particles or α particles. The decay characteristics of some of the important radionuclides routinely used for imaging and therapy are listed in Table 22.4. Among the radionuclides listed in this table, radioisotopes of fluorine, iodine, and astatine are nonmetals and belong to the halogen (Group-7) family. All other radionuclides are metals differing in valency, oxidation state, and coordination chemistry. The γ-emissions of radionuclides decaying by IT or EC are useful for planar and SPECT imaging studies, while PET is based on the annihilation radiation (511 keV photons) from radionuclides decaying by positron (β^+) emission.

It is also important to recognize that several radionuclides are also available as theranostic pair, ideal for both imaging and therapy. Isotopes of the same element (such as ^{123}I, ^{124}I, and ^{131}I) have similar chemistry, and the in vivo behavior of radiotracers labeled with isotopes of the same element will be identical. This contrasts with non-chemically identical matched pairs of isotopes (such as ^{111}In/^{90}Y and ^{68}Ga/^{177}Lu) which may have different biodistribution and PK. Therefore, ^{111}In or ^{68}Ga labeled diagnostic radiopharmaceuticals can only be regarded as chemical/biological surrogates for ^{90}Y, ^{177}Lu, ^{225}Ac, and other trivalent metal-labeled radiopharmaceuticals.

22.3.1   Beta vs. Alpha Dosimetry

Although numerous radionuclides have potential applications in radionuclide therapy, only a very few radionuclides possess favorable nuclear, physical, chemical, and biological characteristics which would identify them as practical for clinical use. The ideal radionuclides for developing TRT are those with an abundance of nonpenetrating radiations, such as charged particles (α^{2+}, β^-, and Auger electrons) and lack of penetrating radiations (γ or X-rays). While penetrating radiation is not essential for TRT, a small amount or abundance with an appropriate energy (100–400 keV) may be useful for imaging studies to demonstrate tumor localization or altered biodistribution. Most of the radionuclides in routine clinical use are β^- emitters (^{131}I, ^{90}Y, ^{177}Lu, ^{89}Sr, and ^{153}Sm) with a wide range of half-lives ranging from 1.95 to 59.5 days (Table 22.4). Depending on the kinetic energy, the average range of electrons in tissue can be between 0.1 and 5.0 mm. As a result, beta particles can pass through several cells (10–1000), a useful prop-

Table 22.4 The most common radionuclides used for imaging and therapy in prostate cancer

Radionuclide	T½	Decay mode Mode	Decay mode %	E_{max} (MeV)	Mean range (mm)	γ-Energy (keV)	Produced by
^{99m}Tc	6.0 hours	IT	98			140	^{99}Mo generator
^{111}In	2.805 days	EC	100			171 and 245	Cyclotron
^{18}F	110 min	$β^+$	97	0.634	0.6		Cyclotron
^{68}Ga	68 min	$β^+$	88.9	1.889	3.50		^{68}Ge generator, Cyclotron
^{64}Cu	12.7 hours	$β^+$	17.9	0.653	0.7		Cyclotron
^{86}Y	14.7 hours	$β^+$	31.9	1.221	3.6		Cyclotron
^{89}Zr	3.27 days	$β^+$	22.8	0.902	1.1	908	Cyclotron
^{90}Y	2.67 days	$β^-$	100	2.28	2.50		^{90}Sr generator
^{177}Lu	6.7 days	$β^-$	79	0.497	0.67	113 and 208.4	Reactor
^{131}I	8.025 days	$β^-$	100	0.606	0.91	364.5	Fission or reactor
^{90}Sr	50.53 days	$β^-$	100	1.496	2.5		Fission
^{153}Sm	1.938 days	$β^-$	100	0.811	1.20	70 and 103	Reactor
^{166}Ho	1.12 days	$β^-$	100	1.85	3.2	80.6	Reactor
^{212}Pb	10.6 hours	$β^-$	100	0.101			^{228}Th/^{224}Ra generator
^{211}At	7.2 hours	$α$	41.8	5.867	0.06	77–92 X-rays	Cyclotron
^{213}Bi	45.6 min	$α$	100	5.9, 8.4	0.08	440	^{225}Ac generator
^{223}Ra	11.435 days	$α$	100	5.78	0.06	690	^{227}Th generator
^{225}Ac	10 days	$α$	100	5.80	0.06	218 and 440	^{229}Th generator, accelerator
^{227}Th	18.7 days	$α$	100	5.90	0.06	236	^{227}Ac generator

erty that has been termed "crossfire effect," which ensures sufficient dose delivery to each cell in a large tissue mass. Beta particles may also cause repairable DNA lesions by inducing single-stranded DNA breaks (SSDB). The biological effect, however, may be sublethal. It is important to match the range of the radionuclide with the anticipated size of the tumor target. Small tumors are more effectively treated by a short-range $β^-$ emitter, while a higher cure rate could be obtained in larger tumors with a long-range $β^-$ emitter [51].

Alpha ($α$) particles are naked helium (^{4}He)$^{2+}$ nuclei with two positive charges and consist of two protons and two neutrons, and are 7300 times heavier than electrons. Alpha particles are monoenergetic and have much higher kinetic energy (5–9 MeV) compared to beta particles.

The range (<100μm) of $α$ particles in tissue is equivalent to only a few cell diameters and this short range is ideally suited for the treatment of small volume cancer tissue. Compared to β-particle emitters, $α$-particle emitters offer several important advantages for TRT. Alpha particles have higher LET in biological tissue. For example, ^{211}At has a mean LET of 97 keV/μm, compared to the LET (0.22 keV/μm) of high energy (2.2 MeV) beta particle of ^{90}Y. As a result of higher LET values, the probability of creating cytotoxic double-stranded breaks (DSBs) of DNA is much higher with $α$ particles and the relative biological effect (RBE) is also significantly higher (3–5 times) compared to that of beta emitters [52]. In addition, cytotoxicity of alpha particles is nearly independent of dose rate and oxygenation status of the cells [53].

22.3.2 Radiolabeling Methods

The labeling of peptides and proteins with radio-nuclides can be performed by direct labeling, with the addition of prosthetic groups. Direct labeling is the method used to label peptides without using intermediates, such as BFCs. The direct labeling technique is, generally, used mostly for radioio-dination and in some cases labeling with Tc-99m. Prosthetic groups are small molecules able to bind with radionuclides in one site of the structure and, simultaneously, with a peptide at a second site. Prosthetic groups are bifunctional agents that consist of a suitable site for radioiodination or fluori-nation and functional groups to allow covalent attachment of the peptide. Radiometals specifi-

cally require bifunctional chelating agents (BFC or BFCA) to obtain the best conjugation of radio-metal with peptides. The bifunctional nature of the chelators means that they can coordinate (form a complex) a metal ion and can also be attached to the peptide. The most common acyclic and cyclic chelators used for radiometal labeling are shown in Figs. 22.10 and 22.11. The choice of a chelator depends on the valency and coordina-tion requirements of the radiometal. For all triva-lent metals (such as ^{111}In, ^{177}Lu, and ^{225}Ac), the macrocyclic chelator DOTA is, generally, used. One of the important requirements is the kinetic stability of the radiometal-chelate complex in vivo. The chemistry of radiolabeling methods is discussed in greater detail in Chaps. 9, 17, and 20.
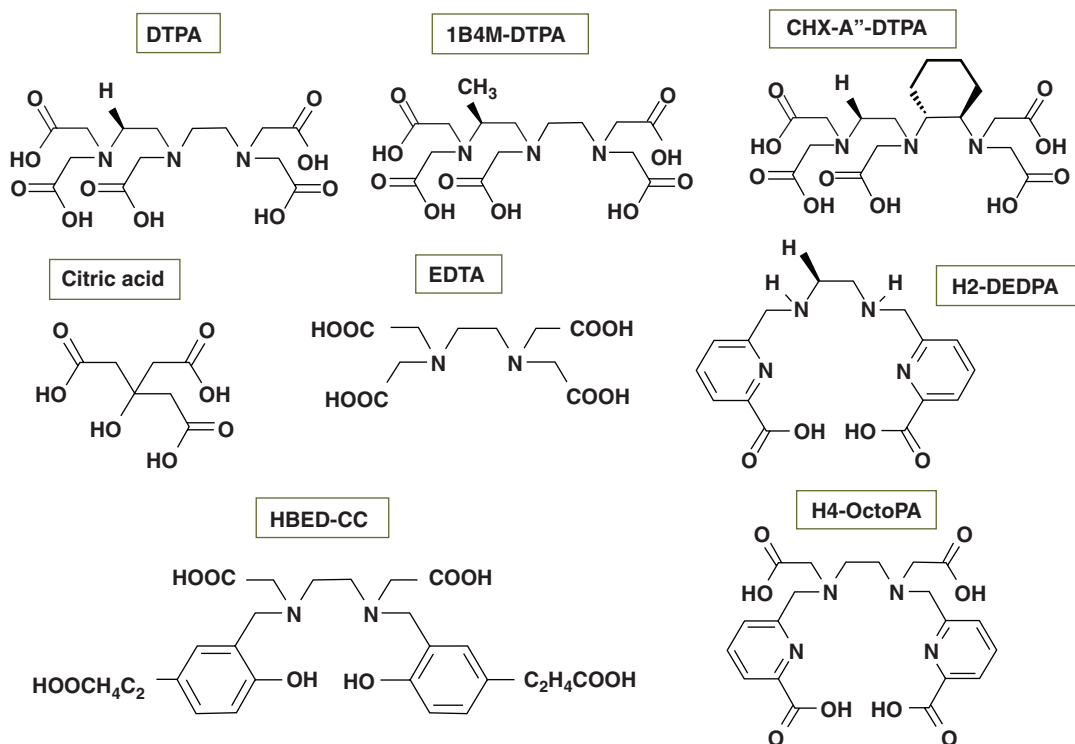
Fig. 22.10 Acyclic chelators used in the development of metal-based radiopharmaceuticals for imaging and therapy
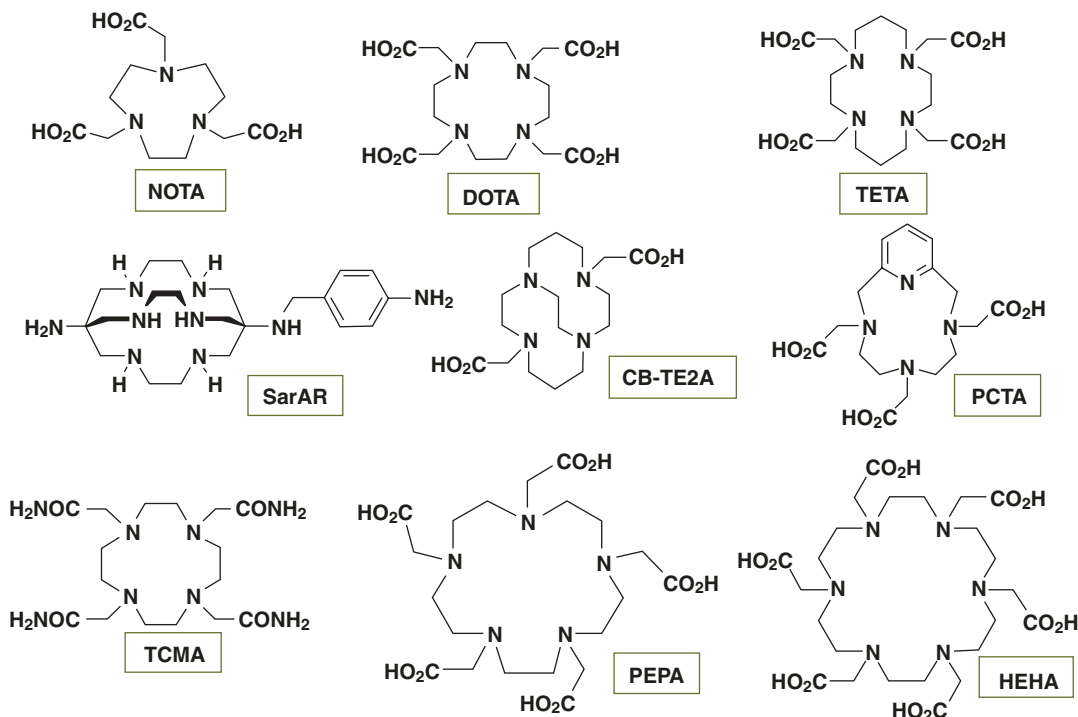
Fig. 22.11 Macrocyclic chelators used in the development of metal-based radiopharmaceuticals for imaging and therapy

22.4 Radiopharmaceuticals for SPECT and PET

The complex and heterogeneous biology of prostate cancer poses major challenges and opportunities for the development of radiopharmaceuticals for single photon emission computed tomography (SPECT) and positron emission tomography (PET). Molecular imaging based on SPECT/CT, PET/CT, and PET/MRI is the combined fusion imaging that can be obtained in a single imaging session. A summary of current, emerging, and future PET-based molecular imaging agents in development is discussed below. The mechanism(s) of tumor localization of several important radiopharmaceuticals, both FDA-approved, and investigational new drugs (IND) are summarized in Tables 22.2 and 22.3. In general, the radioisotope-based molecular imaging technology has the following unique advantages compared to structural imaging techniques:

- Provides information that is unattainable with other imaging technologies or that would require more invasive procedures such as biopsy or surgery.
- Identifies disease in its earliest stages and determines the exact location of a tumor, often before symptoms occur or abnormalities can be detected with other diagnostic tests.
- Determines the extent or severity of the disease, including whether it has spread elsewhere in the body.
- Assesses disease progression and identifies recurrence of disease.
- Selects the most effective TRT based on the unique biologic characteristics of the patient and the molecular properties of a tumor or other disease.
- Accurately assesses the effectiveness of a treatment regimen and determines a patient's response to specific drugs.

22.4.1 Bone Matrix

22.4.1.1 ^{99m}Tc-MDP and ^{99m}Tc-HDP

Prostate cancer most frequently metastasizes to the bone with a predominantly osteoblastic (sclerotic) pathogenesis. Bone scan is the oldest and well-known imaging modality to investigate bone metastases in prostate cancer. ^{99m}Tc-labeled bisphosphonates (Fig. 22.3), such as methylene diphosphonate (MDP), hydroxyl diphosphonate (HDP), and hydroxyethylidene diphosphonate (EHDP), have been used to evaluate bone metastases since the 1980s [54]. The uptake mechanism of bone radiopharmaceuticals in metastatic sites depends on blood flow and osteoblastic activity [55]. The binding of radiotracer to bone is due to physicochemical adsorption (chemisorption) to the hydroxyapatite structure of bone tissue. Bone scan is used for initial staging of intermediate to high-risk disease and for restaging after PSA relapse. It has high sensitivity and the ability to survey the entire skeleton with a simple planar scan. However, it has limited specificity and is not sensitive enough to detect micrometastases. SPECT and SPECT/CT have been shown to improve the sensitivity and reduce the number of equivocal reports for detection of bone metastases in prostate cancer [56]. Besides metastatic lesions, infectious lesions, traumatic and degenerative changes also show increased uptake of bone agents. A quantitative parameter known as the Bone Scan Index (BSI) has been shown to be prognostic for survival and was proposed for stratifying patients entering tumor protocols to measure the extent of tumor involvement of bone and for the assessment of tumor response [57].

^{68}Ga-DOTAZOL

Zoledronic acid, a last-generation bisphosphonate, has shown extremely high hydroxyapatite affinity and inhibition of the farnesyl diphosphate synthase. These properties render it an ideal candidate for theranostics, leading to the development of DOTA-zoledronic acid (DOTA-ZOL) (Fig. 22.3). Preclinical and first clinical evaluations revealed its high potential, and biodistribution and skeletal uptakes were found to be comparable to the ^{68}Ga- or ^{177}Lu-labeled compounds [58–60]. Thus, ^{68}Ga/^{177}Lu-DOTAZOL (or even ^{225}Ac-DOTA-ZOL) provides a set of potential theranostic radiopharmaceuticals, enabling patient-individual dosimetry and pre- and post-therapeutic evaluation.

22.4.1.2 Sodium [^{18}F]Fluoride (NaF)

NaF is one of the early skeletal scintigraphy agents that was approved by the US FDA in 1972, before the introduction of PET imaging technology; however, F-18 fluoride planar bone scan was displaced by the arrival of ^{99m}Tc-labeled diphosphonates, which provided better resolution. [^{18}F]NaF is a marker of bone perfusion and turnover in which ^{18}F fluoride (F$^-$) ions exchange with hydroxyl groups in the hydroxyapatite crystal of bone to form fluoroapatite with higher uptake in new bone, because of higher availability of binding sites [55, 61]. Na^{18}F-PET/CT (Fig. 22.12) is a highly sensitive and specific modality for the detection of bone metastases in patients with high-risk prostate cancer. It is a more sensitive and specific imaging technique than planar and SPECT bone scan, and NaF-PET alone [61]. Dynamic bone scanning with ^{99m}Tc-MDP or ^{18}F-NaF provides functional information sensitive for subtle changes in bone turnover and perfusion, which assists the clinical management of numerous osseous pathologies.

22.4.2 Glucose Metabolism

22.4.2.1 [^{18}F]Fluoro-2-Deoxyglucose (FDG)

Malignancy-induced glucose hypermetabolism is due to the overexpression of cellular membrane glucose transporters (mainly GLUT-1) and enhanced hexokinase enzymatic activity in tumors [62, 63]. The phosphorylation of glucose, an initial and crucial step in cellular metabolism, is catalyzed by the enzyme *hexokinase* (*HK*), which converts glucose to glucose-6-phosphate, and helps to maintain the downhill gradient that results in the transport of glucose into cells through the facilitative glucose transporters. FDG, similar to glucose, enters the cells, converts to FDG-6-phosphate, and gets trapped in the cell.
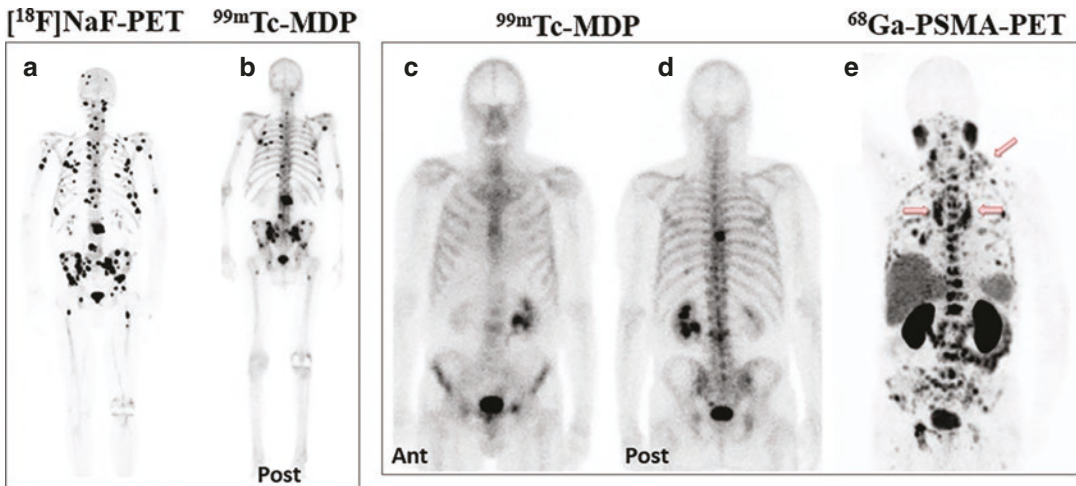
Fig 22.12 [^{18}F]NaF-PET (**a**) detects more bone metastatic lesions compared to ^{99m}Tc-MDP scan (**b**). In a different patient, ^{68}Ga-PSMA-PET (**e**) identifies more metastatic lesions than ^{99m}Tc-MDP. (**c, d**) show Fluoride PET Bone scan

In vitro studies have shown that GLUT1 expression is higher in the poorly differentiated prostate cancer cell lines than in the well-differentiated hormone-sensitive cell lines, suggesting that the level of GLUT1 expression increases with progression of malignancy grade. GLUT1 expression in prostate tumor is also correlated directly to the Gleason score (GS) and androgen level [64]. Therefore, FDG uptake is lower in well-differentiated, low GS and androgen-sensitive prostate cancer than poorly differentiated, high GS, and androgen-resistant tumors. It is well known that prostate cancer, especially, the more differentiated forms, do not exhibit a relevant Warburg effect, thus being characterized by absent or low [^{18}F]FDG avidity. Nevertheless, when progressing to the state of mCRPC, prostate tumors switch to glycolysis as a preferential pathway for producing energy. FDG may also show increased uptake in benign prostate hypertrophy or prostatitis.

FDG-PET/CT is not recommended in detecting primary focus of the cancer and staging of the patients with clinically organ-confined prostate cancer, because of its low sensitivity and specificity [65]. It also has relatively low uptake in the setting of biochemical recurrence or castrate-dependent disease. However, there is evidence that FDG-PET may be useful for restaging after PSA relapse and for assessment of treatment response in CRPC [66, 67]. In particular, FDG-PET is most useful for evaluating lymph node and bone metastases in patients with PSA >2.4 ng/mL and PSA velocity >1.3 ng/mL/year. In summary, FDG-PET/CT has an extremely limited diagnostic value in well-differentiated, androgen-sensitive and low GS prostate cancer. FDG-PET may be useful in the staging of those patients with aggressive primary tumors and can localize the site of disease in a small fraction of men with biochemical failure and negative conventional imaging studies. FDG-PET may be quite useful in treatment response assessment and prognostication of patients with castrate-resistant metastatic prostate cancer [68]. A recent review summarized that FDG-PET/CT has advantages in detecting local recurrence, visceral and lymph node metastases compared to ^{68}Ga-PSMA in partial progressive prostate cancer and castration-resistant prostate cancer patients and emphasized that FDG-PET/CT can compensate for the weakness of PSMA-PET/CT in progressive prostate cancer [69].

22.4.3 Lipid Metabolism

22.4.3.1 [¹¹C]Choline (CH) and [¹⁸F] Fluorocholine (FCH)

Prostate cancer cells rely more on fatty acid metabolism than glycolysis with upregulation and increased activity of lipogenic enzymes, *choline kinase* and *fatty acid synthase* [70].
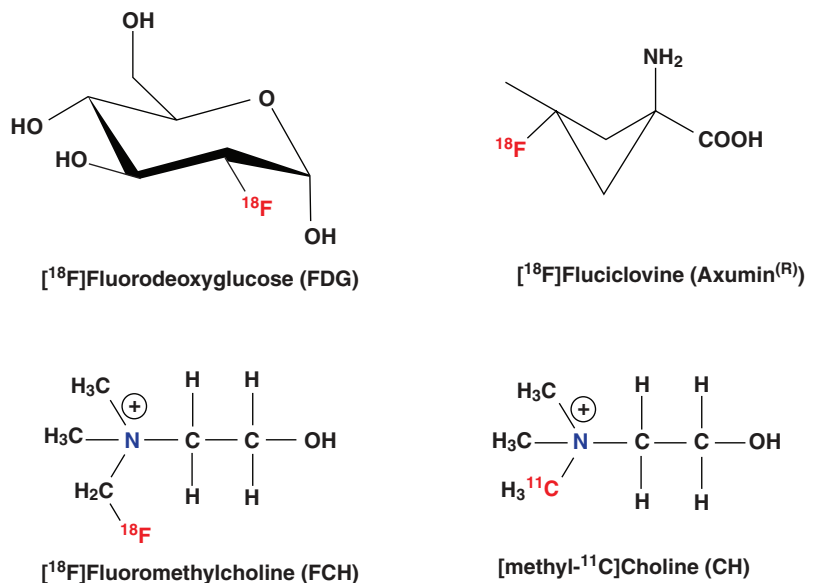
Choline is the fundamental precursor for the synthesis of phosphatidylcholine, which is the essential component of the cell membrane. Choline enters the cell via choline transporters and is used for the biosynthesis of phosphatidylcholine in the tumor cell membrane by *choline kinase*.

[¹¹C]choline was initially developed in Japan for imaging brain tumors [71]. The short half-life of ¹¹C limits the use of CH only to clinical centers with an on-site cyclotron. However, in 2012, the Mayo Clinic in the USA received FDA approval for [¹¹C]Choline-PET to help detect recurrent prostate cancer. Two ¹⁸F-labeled choline derivatives, [¹⁸F]methyl-Fluorocholine (FCH) and [¹⁸F] ethyl-Fluorocholine (eFCH), are currently used in clinical practice. PET/CT with radiolabeled choline is a well-established diagnostic approach for the diagnosis of recurrent prostate cancer after surgery/radiotherapy [50]. Both, CH and FCH (Fig. 22.13) have rapid cancer cell uptake,

rapid blood clearance, relatively minimal excretion in the urine, and high diffuse liver uptake. FCH, however, shows more urinary excretion and intense bladder activity compared to CH.

The diagnostic potential of both, CH and FCH in detecting and staging or restaging of prostate cancer has been reviewed extensively [72, 73]. These two radiotracers are not ideal for initial staging due to false positives in prostatitis and BPH and false negatives in small (<5 mm) or necrotic tumors [74]. However, they have shown promise for restaging after PSA relapse, with high sensitivity for local recurrence, nodal metastases, and bone metastases. The current recommendation is to consider CH-PET/CT as the first-line diagnostic procedure in patients with biochemical relapse showing PSA levels greater than 1 ng/mL, PSA velocity higher than 1 ng/mL/year, or PSA doubling time <6 months [75, 76]. Overall, there is limited but, promising evidence for the use of choline PET/CT to stage patients with untreated, high-risk prostate cancer. Recent studies with ⁶⁸Ga-PSMA-PET indicate that PSMA-PET is superior to Choline-PET (Fig. 22.14) in primary staging as well as in secondary staging [78]. FCH-PET, however, may be superior in some bone lesions and in a few hormone-resistant high-risk PC patients [77].

Fig. 22.13 PET radiopharmaceuticals used for molecular imaging in prostate cancer

[¹⁸F]Fluorodeoxyglucose (FDG)

[¹⁸F]Fluciclovine (Axumin⁽ᴿ⁾)

[¹⁸F]Fluoromethylcholine (FCH)

[methyl-¹¹C]Choline (CH)
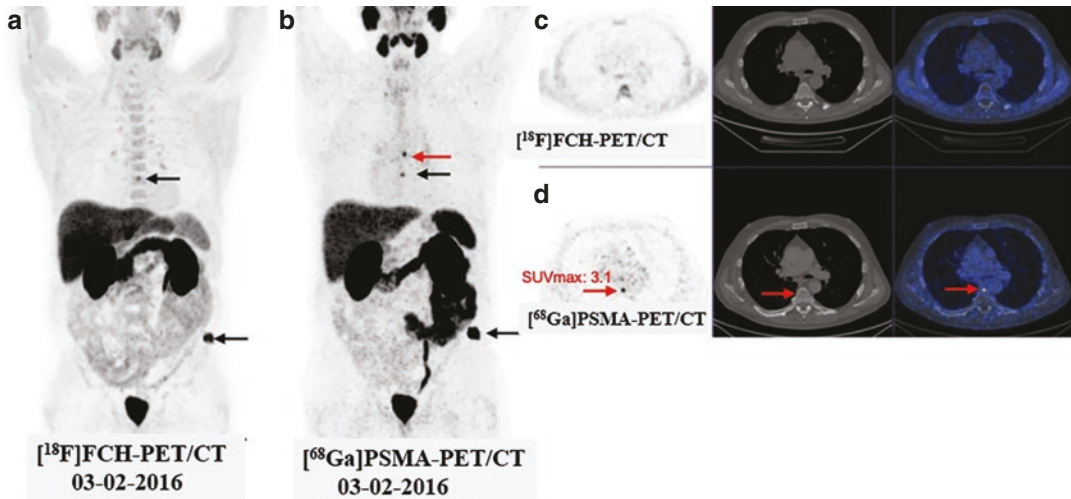
Fig. 22.14 Comparison of FCH-PET and Ga-PSMA-PET in prostate cancer recurrence: FCH-PET (**a**, **c**) revealed multiple bone metastases (arrows) in the left ilium and T10 vertebra corresponding with the sclerotic changes on CT. Ga-PSMA-PET (**b**, **d**) detected additional small bone metastasis on T9 vertebra (red arrows) without relevant morphological changes on CT. PSMA-PET detected small skeletal metastases (GS = 8, PSA: 0.7 ng/mL). (Figure from Paymani et al. [77])

22.4.4 Amino Acid (AA) Transport

Since amino acids are essential to cell metabolism and growth, AA transporter systems are overexpressed in prostate cancer, specifically, large neutral amino acid transporters (system L: LAT1, LAT3, and LAT4) and alanine-serine-cysteine transporters (system ASC: ASCT1 and ASCT2). Of these, LAT3, ASCT1, and ASCT2 are upregulated with androgen simulation and LAT1 and ASCT2 are associated with a more aggressive tumor phenotype [79, 80]. Prostate cancer may be imaged using both radiolabeled natural and synthetic amino acids. [11C]methionine has shown potential for initial evaluation of low- and high-grade primary prostate tumors [81]; however, it is not optimal because of the accumulation of metabolites in nontarget organs.

22.4.4.1 [18F]Fluciclovine (Axumin)
Fluciclovine (18F), also known as anti-1-amino-3-18F-fluorocyclobutane-1-carboxylic acid (anti-3[18F] FACBC) (Fig. 22.13), is a synthetic nonmetabolized, L-leucine analog that can accumulate in prostate cancer via overexpression of the ASC transporters [82]. Although it is transported by the AA transporter system, it does not undergo terminally incorporative metabolism within the body [83]. The distribution of the tracer in the body differs from choline and FDG, as kidney uptake of FACBC is negligible, and no activity is found in the urinary tract. There is low native brain uptake compared to FDG, which may enhance detection of brain metastases or primary brain tumors. The more intense native liver and pancreatic uptake seen with this agent would be expected to limit disease detection in those organs. FACBC-PET has shown early clinical success in imaging primary and recurrent disease in the prostate, pelvic lymph nodes, and bone, with relatively high tumor uptake with little urinary excretion, and improved sensitivity compared to ProstaScint™ imaging [84].

In 2016, [18F]fluciclovine was FDA approved for the localization of recurrent prostate cancer in patients with elevated PSA levels. Comprehensive clinical data demonstrate that 18F-fluciclovine is beneficial in the identification of the site of suspected recurrent disease. [18F]fluciclovine demonstrates improved accuracy when compared with conventional imaging modalities for whole-body staging. The detec-

tion of biochemical recurrence using [18F] Fluciclovine-PET was compared to 68Ga-PSMA-PET [85, 86]. These early reports indicate improved detection rates for PSMA-PET when compared with fluciclovine-PET in patients with recurrent PCa. Figure 22.15 shows comparison of Fluciclovine-PET to Ga-PSMA-PET. However, further studies are needed to compare [18F]fluciclovine-PET studies with PSMA radiotracers, and to characterize the patterns of bone uptake more completely, and also the uptake by other malignant tissues [79, 87].

22.4.5 Androgen Receptor

22.4.5.1 [18F]FDHT

Prostate cancer growth and progression is stimulated by androgens. Since the AR is the key driver of prostate differentiation and PC progression [22], inhibiting the central AR signaling by ADT it is the cornerstone of advanced PC treatment. [18F]Fluoro-16β-5α-dihydrotestosterone ([18F] FDHT) (Fig. 22.4), a ligand that targets the ligand-binding domain of AR, was originally developed to assess AR occupancy [25–27]. FDHT-PET can be used to evaluate the AR expression levels and
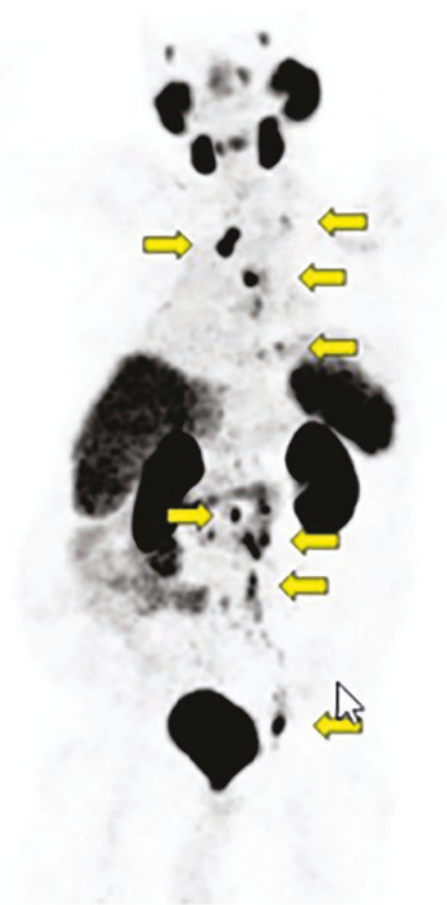

Fig. 22.15 In a patient with prostate cancer 68Ga-PSMA-11 PET indicates (arrows) intense uptake in pelvic, abdominal, thoracic, and supraclavicular lymph nodes (LNs). Corresponding LNs on 18F-fluciclovine-PET show no uptake [85]

receptor occupancy, and enables detection of AR-positive metastatic lesions as indicated by increased AR concentrations. Following treatment with AR antagonists, a decrease in FDHT uptake in the metastatic lesions is indicative of treatment response [88]. [18F]FDHT-PET scans in CRPC patients treated with MDV3100 (AR-mediated drug) found that tumors in nearly all patients showed a decrease in [18F]FDHT binding, indicating that MDV3100 can occupy the AR ligand-binding domain and preclude radiotracer binding. However, these [18F]FDHT-PET "responses" did not correlate with declines in serum PSA or tumor response [88, 89]. A recent study reported that baseline [18F]FDHT-PET/CT using SUV_{peak} of all metastatic lesions predicts treatment response in patients with mCRPC treated with enzalutamide [90].

Direct comparison of FDHT-PET scans with FDG-PET studies has suggested that there may be diverse metabolic phenotypes (Fig. 22.16) of castrate-resistant cancers (androgen receptor predominant, glycolysis-predominant, or androgen receptor/glycolysis-concordant) and that 18F-FDHT is probably suited as a pharmacodynamic response marker, rather than a treatment response marker [91]. Therefore, PET studies to study AR expression (with FDHT) and glycolysis (with FDG) have the ability to determine heterogeneity of imaging phenotypes, which may be useful in distinguishing patients who will benefit from AR inhibitors from those who need alternative treatments [24].

Preclinical studies suggest that androgen blockade appears to increase expression of PSMA in both hormone-sensitive and castrate-resistant
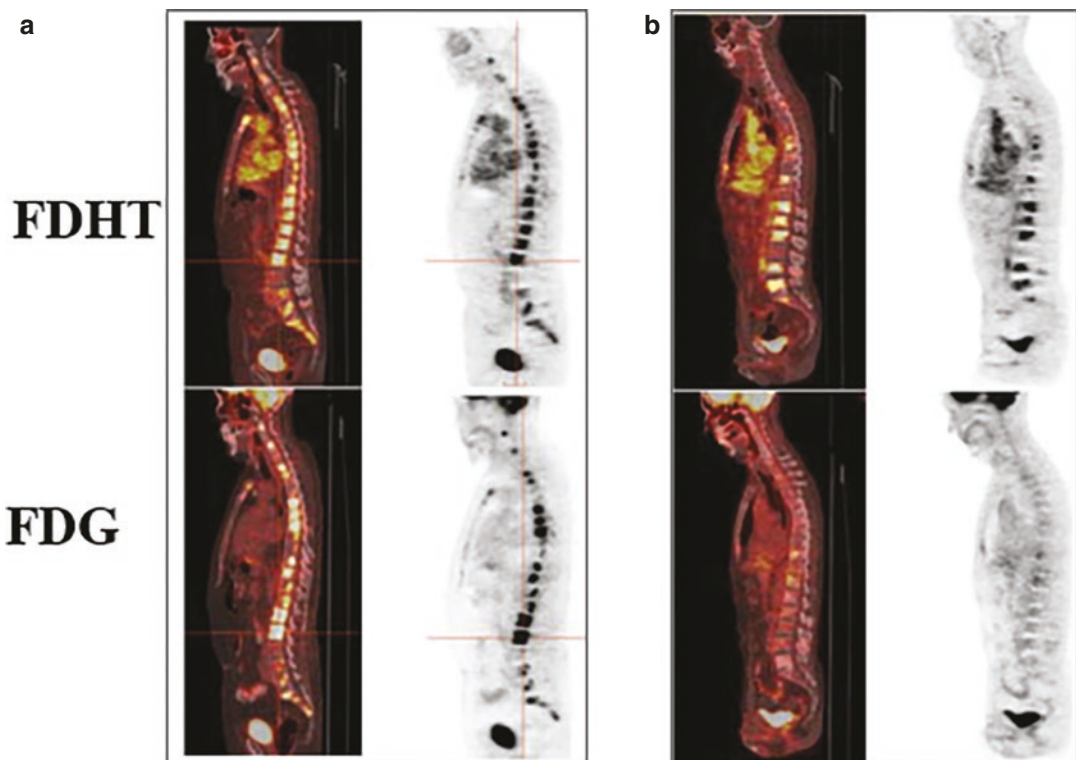
Fig. 22.16 [18F]FDHT vs. [18F]FDG phenotypes in CRPC patient with multiple osteoblastic metastases. The scans in (**a**) show uptake in bone lesions consistent with a "Glycolysis/AR Concordant" phenotype. While scans in (**b**) demonstrate intense FDHT uptake and relatively low level FDG uptake, consistent with an "AR Predominant" phenotype. (From Fox et al. [91])

xenotypes. Recently, Ga-PSMA-PET studies demonstrated higher tumor uptake suggesting enhanced PSMA expression following treatment with enzalutamide [92]. Since PSMA expression is influenced by AR signaling, further investigations should help to clarify the relative value of FDHT-PET vs. PSMA-PET imaging in guiding therapies for prostate cancer. It appears that the three molecular imaging modalities based on FDHT, FDG, and PSMA will have distinct and complementary roles to play in the management of patients with mCRPC.

22.4.5.2 [^{18}F]Enzalutamide (FEZT)

FDHT shows high specific binding to the AR but, is rapidly metabolized in humans [93]. The circulating radiolabeled metabolites show high background activity in blood and are cleared via the kidneys into the urine. Enzalutamide (Xtandi®) is a pure AR antagonist that possesses an AR affinity similar to that of dihydrotestosterone and is currently used in androgen therapy. Enzalutamide and its primary metabolite *N*-desmethylenzalutamide have an AR affinity comparable to that of FDHT but, are excreted mainly via the hepatic route [94]. It has been recently reported that FEZT (Fig. 22.4) may have more favorable properties for imaging of AR density with PET than FDHT [94]. Preclinical studies in AR-positive LnCaP xenograft model showed about three times higher tumor uptake for FEZT than for FDHT. Also, at 1 h after tracer injection, 93% of FEZT in plasma was still intact, compared with only 3% of FDHT.

22.4.6 Radiolabeled Antibodies

### 22.4.6.1 ^{111}In-Capromab Pendetide (ProstaScint™)

The mAb 7E11-C5.3 was the first anti-PSMA mAb originally developed with a type of prostate cancer cell line known as LNCaP cells [35]. This murine mAb was later conjugated to the linker-chelator, glycyl-tyrosyl-(*N*,ε-diethylenetriaminepentaacetic acid) lysine hydrochloride (GYK-DTPA-HCl), radiolabeled with ^{111}In and was commercialized as an imaging agent, known as ^{111}In capromab pendetide (ProstaScint™) [95]. Since it recognizes and

binds to an intracellular epitope of PSMA, only the fixed cells and necrotic cells but not the intact viable cells, bind to the 7E11 mAb. The FDA in 1996, however, approved ProStacint™ as a staging agent indicated for the detection of recurrent prostate cancer in post-prostatectomy patients with a rising PSA and negative or equivocal standard metastatic evaluation, in whom there is high clinical suspicion of occult metastatic disease, and for newly diagnosed patients with biopsy-proven prostate cancer thought to be at high risk for lymph node metastasis. In patients with prostate carcinoma who are at high risk for metastatic disease, the sensitivity was 77% and the specificity was 86% [96]. Subsequent publications have revealed wide variance in the efficacy; such as sensitivity of 67% for disease detection in prostate bed, but a sensitivity of only 10% for extraprostatic disease detection. This agent repeatedly failed in the clinical setting, likely due to poor pharmacokinetics and failure to reach its target epitope on the intracellular portion of PSMA [97].

22.4.6.2 ^{177}In-huJ591 and ^{177}Lu-huJ591 mAb

J591 mAb targets the extracellular portion of PSMA and, therefore, binds to the viable tumor cells [41, 98]. The bifunctional DOTA chelator was conjugated to humanized J591 mAb. The DOTA-J591 mAb (5–6 DOTAs/IgG) was labeled with ^{111}In for imaging studies and ^{90}Y or ^{177}Lu for RIT [99]. Saturation binding studies demonstrated that J591 mAb binds to PSMA with extremely high affinity (K_d = 1.83 ± 1.21 nM). Based on ^{131}I-J591 mAb, it was estimated that LNCaP tumor cells express approximately a million PSMA-binding sites/cell [42].

Planar and SPECT imaging studies with ^{111}In and/or ^{177}Lu DOTA-huJ591 (Fig. 22.17) have shown accurate detection of prostate cancer bone and soft tissue metastases, as well as uptake in the tumor neovasculature of many solid tumors [100–104]. In a phase I study with 53 patients, ^{111}In-J591 accurately targeted bone and/or soft tissue lesions in 98% of the eligible patients. In a phase I dose escalation study with ^{177}Lu-J591, the planar/SPECT imaging detected almost 100% of the lesions identified by conventional imaging studies. These imaging studies indicated that
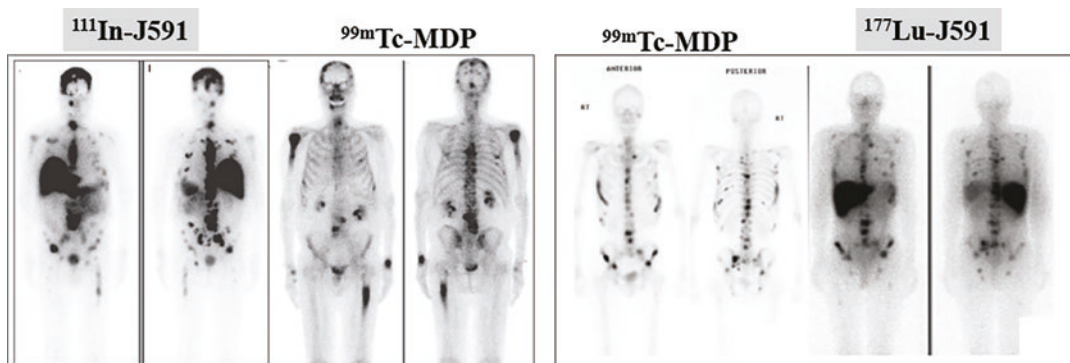
Fig. 22.17 J591 mAb targeting of PSMA in patients with prostate cancer. Panel on left shows comparison of ^{111}In-J591 with bone scan and panel on right shows comparison of ^{177}Lu-J591 with bone scan. (Images provided by Dr. Tagawa at Weill Cornell Medicine, NY)

J591 imaging of PSMA expression is a prognostic tool in patients with mCRPC.

22.4.6.3   [89]Zr-huJ591 mAb

[89]Zr decays in two ways (23% β^+ and 77% *EC*) with a half-life (*T½* = 3.3 days) and ideal for PET/CT imaging with [89]Zr-labeled antibodies. Also, the [89]Zr has a relatively short positron range (shorter than ^{18}F) by emitting low energy β^+ particles (E_{mean} = 396 keV), which facilitates high-resolution PET imaging. Compared to [^{18}F]FDG and CT, patients generally receive higher radiation from [89]Zr-labeled mAb PET (~20–40 mSv for 37–74 MBq) [105].

[89]Zr-huJ591 mAb was used for PET imaging studies to detect PSMA-positive prostate cancer. Early studies have shown inconsistent results for the diagnostic performance of primary prostate cancers [106]. However, in patients with metastatic prostate cancers (n = 10), the sensitivity for detecting primary tumors increased to 100%. In patients (n = 50) with mCRPC [89]Zr-J591-PET had a higher sensitivity for bone metastasis than conventional imaging methods, while conventional imaging methods were more sensitive for soft tissue lesions [107, 108].

While imaging with radiolabeled whole IgG mAb approach is highly promising the optimal time for patient imaging after injection in terms of achieving adequate tumor to background ratios was 7 ± 1 days. Although radiolabeled antibodies offer the potential for tumor targeting, their effectiveness as diagnostic radiopharmaceutical is limited by a long plasma half-life, poor tumor penetrability, and the nonspecific localization exhibited with immunoglobulins.

22.4.6.4   [89]Zr-Df-IAB2M Minibody

IAB2M is an 80-kDa minibody genetically engineered from the parent J591 mAb. [89]Zr-IAB2M showed rapid accumulation in tumors and a fast clearance from the blood within 24 h in a prostate cancer model [109]. The [89]Zr-IAB2M uptake of bone and lymph node metastases was discernible in as little as 24 h and lasted up to 120 h in patients with prostate cancer [110]. The [89]Zr-IAB2M uptake correlated with PSMA expression [111]. With [89]Zr, the advantage of minibody is significant reduction of effective dose (0.41–0.68 mSv/MBq) compared to whole IgG. Figure 22.18 shows the [89]Zr-IAB2M PSMA targeting more metastatic prostate cancer lesions compared to bone scan, and FDG-PET [111].

22.4.6.5   [89]Zr-DFO-MSTP2109A, Anti-STEP-1 Antibody

The 6-transmembrane epithelial antigen of the prostate (STEAP) family is comprised of four novel cell surface markers (STEAP 1–4) highly expressed in prostate cancer [112]. It is also present in other cancers but, has little cross-reactivity with other normal tissues. STEAP1 is composed of 339 amino acid cell surface markers. Functionally, it appears to be an ion channel or transporter protein and may have roles in multiple biological processes, including cell adhesion, pro-

^{99m}Tc-MDP   [^{18}F]FDG ^{89}Zr-IAB2M
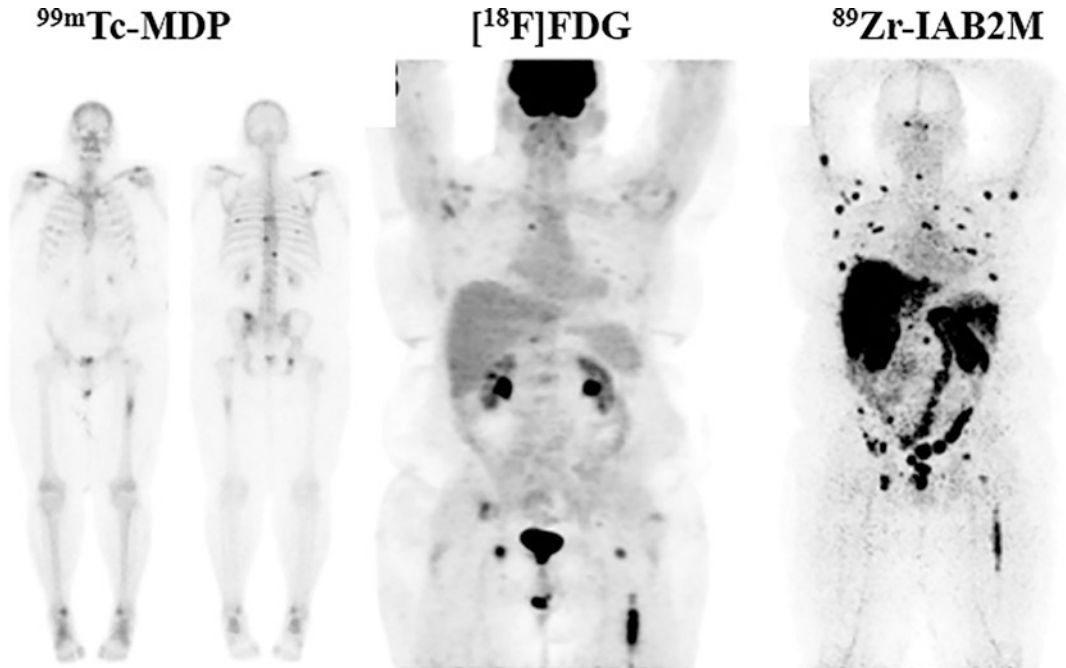
Fig. 22.18 ^{89}Zr-IAB2M-PET imaging in mCRPC. Targeting with IAB2M (minibody fragment from J591 mAb). Comparison with bone scan and FDG-PET. ^{89}Zr-IAB2M scan shows more images than bone scan or FDG-PET. (From Pandit-Taskar et al. [111])

liferation and invasiveness, intracellular communication, and tumor growth inhibition, and iron metabolism. STEAP1 overexpression in prostate cancer and its bone metastases has been very well documented, showing correlation between increased expression and tumor aggressiveness.

^{89}Zr-DFO-MSTP2109A mAb may have the potential to be used as a companion imaging agent for therapies that are being developed to target STEAP1. A phase 1 study evaluated the safety, biodistribution, and tumor targeting in patients with mCRPC [113]. There was no significant acute or subacute toxicity. Favorable biodistribution and enhanced lesion uptake (in both bone and soft tissue) were observed. The best lesion discrimination was seen around 6 days post administration.

22.4.7 Small-Molecule PSMA Inhibitors

Small molecules that interact specifically with PSMA and carry appropriate radionuclides for PET and SPECT provide an ideal molecular imaging option for prostate cancer. Smaller molecular weight compounds with higher permeability into solid tumors will likely have a definitive advantage in obtaining higher percent uptake per gram of tumor tissue and a high percentage of specific binding. Smaller molecules will likely also display improved blood clearance and tissue distribution in normal tissues compared to intact immunoglobulins making lesion detection more conspicuous.

Several groups have reported on the development of small-molecule inhibitors of PSMA based on the structural motifs of various NAALADASE inhibitors comprising two amino acids joined through their NH_2 groups by a urea linkage (glutamate urea heterodimers). Glutamate-ureido (Glu-ureido) based inhibitors are by far the most explored and clinically used class of PSMA agents. The urea-based PSMA-binding motifs are present in three forms: glutamate-urea-glutamate (*glu-urea-glu*) also known as DUPA motif, glutamate-urea-cysteine

(*glu-urea-cys*), or glutamate-urea-lysine (*glu-urea-lys*). Many of the current radiolabeled PSMA inhibitors used in the clinic for imaging and therapy (Tables 22.2 and 22.3) are based on the urea-based motif or pharmacophore.

22.4.7.1 DCFBC and DCFPyl

In 2002, Dr. Pomper's group at John Hopkins School of Medicine (JHSM) reported the synthesis of the first radiolabeled PSMA inhibitor, [11C]MeCys-C(O)-Glu ([11C]MCG or [11C]DCMC) (Fig. 22.19) which binds to PSMA with high potency ($IC_{50} = 1.4$ nM) [114]. Three years later, based on animal studies, [11C]DCMC was proposed for imaging prostate cancer and the authors stated that [11C]DCMC is not a substrate for PSMA, but is bound to the active site of the enzyme electrostatically so that PSMA is behaving like a receptor and not as an enzyme in this type of imaging studies [115].

[18F]DCFBC (Fig. 22.19) was the first 18F labeled PSMA inhibitor developed in 2008 at JHSM based on Cys-Urea-Glu pharmacophore and was successfully evaluated in several clinical studies [116]. The major drawback of this tracer was slow blood clearance and high background activity. As a result, early imaging studies did not provide optimal sensitivity.

In a prospective study in patients ($n = 68$) with documented biochemical recurrence after primary local therapy (prostatectomy and/or post radiation therapy) with negative conventional imaging, [18F]DCFBC-PET was able to identify recurrence with PSA >0.78 ng/mL in 60.3% of patients, which led clinicians to change the treatment strategy in 51% of patients [117].

[18F]DCFPyl (Pylarify™)

The next generation compound from JHSM is [18F]DCFPyl (Fig. 22.19), developed based on Lys-Urea-Glu motif, was hydrophilic, and showed faster renal excretion [118]. In patients with biochemical recurrence, direct comparison of [18F]DCFPyl with 68Ga-PSMA-11 indicated that [18F]
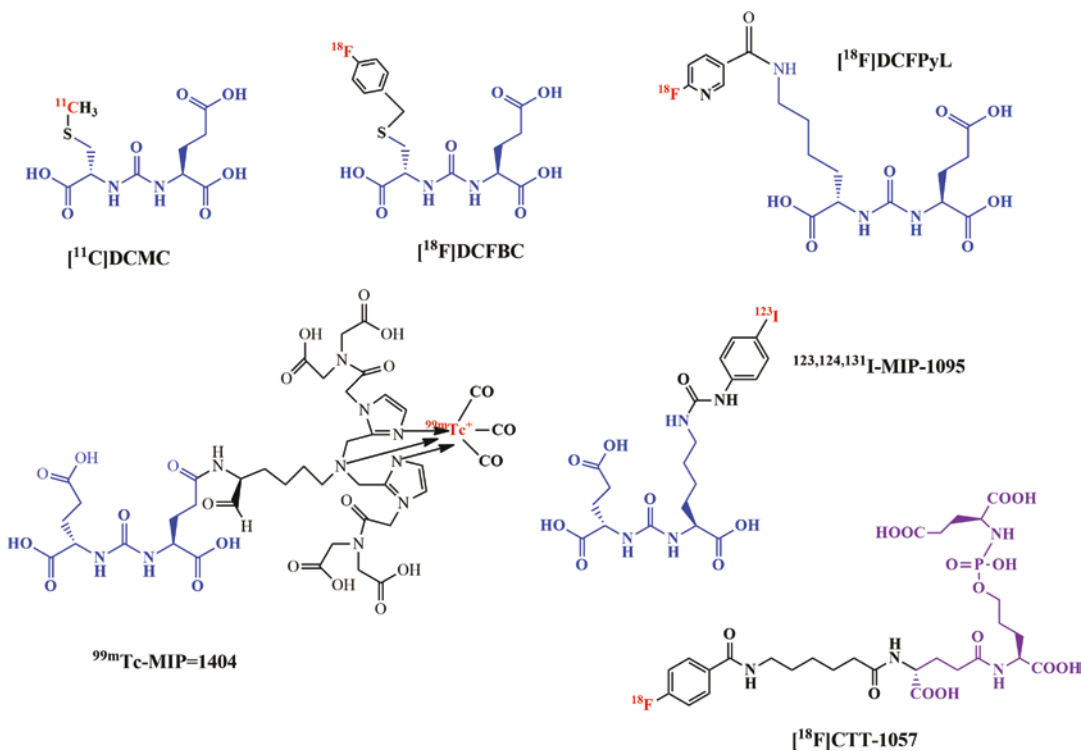
Fig. 22.19 Small-molecule PSMA inhibitors labeled with 18F, 99mTc, and 123/131I. Except for CTT-1057 ligand (phosphoramide derivative), all the other ligands share the urea-glutamate pharmacophore (shown in blue color)

DCFPyL is noninferior to ^{68}Ga-PSMA-11, and that imaging with [^{18}F]DCFPyL-PET may even exhibit improved sensitivity in localizing relapsed tumors after prostatectomy for moderately increased PSA levels [119]. A pilot study comparing [^{18}F]DCFPyl to [^{18}F]PSMA-1007 observed that excellent image quality was achieved with both agents, resulting in identical clinical findings. Nonurinary excretion of ^{18}F-PSMA-1007, however, might present some advantage with regard to delineation of local recurrence or pelvic lymph node metastasis in selected patients; the lower hepatic background might favor [^{18}F]DCFPyL in late stages, when rare cases of liver metastases can occur [120].

The FDA approval was based on data from two studies, the OSPREY and CONDOR trials, investigating the safety and diagnostic performance of ^{18}F-DCFPyL in prostate cancer. In the phase 2/3 OSPREY trial, improvements in the specificity (96–99%) and positive predictive value (78–91%) of the agent were observed when compared with conventional imaging for metastatic prostate cancer. Eligible patients in the OSPREY trial were divided into two cohorts, with cohort A including patients with high-risk, locally advanced prostate cancer, and cohort B including patients with metastatic or recurrent disease. In the phase 3 CONDOR study, a median PSA level of 0.8 ng/mL was observed among the 208 evaluable patients, with 68.8% having a PSA level of less than 2.0 ng/mL. The primary end point of correct localization rates (CLRs), identified by PyL–PET/CT and evaluated by 3 blinded independent central readers was observed at 85.6% (95% CI, 78.8–92.3%), 87.0% (95% CI, 80.4–93.6%), and 84.8% (95% CI, 77.8–91.9%) [121] (Fig. 22.20).
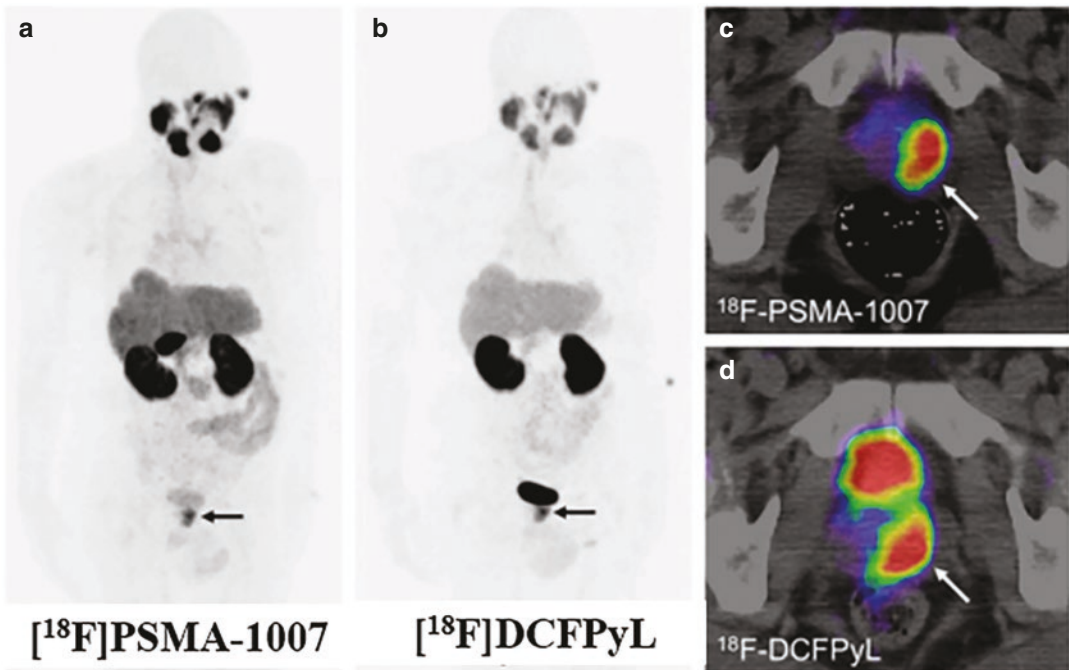
Fig. 22.20 [^{18}F]DCFPyl vs. ^{18}F-PSMA-1007 PET/CT in a patient with newly diagnosed prostate cancer with high PSA (95.43 ng/mL) and positive biopsy (GS = 8). DCFPyL (**b**, **d**) detects (SUV$_{max}$ = 18.08) prostate cancer confined to prostate gland. PSMA-1007 (**a**, **c**) (SUVmax = 11.77) also provides the same diagnosis [120]

22.4.7.2   MIP-1095 and MIP-1404

In 2006, Dr. Babich's group at Molecular Insight Pharmaceuticals (MIP) company (later acquired by Progenics Pharmaceuticals Inc) started a program to design and synthesize a series of heterodimeric inhibitors of PSMA having Lys-urea-Glu pharmacophore that could be radiolabeled with different isotopes including halogens. They reported the development of two high-affinity radioiodinated PSMA inhibitors ^{123}I-PSMA-1072 ($Ki = 5$ nM) and ^{123}I-PSMA-1095 ($Ki = 0.3$ nM) for SPECT imaging studies [122]. The first human studies demonstrated that these tracers detect lesions in the prostate gland, soft tissue, lymph nodes, and distant metastases and clearly documented the potential utility of PSMA imaging at 4 h after injection based on planar and SPECT imaging studies [123]. Direct comparison with ProstaScint imaging clearly documented that ^{123}I-MIP-1072 identified several metastatic lesions in the pelvic lymph nodes not detected by anti-PSMA antibody, ProstaScint imaging. Based on these early clinical results, MIP-1095 (Fig. 22.19) was labeled with [131]I (a radionuclide that emits a beta particle) for targeted therapy of metastatic prostate cancer. [124/131]I-MIP-1095 was also developed for PET imaging studies and TRT of mCRPC [124].

#### ^{99m}Tc-MIP-1404 (Trofolastat™)

Subsequently, in 2012, Dr. Babich's group also reported the development of two high-affinity ^{99m}Tc-labeled PSMA inhibitors, ^{99m}Tc-MIP-1404 (Fig. 22.19) and ^{99m}Tc-MIP-1405, based on Glu-Urea-Glu and Glu-Urea-Lys pharmacophores and tricarbonyl core chemistry [125]. The first human studies in patients with mCRPC showed both ^{99m}Tc tracers localized to lesions in bone and soft tissue that correlated with radiologic evidence of metastatic disease identified by the bone scan [126, 127]. In a 71-year-old patient who had prior prostatectomy and with a rising PSA (1.37–8.9 ng/mL over a period of 4 months), PSMA imaging with ^{99m}Tc-MIP-1404 (in March) detected more metastatic lesions earlier compared to the two bone scans performed either before (in January) or after (in June) the PSMA scan (Fig. 22.21). Based on these results a preliminary phase I study and a multicenter phase II study were conducted in high-risk prostate cancer patients scheduled for prostatectomy and extended pelvic node lymph node dissection. In all subjects with Gleason score > 7, [99m]Tc-
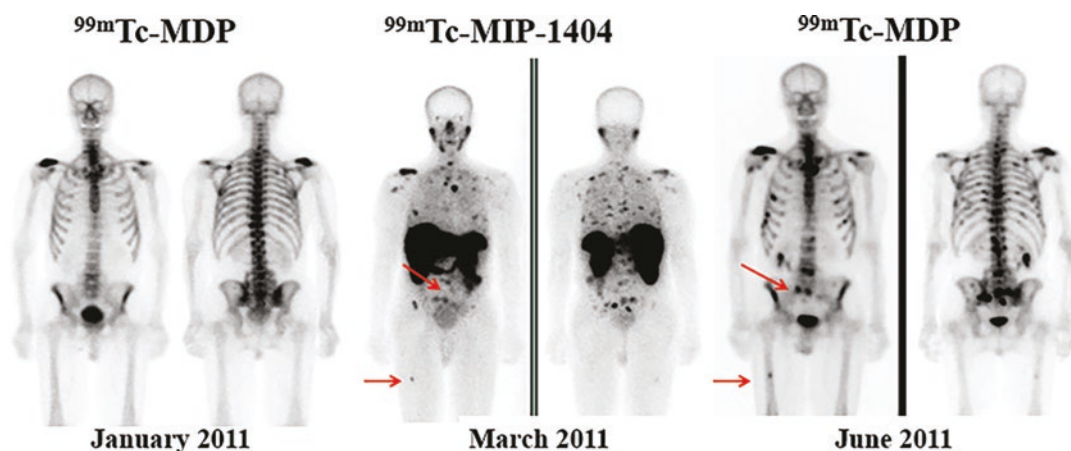
Fig. 22.21 ^{99m}Tc-MIP-1404 planar whole-body images in a patient who had prior prostatectomy and with a rising PSA (1.37–8.9 ng/mL over a period of 4 months), PSMA imaging with ^{99m}Tc-MIP-1404 (in March) detected more metastatic lesions earlier compared to the two bone scans performed either before (in January) or after (in June) the PSMA scan [126, 127]
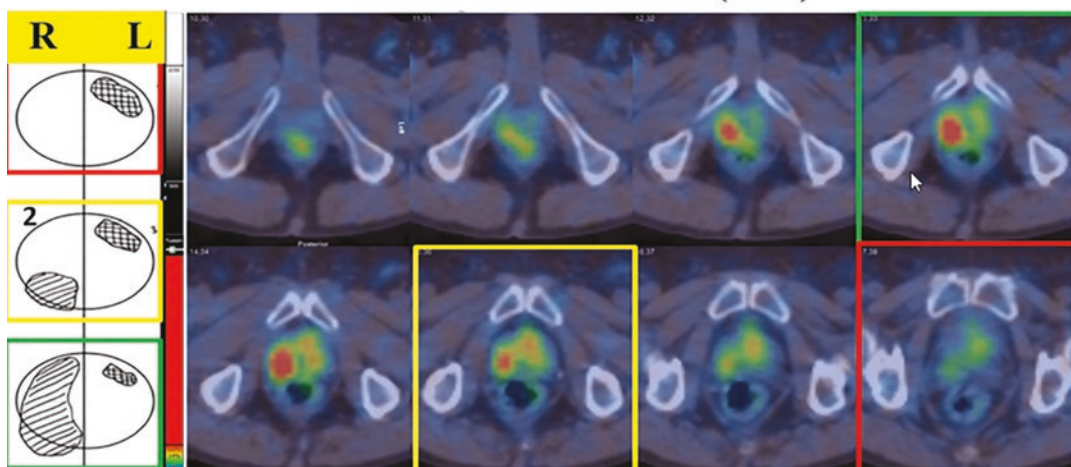
Fig. 22.22 99mTc-MIP-1404 images in a high-risk prostate cancer patient scheduled for prostatectomy and extended pelvic node lymph node dissection. 99mTc-MIP-1404 SPECT clearly identified the prostate cancer foci (Gleason score > 7) in the prostate gland, confirmed by histopathology (Vallabhajosula et al. Weill Cornell Medicine, NY)

MIP-1404 SPECT clearly identified the PCa foci in the prostate gland, confirmed by histopathology (Fig. 22.22), and PSMA staining [128]. Because 99mTc-MIP-1404 (Trofolastat™) showed minimal urinary excretion, it had a distinct advantage for detecting prostate cancer in the gland and pelvis at initial stages of the disease and was selected for phase II/III studies to determine sensitivity, and specificity to detect prostate cancer in high-risk patients. Trofolastat™ has been investigated in several clinical trials resulting as the first PSMA imaging agent to finalize phase 3 clinical trials [129]. It is therefore expected that 99mTc-MIP-1404 may be available as a "technetium instant kit" in the near future.

22.4.7.3   PSMA-11, PSMA-617, PSMA-1007, and PSMA-I&T

**68Ga-PSMA-HBED-CC (or 68Ga-PSMA-11)**
In 2012, the development of PSMA-HBED-CC (also known as PSMA-11 or DKFZ-PSMA-11) at the German Cancer Research Centre (GCRC) and the University Hospital at Heidelberg by Drs. Eder, Haberkorn, and Afshar-Oromieh should be regarded as a major milestone in the development of radiolabeled PSMA inhibitors for molecular imaging and targeted therapy.

PSMA-11 consists of a Glu-urea-Lys motif conjugated with the highly efficient and Ga-specific acyclic chelator HBED-CC (Fig. 22.10) via an aminohexanoic acid (Ahx) spacer [130]. The advantage of HBED-CC chelator is that it can form efficient 68Ga complex at room temperature with extremely high thermodynamic stability. In the first human studies, direct comparison to [18F] FCH, 68Ga-PSMA-targeted PET imaging was able to detect lesions much earlier in patients with low PSA values and showed reduced background activity in healthy tissue [131]. Subsequently, several clinical studies documented the clinical utility of 68Ga-PSMA-11 (Fig. 22.23) for molecular imaging of prostate cancer [132].

The FDA approval of 68Ga-PSMA-11 [133] was based on evidence from two clinical trials in patients with prostate cancer. The trials were conducted at two different sites in the USA (FDA package insert). Trial-1 enrolled patients who were recently diagnosed with prostate cancer and were awaiting surgery for the removal of the prostate and the nearby lymph nodes. Trial-2 enrolled
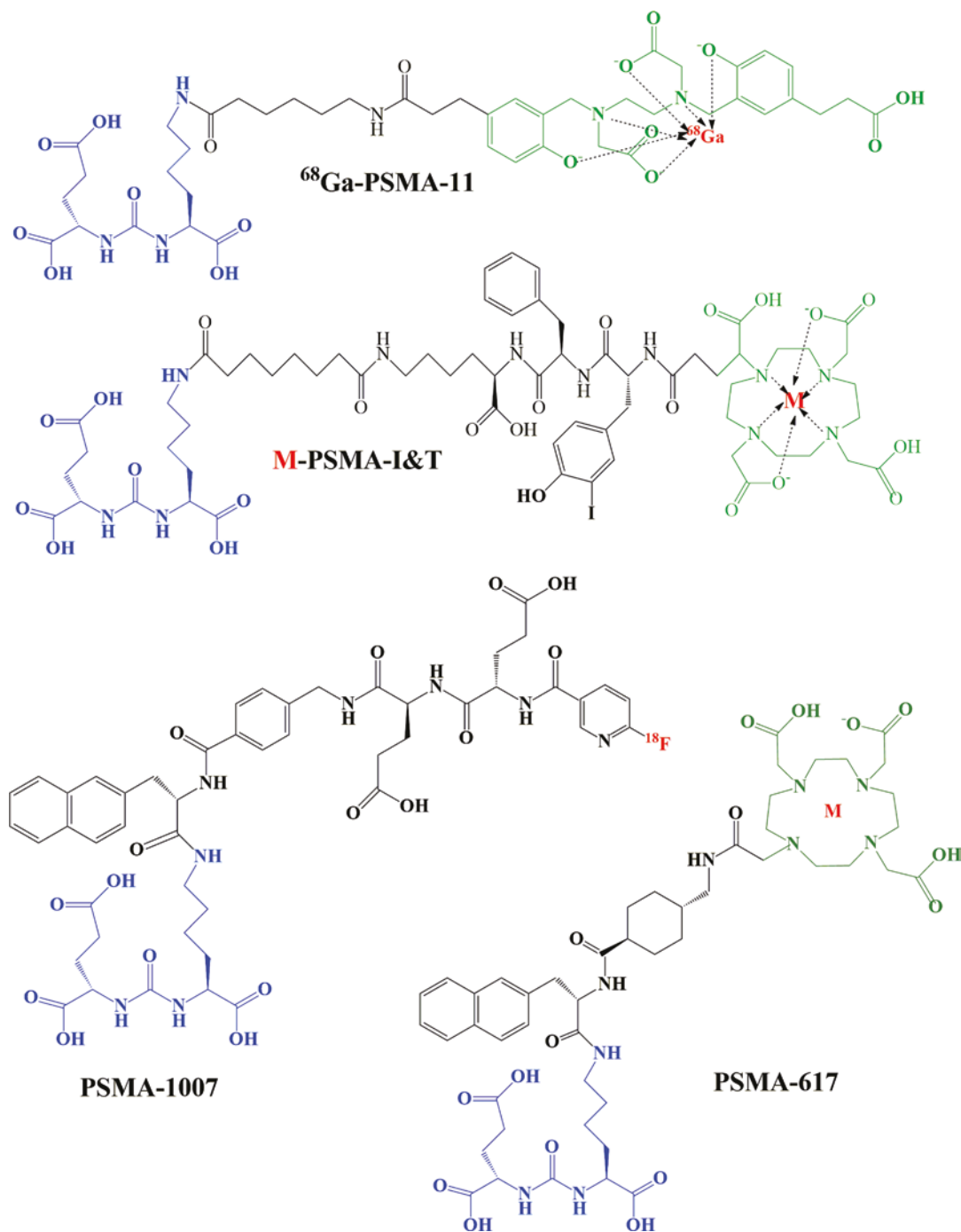
Fig. 22.23 Small-molecule PSMA inhibitors (PSMA-11, PSMA-617, and PSMA-I&T) were developed to complex trivalent metals, such as ^{68}Ga, ^{111}In, ^{177}Lu, and [225]Ac. PSMA-11 is based on HBED-CC chelator, while PSMA-617 and PSMA-I&T are based on DOTA chelator. All the ligands share the urea-glutamate pharmacophore (shown in blue color)

patients who were already treated for prostate cancer but, had rising PSA levels, suspicious for cancer spreading. In patients scheduled for radical prostatectomy, the positive predictive value was 61% and the negative predictive value was 84%. The sensitivity was 47% and specificity was 90%. In patients with biochemical recurrence, the likelihood of identifying a ^{68}Ga-PSMA-11 PET positive lesion generally increased with higher serum PSA level (36% at <0.5 ng/mL to 91% at >2.0 ng/mL).

PSMA-11, PSMA-617, PSMA-1007, and PSMA-I&T

In order to develop a theranostic PSMA inhibitor, the investigators at the GCRC in Heidelberg, conjugated the same Glu-Urea-Lys pharmacophore with DOTAGA chelator using a modified linker with D-amino acids and, thus, developed the first theranostic PSMA inhibitor, named PSMA-I&T, for imaging and therapy of prostate cancer [134,

135]. The targeting of PSMA with ^{177}Lu-PSMA-I&T was shown to be as good as that of ^{68}Ga-PSMA-11 (Fig. 22.24). Some clinical studies evaluated the potential of ^{68}Ga-PSMA I&T for the detection of primary prostate cancer before prostatectomy [43].

The HBED-CC chelator used for developing ^{68}Ga-PSMA-11 is not appropriate for labeling therapeutic radiometals such as ^{177}Lu, ^{90}Y, and [225]Ac. To overcome this restraint, the investigators at the GCRC developed two high-affinity PSMA inhibitors, PSMA-617 and PSMA-I&T, based on Glu-Urea-Lys pharmacophore and DOTA or DOTAGA chelators (Fig. 22.23). In addition, the choice of linker/spacer has a significant impact on tumor targeting, as well as on the pharmacokinetics. PSMA-617 was synthesized by conjugating DOTA chelator to the Glu-Urea-Lys motif by a naphthalic spacer [136]. PSMA-I&T was synthesized by DOTAGA chelator to the same Glu-Urea-Lys scaffold by a spacer con-
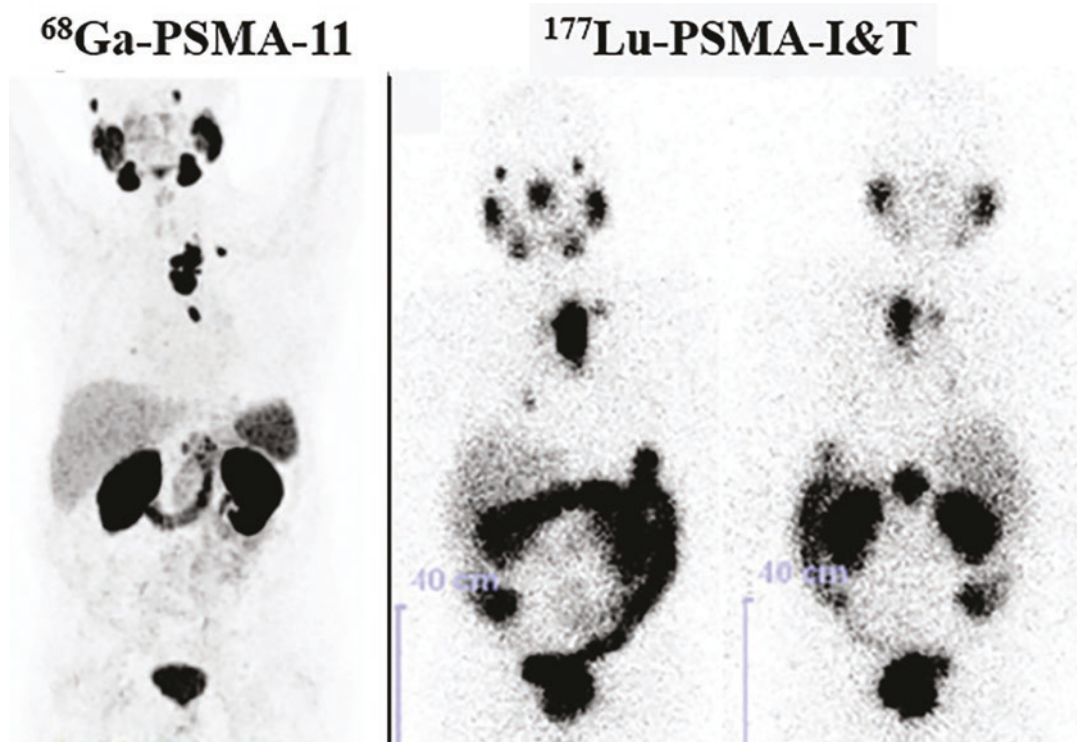
Fig. 22.24 PSMA targeting with ^{68}Ga and ^{177}Lu labeled small-molecule PSMA inhibitors. ^{68}Ga-PSMA-PET/CT showed intense tracer accumulation in mediastinal lymph node metastases. Correspondingly, these mediastinal lymph nodes demonstrated high ^{177}Lu-PSMA-I&T uptake 47 h after therapy with 5.7 GBq of ^{177}Lu-PSMA-I&T [134]

taining D-Phe-D-Phe-Lys amino acid residues. Further substitution of the D-Phenylalanine residues in the peptide linker by 3-iodo-D-tyrosine resulted in the final compound, DOTAGA-(I-y)-fk-(Sub-kuE), named PSMA-I&T (for imaging and therapy) since it can be used to label with either ^{68}Ga or [177]Lu [134].

^{177}Lu-PSMA-617 was quickly used as a therapeutic ligand because it has higher tumor uptake at later time points, lower spleen uptake, and highly efficient clearance from the kidneys [136]. Some studies, however, showed lower tumor uptake compared to PSMA-11 whereas the tissue distribution pattern and kinetics of PSMA-I&T are comparable to PSMA-11 [134].

The investigators at GCRC were also successful in developing a ^{18}F-labeled PSMA inhibitor [^{18}F]PSMA-1007. PSMA-1007 shares the same Glu-Urea-Lys motif and the naphthalene-based linker region as PSMA-617. The only difference is the ^{18}F radiolabeling moiety. The pharmacophore conjugated with NaI but, the linker is replaced by 4-carboxy-benzylamine residue followed by two glutamic acid residues and conjugated with 6-[^{18}F]fluronicotinic acid [137, 138]. In a pilot clinical study, [^{18}F]PSMA-1007 was directly compared to [^{18}F]DCFPyl in patients with newly diagnosed prostate cancer (Fig.

22.20). Excellent imaging quality was achieved with both tracers, resulting in identical clinical findings. With PSMA-1007, however, unlike the other PSMA inhibitors, excretion is mainly by hepatobiliary system and nonurinary excretion of [^{18}F]PSMA-1007 might present some advantage with regard to delineation of local recurrence or pelvic lymph node metastasis in selected patients [120].

22.4.7.4   rhPSMA-7.3

A unique and novel class of theranostic agents named radiohybrid (rh) PSMA inhibitors based on Glu-Urea-Lys pharmacophore were developed by Dr. Wester and colleagues at the Technical University of Munich, Garching, Germany (TUMG) [139, 140]. Radiohybrid concept represents a molecular species that offers two binding sites for radionuclides, a silicon-fluoride acceptor (SiFA) for ^{18}F and a chelator (such as DOTA) for radiometallation. One of these binding sites is radiolabeled, the other one labeled with a stable nuclide, thus is silent. These pairs of compounds (Fig. 22.25), either pure imaging pairs (A) or theranostic pairs (B), represent chemically identical species (monozygotic chemical twins) and thus exhibit identical in vivo characteristics (e.g., affinity, lipophilicity, pharmacokinetics). The lead compound [^{18}F]Ga-rhPSMA-7 with [nat]Ga-

[18F]rh-PSMA-7
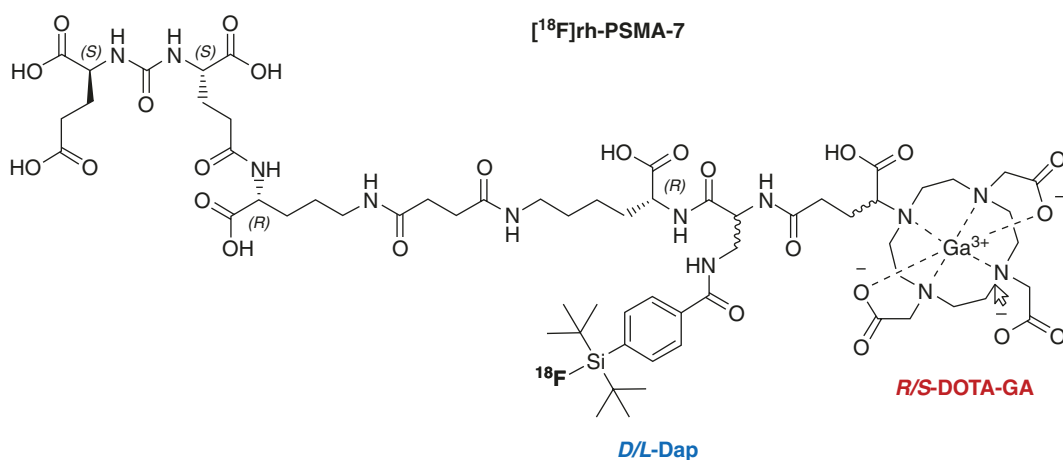
Fig. 22.25 Diastereomeric mixture [^{18}F,[nat]Ga]rhPSMA-7 is composed of the four isomers [^{18}F, [nat]Ga]rhPSMA-7.1 to 7.4, differing in the stereoconfiguration of diaminopropionic acid (D-/L-Dap) and DOTA-GA (R-/S-DOTAGA). The predominant species is [^{18}F,[nat]Ga]rhPSMA-7.3 [139, 140]

DOTAGA complex was evaluated in patients with biochemical recurrence [141]. The biodistribution was found to be similar to that of established PSMA ligands, and [^{18}F,[nat]Ga]rhPSMA-7 PET/CT demonstrated high detection rates in early biochemical recurrence after radical prostatectomy, especially among patients with low PSA values. [^{18}F]Ga-rhPSMA-7, however, represents a mixture of four stereoisomers (7.1, 7.2, 7.3, 7.4), differing in the stereo-configuration of the diaminopropionic acid branching unit (D-Dap or L-Dap) and the glutamic acid pendant arm at the DOTA-GA-chelator (R-DOTA-GA or S-DOTA-GA) [139, 140]. Based on preclinical studies, [^{18}F,[nat]Ga]rhPSMA-7.3 was identified as the preferred isomer since it showed high tumor accumulation, low uptake by the liver and kidney with low blood levels. [^{18}F]-rhPSMA-7.3 is currently in phase III trials (sponsored by BlueEarth Diagnostics) for prostate cancer (PCa) imaging. In order to assess the role in primary staging, [^{18}F]-rhPSMA-7.3 PET/CT studies in patients ($n = 279$) with primary prostate cancer were evaluated [142]. [^{18}F]-rhPSMA-7.3 offers superior diagnostic performance to morphological imaging for primary N-staging of newly diagnosed PCa, shows lower inter-reader variation, and offers good distinction between primary tumor and bladder background activity. In preclinical studies, the in vivo behavior of the therapeutic analog ^{177}Lu-rhPSMA-7.3 was compared to [^{177}Lu]PSMA-I&T [143]. Based on the results, ^{19}F/^{177}Lu-rhPSMA-7.3 can be considered a suitable candidate for clinical translation due to similar clearance kinetics and radiation dose to healthy organs but, superior tumor uptake and retention compared with ^{177}Lu-PSMA-I&T.

22.4.7.5 Albumin-Binding PSMA Inhibitors

The plasma protein human serum albumin (HAS) has a long half-life of about 19 days and, because of its high molecular weight (67 kDa), it has low renal clearance making the protein a valuable candidate as a drug delivery system and a means to extend the half-life of peptides [144–146]. HSA is a widely recognized carrier for the passive targeting to solid tumors and has been frequently used to develop drug conjugates for longer plasma half-life. The covalent or noncovalent attachment of peptides to albumin can reduce the glomerular filtration rate and extend the half-life of peptides by increasing the size of peptide-based drugs. Albumin is also found to specifically target tumor regions because of its enhanced permeability and retention (EPR) effect as well as albumin receptor binding, which is a unique advantage as the carrier for tumor-targeted drug delivery [145].

Albumin-binding ligands based on the lead structure 4-(*p*-iodophenyl)butyric acid (IPBA) have been identified by screening DNA-encoded chemical libraries [147]. The best derivative of IPBA, known as Albutag, was used to develop radiolabeled folate conjugates for imaging and therapy [148]. Albutag was also used to develop a novel class of trifunctional ligands, consisting of the high-affinity PSMA-binding domain, the Albutag, and the DOTA chelator, to facilitate the modification of the three moieties independently and ultimately enable the generation of spatial optimized conjugates PSMA conjugates for prostate cancer theranostics [149]. Preclinical studies demonstrated that the trifunctional ligands had high and persistent tumor uptake with absorbed doses that were four times greater than those observed for a similar compound lacking the albumin-binding moiety. It was also reported that the tumor uptake of the lead compound ^{177}Lu-RPS-077 continues to increase up to 24 h after injection and that the washout by 96 h was not significant. The tumor AUC and tumor-to-kidney ratio of ^{177}Lu-RPS-072 are significantly enhanced compared with any other small molecule investigated in a LNCaP xenograft model. Therefore ^{177}Lu-RPS-072 exhibits an increased therapeutic index, shows the potential to increase the dose delivered to tumors, and is a highly promising candidate for targeted radioligand therapy [149]. Albutag was also used to develop albumin-binding PSMA-targeting PET radioligands based on NODAGA chelator [150].

Recently, a new class of PSMA radioligands comprising ibuprofen as an albumin-binding entity was reported [151]. The isobutylphenyl propionic acid, known under the name "ibuprofen," is a nonsteroidal anti-inflammatory drug

(NSAID), which binds to plasma proteins. To develop radiometal-labeled PSMA inhibitors, several glutamate-urea-based PSMA ligands were synthesized with ibuprofen, conjugated via variable amino acid-based linker entities. The lead compound ^{177}Lu-Ibu-DAB-PSMA, in which ibuprofen was conjugated via a positively charged diaminobutyric acid (DAB) entity, showed distinguished tumor uptake and the most favorable tumor-to-blood and tumor-to-kidney ratios [151].

The benefit of an enhanced tumor uptake of long-circulating PSMA radioligands is, however, compromised by an increased retention of activity in healthy organs and tissues including the kidneys, and bone marrow, which may limit the number of therapy cycles that can be applied. Albumin-binding properties have, thus, to be carefully balanced to achieve an increased tumor uptake while keeping background activity as low as possible [152].

22.4.8 Bombesin and GRPR Analogs

A variety of radiolabeled GRPR agonists (such as ^{68}Ga/^{177}Lu-AMBA, ^{68}Ga/^{177}Lu-PESIN) have been developed for targeting GRPR-positive tumors and were evaluated in preclinical and clinical studies [49, 50, 153]. Several recent reports have shown that GRPR antagonists show properties superior to GRPR agonists, affording higher tumor uptake and lower accumulation in physiologic GRPR-positive nontarget tissues [154]. GRPR agonists activate the receptor and induce side effects. GRPR antagonists, however, are expected to have no adverse effects [49]. Several GRPR antagonists (such as ^{68}Ga-RM26, ^{68}Ga-RM2 (also referred to as ^{68}Ga-BAY86-7548), ^{64}Cu-CB-TE2A-AR06, ^{68}Ga-SB3) were evaluated in clinical studies to assess the potential clinical utility to detect primary prostate cancer lesions. The amino acid sequence of bombesin and analogs is shown in Fig. 22.9.

RM26 with high affinity was discovered by peptide backbone modification of bombesin analogs [155]. A pilot PET study with ^{68}Ga-NOTA-RM26 in 28 patients with newly diagnosed and post-therapy prostate cancer demonstrated that RM26 can detect both primary prostate cancer and metastases with high efficiency. There was a significant positive correlation between SUV derived from ^{68}Ga-RM26 PET and the expression level of GRPR [155]. Several pilot clinical studies with ^{68}Ga-RM2 (^{68}Ga-labeled DOTA-4-amino-1-carboxymethyl-piperidine-D-Phe-Gln-Trp-Ala-Val-Gly-His-Sta-Leu-NH$_2$) also showed GRPR-PET may have a potential clinical role in the molecular imaging and TRT of prostate cancer [156–158]. ^{68}Ga-RM2 has the highest physiologic uptake in the pancreas followed by moderate uptake of the tracer in the liver, spleen, and urinary excretion [159]. It has garnered interest as a target for prostate theranostics, especially, due to the lack of salivary gland uptake which is prominently seen in ^{68}Ga-PSMA-PET. A recent study examined the use of [^{68}Ga]RM2-PET/CT (GRPR antagonist) in patients with known biochemical recurrence of prostate cancer and negative or equivocal [^{18}F]fluoroethylcholine-PET/CT and demonstrated that [^{68}Ga] RM2-PET/CT was helpful in localizing the recurrence in such cases [157, 159]. Based on a direct comparison with [^{18}F]DCFPyl-PET (Fig. 22.26) it was concluded that ^{68}Ga-RM2 remains a valuable radiopharmaceutical even when compared with the more widely used ^{68}Ga-PSMA11/^{18}F-DCFPyL in the evaluation of biochemical recurrence of prostate cancer [160]. The first clinical data with ^{68}Ga-NeoBOMB1 in a group of prostate cancer patients highlighted its ability to visualize primary tumors, as well as liver metastases and bone lesions [161].

A recent review suggests that GRPR-targeted imaging may constitute a relevant addition for those patients with PSMA-negative tumors, or those with low-grade tumors that do not show on MRI nor PSMA-PET scans because retrospective studies have revealed that PSMA expression was inversely correlated with GRPR, underscoring the potential value of their combined use [153].
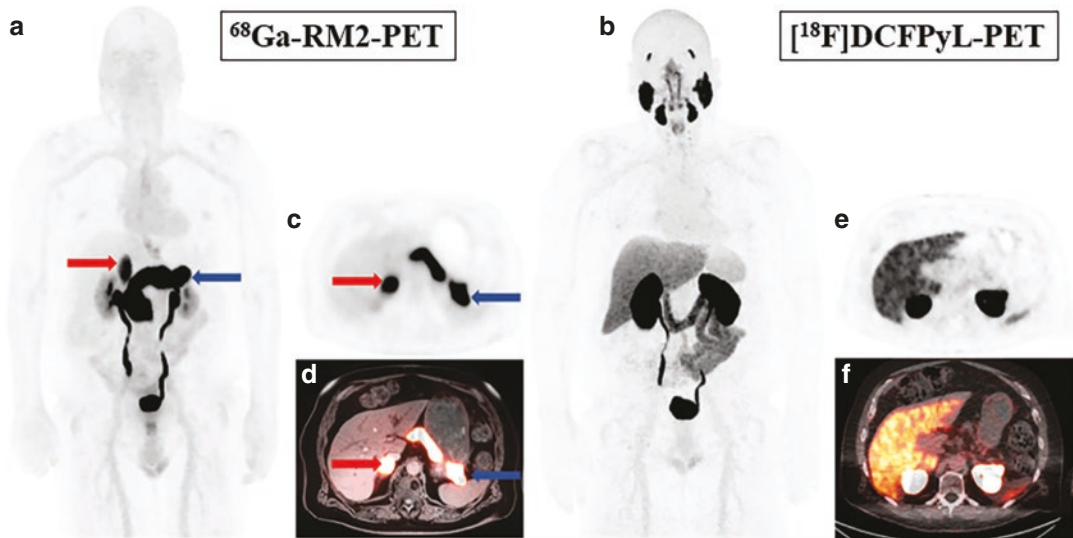
Fig. 22.26 Comparison of ^{68}Ga-RM2-PET (bombesin analog for GRPR) with PSMA ligand, [^{18}F]DCFPyL-PET in a patient presenting with prostate cancer biochemical recurrence (BCR) (PSA 11.6 ng/mL and PSA velocity 12.2 ng/mL/year). ^{68}Ga-RM2 scans (**a**, **c**, **d**) compared to [^{18}F]DCFPyL (**b**, **e**, **f**). Red arrows mark right adrenal lesion clearly seen on GRPR-PET but not prospectively identified on PSMA-PET given similar uptake in the adrenal gland and liver parenchyma. Blue arrows mark physiologic ^{68}Ga-RM2 uptake in the pancreas [160]

22.5   Radiopharmaceuticals for Bone Pain Palliation

As discussed in Sect. 22.2.1, bone is the most common and preferred site for metastatic involvement in prostate cancer. The presence of bone metastases implies poorer prognosis, shortens survival, and is associated with a multitude of complications, including severe bone pain, pathological fracture, spinal cord compression, hypercalcemia, etc. [19]. Bone metastases in prostate cancers are typically characterized by an osteoblastic picture due to excess bone deposition [19].

Several radiopharmaceuticals were developed based on β^- emitting radionuclides, as shown in Table 22.3 [21, 162, 163]. Studies in radiobiology indicate that radiation doses delivered to bone metastases at higher dose rates would have a higher RBE. Therefore, the advantage of shorter-lived radionuclides at higher dose rates in comparison with longer lived radionuclides at lower dose rates will also depend on biokinetics of the radiopharmaceutical and how the dose rate in target tissue compares to the dose rate in critical organs [163]. These radiopharmaceuticals can broadly be classified into two categories based on the mechanism by which they get accumulated in the skeleton: Ca^{2+} analogs and diphosphonate complexes of radiometals due to the affinity of phosphonates towards calcium in the actively growing bone.

^{32}P as sodium orthophosphate administered orally (444 MBq) or intravenously (185 MBq) was used for the treatment of metastatic bone pain till the 1980s. ^{32}P is bound to hydroxyapatite of the inorganic bone matrix. In spite of its efficacious nature, the use of this agent declined owing due to the high energy β^- particle emission, which causes severe bone marrow toxicity including myelosuppression and pancytopenia [162]. Moreover, because of the radionuclide being a pure β^- particle emitter, simultaneous pharmacokinetic evaluation and dosimetric assessment cannot be done.

22.5.1 ^{89}Sr Dichloride (Metastron®)

The first use of ^{89}Sr for bone pain palliation was reported in 1942 [164]. Since it is a Ca^{2+} analog, ^{89}Sr^{2+} cation is internalized to the inorganic bone

matrix and the biochemical uptake is in proportion to local osteoblastic activity, which is tenfold higher in metastatic lesions. After localization, it still remains in the tumoral sites for 100 days. The excretion occurs predominantly from kidneys, limiting its use in the setting of renal failure. The recommended dose is 150 MBq. Based on the latest meta-analysis, an overall response rate of 70% has been reported, commencing typically within 14–28 days of administration and lasting up to 15 months [21]. The efficacy of ^{89}Sr chloride in bone pain palliation has been compared to other radiopharmaceuticals (such as [153]Sm-EDTMP and [186/188]Re-HEDP) revealing no significant difference. The hematological toxicity (myelosuppression) is the major side effect which is due to high energy β^- particles and like ^{32}P, it cannot be used for simultaneous pharmacokinetic evaluation and dosimetry studies.

22.5.2 Bisphosphonates: [153]Sm-EDTMP (Quadramet®)

The first clinical use of bone pain palliation with [153]Sm was reported in 1989 [165]. It is used with the chelator ethylenediamine tetramethylenephosphonate ([153]Sm-EDTMP), which is supplied as [153]Sm-lexidronam-pentasodium (Quadramet) (Fig. 22.3) with a recommended activity of 37 MBq/kg body weight. It is a well-known radiopharmaceutical for bone pain palliation and since it received FDA approval, it has been widely used in various osteoblastic metastatic lesions, especially in prostate and breast cancer. It has shown high uptake in the skeleton with $62 \pm 13\%$ at 24 h post-injection [163]. It rapidly binds to hydroxyapatite crystals, leading to less than 1% availability in the blood 5 h after injection. No specific uptake has been observed outside the skeleton, and excretion occurs mainly through the kidneys. The pharmacokinetics of [153]Sm-EDTMP is favored over [186]Re-HEDP with lower urinary excretion and potentially higher bone and lesion uptake [163]. Pain palliation is usually experienced within 1 week and frequently within 48 h of administration of [153]Sm-EDTMP. The pain reduction occurs as early as in the first week after injection, lasting for about 2–3 months [21]. Compared to ^{89}Sr, the moderate energy β^- emission reduces the possibility of bone marrow ablation and the adequate γ-emission of suitable energy of photons (103 keV) helps biodistribution and dosimetry studies. Overall, [153]Sm–EDTMP has been successfully used for pain control for three decades. One of the major drawbacks, however, is its relatively shorter half-life (46.3 h) which causes significant loss of activity due to radioactive decay in shipment.

22.5.2.1 Investigational Agents

Several other radiolabeled diphosphonates have been investigated in small clinical studies. [186/188]Re-HEDP complex behaves similar to ^{99m}Tc bone agents. Approximately 40% is localized in the skeleton at 24 h but, significantly less uptake compared to [153]Sm-EDTA. Repeated doses of [188]Re–HEDP, compared to a single administration, have shown improvement in PFS and OS, as well as a reduction of PSA levels in approximately half of the patients. The apparent antitumoral effect may be explained by higher β^- energy and tissue penetration, as well as a higher dose rate of [188]Re–HEDP administration due to very short physical half-life of 0.7 days [163]. I[188]Re-HEDP has not been approved in many countries for clinical use and the number of prospective trials with large populations is limited. The potential advantages include the availability of a long-lived on-site generator ([188]W→[188]Re), favorable pain control, the potential impact on OS, and cost-effectiveness.

^{177}Lu-EDTMP and ^{177}Lu-DOTAZOL

[177]Lu has been proposed as a possible radionuclide for bone pain palliation. It has the theoretical advantage of reduced bone marrow toxicity due to low energy beta particle energy and mean tissue range of 0.2 mm. ^{177}Lu–EDTMP has been studied as a safe and effective potential palliative therapy in painful bone metastases, due to rapid skeletal accumulation and minimal uptake in other organs. ^{177}Lu–DOTMP has also been investigated revealing rather similar characteristics to ^{177}Lu–EDTMP. Yet, the latter exhibits slightly higher skeletal uptake as well as retention in the liver and kidneys

[21]. ^{177}Lu-EDTMP has been compared to [153]Sm-EDTMP. Reportedly, they both have subjected bone metastases to similar radiation doses. Likewise, the response rate of approximately 75–80% has been noted for both radiopharmaceuticals. In addition, the cocktail of both these agents has shown safety in administration and pain relief/reduction in 24/25 patients [21]. [177]Lu labeled with zoledronic acid (^{177}Lu-DOTA[ZOL]) (Fig. 22.3) is another investigational radiopharmaceutical with promising preliminary biodistribution and post-therapy dosimetry results. It also possesses a potential theragnostic application (using ^{68}Ga-DOTAZOL-PET) for the treatment of bone metastases [59, 60]. A recommended therapeutic activity was described with 45 MBq/kg for ^{177}Lu-EDTMP and higher activity of 5780 MBq for ^{177}Lu-DOTA[ZOL]. A systematic review and meta-analysis conclude that ^{177}Lu-EDTMP seems to have a comparable efficacy and safety profile as that of the frequently administered radiopharmaceuticals for bone palliation [166].

## 22.6   Radiopharmaceuticals for Targeted Therapy

22.6.1   [223]Ra Dichloride (Xofigo)

[223]Ra ($T_{1/2}$ = 11.4 days) decays to stable [207]Pb with five intermediate radionuclide progenies and a total of five α particles (Fig. 22.27). Currently, the clinical and commercial production of [223]RaCl$_2$ (Bayer Health Care Pharmaceuticals) involves [227]Ac and [227]Th isolation from a [231]Pa source (3.28×10^4 year) [167]. In 2013, [[223]Ra]radium dichloride (Xofigo®; formerly alpharadin) became the first and only alpha-emitting radiopharmaceutical to receive FDA and EMEA approval for clinical use, with an intended purpose to treat patients with CRPC, symptomatic bone metastases, and no known visceral metastatic disease. [223]Ra[2+] mimics calcium and forms complexes with the bone mineral hydroxyapatite at areas of increased bone turnover, such as bone metastases. The high LET (80 keV/μm) leads to a high frequency of DSDBs in adjacent cells, resulting in an antitumor effect on bone metastases. As shown in Table 22.5, the dose to metastatic lesions is around 25 Gy from one cycle of [223]Ra administration and is comparable to the dose from radiopharmaceuticals for bone pain palliation. The RBE effect, however, will be significantly higher compared to the beta emitters.

[223]Ra dichloride injection is supplied as a single-use vial at a concentration of 1000 kBq/mL (27 microcurie/mL) at the reference date with a total radioactivity of 6000 kBq/vial (162 microcurie/vial) at the reference date. The recommended dose regimen of Xofigo is 50 kBq (1.35 microcurie) per kg body weight, given at 4-week intervals for six injections.

After intravenous injection, radium-223 is rapidly cleared from the blood and is distributed primarily into bone or is excreted into the intestine. At 4 h, about 4% of the injected radioactivity remained in blood, decreasing to <1% at 24 h after the injection. At 10 min post-injection, radioactivity was observed in bone and in the intestine. At 4 h, the bone uptake was 61% of the
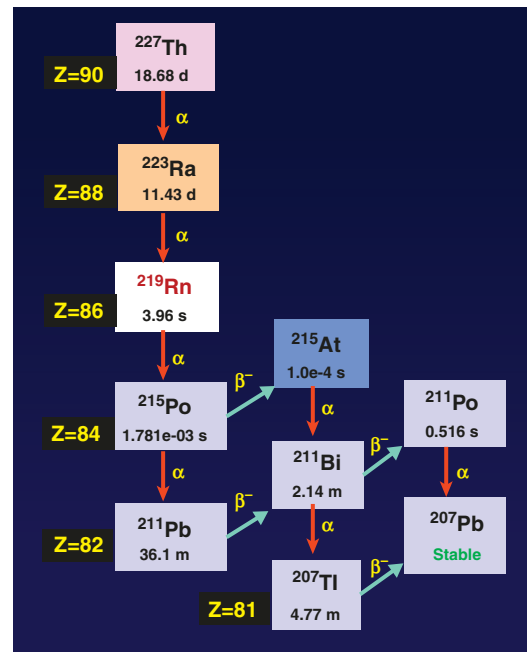
Fig. 22.27 Radium-223 is the daughter of Thorium-227. The decay scheme of Ra-223 shows both alpha and beta particle emissions before it reaches stable Pb-207

Table 22.5 Dosimetry[a] of radiopharmaceuticals for bone pain palliation

Radiopharmaceuticals	$T_{1/2}$ (Days)	B_{Emax} (MeV)	γ-Photons (keV)	Range (mm) Max	Range (mm) Mean	Dose (mMq)	Red marrow dose (mGy/ MBq)	Bone Mets. (Gy)
[^{32}P]sodium orthophosphate	14.26	1.71		8.1	2.5	444	6.5	
^{89}Sr-dichloride	50.53	1.46	910 (0.01%)	6.6	1.9	150	19.0	0.03–50.0
^{153}Sm-EDTMP (*Quadramet*)	1.9292	0.81	103 (28%)	3.0	0.4	37/kg	0.89 ± 0.03	2.9–14.1
^{186}Re-HEDP	3.78	1.07	135 (9%)	4.5	0.8	1285	0.8	40.1
^{188}Re-HEDP	0.71	2.12	155 (15%)	10.45	2.8	~3000	0.61 ± 0.21	12.6 ± 6.6
^{177}Lu-EDTMP	6.71	0.49	113 (6%)	1.5	0.2	45/kg	0.80 ± 0.15	
^{177}Lu-DOTA^{ZOL}			208 (11%)			5780	0.36 ± 0.12	4.21 ± 2.4
^{223}Ra dichloride[b]	11.4	5–7.5 MeV α		<0.1 mm		0.05/kg	139.0	25.6

[a] Dosimetry values from Liepe et al. [163]

[b] The dosimetry data for ^{223}Ra is from Xofigo package insert

administered activity. Approximately 63% of the administered radioactivity was excreted from the body within 7 days after injection (after correcting for decay). Fecal excretion is the major route of elimination from the body (Xofigo-2013 PI).

The efficacy and safety of Xofigo were evaluated in a double-blind, randomized, placebo-controlled phase 3 clinical trial of patients with CRPC with symptomatic bone metastases. Patients receiving the treatment with ^{223}Ra exhibited a 3.6-month prolonged survival time (PST) over the placebo group and a 5.8 month improved timeframe before the occurrence of a systematic skeletal-related event with a reduction of occurrence of spinal compression [168, 169].

22.6.2 RIT with ^{177}Lu- or ^{225}Ac-Labeled J591 mAb

As discussed in Sect. 22.4.6.2, the clinical trials with ^{90}Y- or ^{177}Lu-labeled huJ591 mAbs started 20 years ago at Weill Cornell Medicine in New York. Two independent RIT phase I trials have been performed using ^{90}Y- or ^{177}Lu-labeled DOTA-huJ591 in patients with mCRPC [101, 170, 171]. All patients received a total of 20 mg of J591 mAb containing both radiolabeled DOTA-J591 and naked J591 mAb. These trials defined the maximum tolerated dose (MTD),

dosimetry, pharmacokinetics, and human anti-humanized antibody (HAHA) response, and demonstrated preliminary evidence of antitumor activity. With ^{90}Y, 0.647 GBq/m^2 dose level was determined to be the MTD. With ^{177}Lu, 2.59 GBq/m^2 dose level was determined to be the MTD. ^{177}Lu was chosen for further development based upon its physical properties, especially since the low energy beta particles deliver a lower radiation dose to bone marrow relative to the higher energy beta particles from ^{90}Y [102–104].

22.6.2.1 RIT with ^{177}Lu-DOTA-huJ591 mAb

In a dual-center phase II study, two cohorts of patients (total $n = 47$) with progressive mCRP received one dose of ^{177}Lu-J591 (2.405 GBq/m^2, or 2.59 GBq/m^2). Sites of prostate cancer metastases were targeted in 94% of patients as determined by planar imaging. All patients experienced reversible hematologic toxicity with grade 4 thrombocytopenia occurring in 47% of patients. In atients ($n = 32$) who received a single dose of 2.59 GBq/m^2, >30% PSA decline was observed in 47% of patients, and longer survival of 21.8 months [137, 138]. The safety and efficacy data of phase II study are summarized in Table 22.6.

Dose fractionation is a practical strategy to decrease the dose to bone marrow while increasing the cumulative radiation dose to the tumor at

an optimal dose rate [102–104, 174]. A phase I/II clinical study with a phase I dose escalation component followed by phase IIa dosing was performed using two dosing cohorts selected for exploration (2.96 GBq and 3.33 GBq/m² total dose divided into two doses 2 weeks apart). As demonstrated before, there appeared to be a dose-dependent response for PSA decline and overall survival. At the highest cumulative dose (3.33 GBQ/m²), 35% of patients had reversible grade 4 neutropenia, and 58.8% of patients had thrombocytopenia. This dose showed a greater PSA decline with a median survival of 3.5 years [175, 176]. The safety and efficacy data are given in Table 22.6. In addition, those with lower PSMA uptake on ^{177}Lu SPECT had lower likelihood of significant PSA decline.

In order to evaluate the value of combination therapy, a phase 1 clinical study tested the therapeutic value of combination of docetaxel chemotherapy with fractionated dose ^{177}Lu-J591 mAb therapy [177]. In a pilot study 15 patients with mCRPC received standard docetaxel (75 mg/m²) in 21-day cycles, with cohorts receiving escalating fractionated doses of ^{177}Lu-J591 during cycle 3 (highest planned total dose 80 mCi/m²). This study demonstrated the safety of the combination with early evidence of activity, with 73% achieving >50% PSA decline. Toxicities were comparable to prior ^{177}Lu-J591 studies [177]. Although 2-dose fractionation appears attractive alone or with docetaxel a pilot study explored the value of "hyper-fractionated" ^{177}Lu-J591 in which low-dose ^{177}Lu-J591 (25 mCi/m²) was administered every 2 weeks until greater than grade 2 toxicity

emerged [178]. As designed, dosing was limited by myelosuppression (especially thrombocytopenia) but, the regimen did not appear more favorable than 2-dose fractionation and is also less convenient for patients, so the regimen is not being further explored.

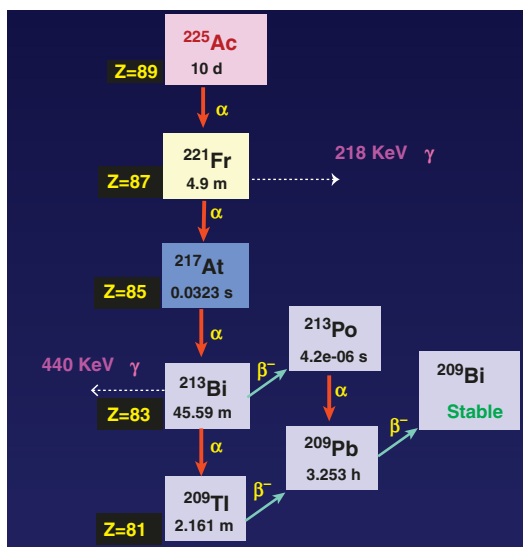### 22.6.2.2 RIT with [225]Ac-DOTA-huJ591 mAb

Twenty years ago, [213]Bi-J591 was proposed as a radiopharmaceutical for α-particle therapy of prostate cancer [179]. While [213]Bi demonstrated promising efficacy in the preclinical setting, it is not an appropriate radionuclide for whole IgG mAb with a longer circulation time. An alternative to [213]Bi was to utilize its parent nuclide, [225]Ac, which has a 10-day half-life and 5 net α particles and 3 beta particles per decay (Fig. 22.28). Also, as a trivalent metal, [225]Ac binds to the same DOTA chelator like [177]Lu.

Based on human biodistribution data, and assuming RBE for alpha emitters is 5, the radiation dosimetry calculations suggested that administration of 6.06 MBq (164μCi) of [225]Ac-J591 mAb may deliver ~2.0 Gy to bone marrow. A phase I dose escalation study was designed to determine the dose-limiting toxicity (DLT) and the maximum tolerated dose (MTD) of [225]Ac-J591 in a single dose regimen [180, 181]. Patients received doses starting from 13.3 kBq/kg to a maximum of 93.3 kBq/kg (for an average person of 75 kg, the maximum dose administered is 7 MBq). Thirty-two patients with progressive mCRPC were treated with [225]Ac-J591 in this protocol. In the dose escalation phase of the study,

Table 22.6 Safety and Efficacy of RIT in mCRP with ^{177}Lu-huJ591: PSA decline and toxicity

Response	Single dose		Cumulative dose given in two doses		
	2.405 GBq/m²	2.59 GBq/m²	1.48–2.59 GBq/m²	2.96 GBq/m²	3.33 GBq/m²
Number of patients (*n*)	15	32	16	16	17
Any PSA decline (%)	46.7	65.6	37.5	50.0	87.5
>30% PSA decline (%)	13.3	46.9	12.5	25.0	58.8
>50% PSA decline (%)	6.7	12.5	6.3	12.5	29.4
Median survival (months)	*11.9*	*21.8*	*14.6*	*19.6*	*42.3*
Platelets grade-4	27.0	56.3	20.0	43.8	58.8
Platelet transfusion	7.0	41.0	0.0	31.3	52.9
Neutropenia grade-4	0.0	37.5	0.0	31.3	29.4
Febrile neutropenia	0.0	2.1	0.0	0.0	5.8

there was one patient who had grade 4 thrombocytopenia and anemia. However, there was no MTD, and the recommended phase 2 dose of the compound is 93.3 kBq/kg. Overall, 68.8% of patients had at least some level of PSA decline

and 43.8% had a PSA decline of over 50%. The median biochemical progression-free survival in the entire population was 5.1 months and the median overall survival was 11.1 months. There were no cases of severe xerostomia. The study concluded that PSMA targeting with ^{225}Ac-J591 mAb is tolerable with early evidence of clinical activity (Fig. 22.29) in a pretreated population with favorable patient-reported outcomes. Studies administering multiple or subsequent doses and/or combination therapy are underway.


Fig. 22.28 The decay scheme of Ac-225 shows both alpha and beta particle emissions before it reaches stable Bi-209. The gamma photons for the daughters Fr-221 and Bi-213 are used to identify Ac-225 when the parent and daughters are in secular equilibrium

22.6.3 Small-Molecule PSMA Inhibitors

22.6.3.1 Lu 177 Vipivotide Tetraxetan (Pluvicto, ^{177}Lu-PSMA-617)

As discussed in Sect. 22.4.7.3, the design and synthesis of PSMA-617 was reported in 2015 by the Heidelberg group. Based on ^{68}Ga-PSMA-617 PET scan, they demonstrated the PSMA targeting potential of PSMA-617 [136]. The first clinical experience with ^{177}Lu-PSMA-617 targeted therapy in patients with advanced mCRPC resistant to or with contraindications to other conventional therapies and PSMA-positive tumor phenotypes demonstrated that ^{177}Lu-PSMA-617
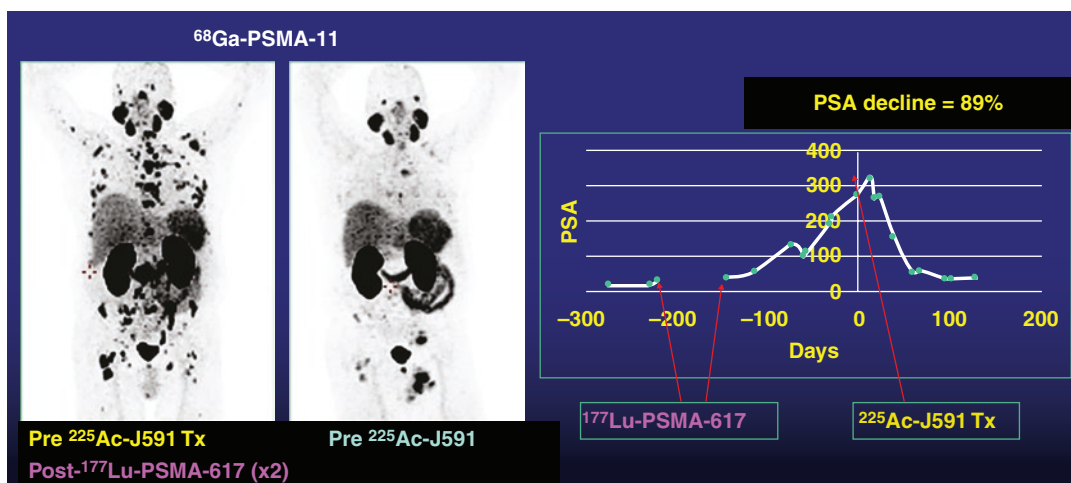
Fig. 22.29 ^{225}Ac-J591 mAb targeted therapy in a patient with mCRPC. The patient had prior treatment with 2 cycles of ^{177}Lu-PSMA-617 and when the disease was progressive received 4 MBq of 225Ac-J591. 68Ga-PSMA PET

scans before and after treatment show evidence of treatment response. The patient also had 86% decline in PSA level. (Images provided by Dr. Tagawa at Weill Cornell Medicine, NY)
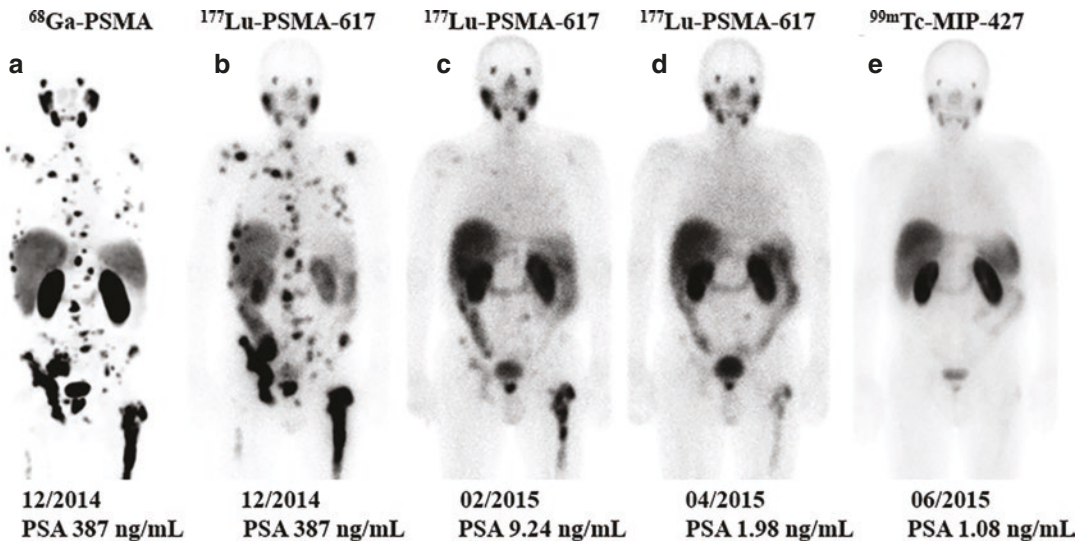
Fig. 22.30 ^{177}Lu-PSMA-617 therapy in a patient with PSMA-positive mCRPC (6 GBq/cycle, 3 cycles 2 months apart). Scan (**a**) represents 68Ga-PSMA-PET; scans (**b–d**) represent planar images after ^{177}Lu therapy dose. Scan (**e**) represents planar image with ^{99m}Tc-PSMA tracer. Scans (**c–e**) show good response to ^{177}Lu-PSMA-617 therapy [182, 183]

is a promising new option for therapy of mCRPC (Fig. 22.30) [182, 183]. Thirty patients received 1–3 cycles of ^{177}Lu-PSMA-617 (4 or 6 GBq/cycle). Dosimetry studies revealed kidney doses (~0.75 Gy/GBq), red marrow doses (0.03 Gy/GBq), and salivary gland doses (1.4 Gy/GBq), irrespective of tumor burden and consistent on subsequent cycles. Mean tumor-absorbed dose ranged from 6 to 22 Gy/GBq during the first cycle.

To assess the benefit of higher ^{177}Lu dose rate on the safety, a phase 1/II dose escalation study of fractionated dose of ^{177}Lu-PSMA-617 for progressive mCRPC was conducted at Weill Cornell Medicine in New York. Patients received two doses of ^{177}Lu-PSMA-617 in a cycle (cumulative dose of 7.4–22 GBq), 2 weeks apart. The study concluded that a single fractionated cycle of up to 22.2 GBq of ^{177}Lu-PSMA-617 is safe, with encouraging early efficacy signals, even without selection for PSMA expression by imaging. A trend for dose-response was observed [175, 176].

A single-arm, single-center phase 2 trial was performed in patients with mCRPC who progressed after standard treatments [184]. Fifty eligible patients received 7.5 GBq/cycle, 4 cycles at six weekly intervals. The study concluded that treatment with [^{177}Lu]-PSMA-617 has high response rates, low toxic effects, and reduction of pain in men with mCRPC who have progressed after conventional treatments. A randomized, multicenter open label phase 2 trial (TheraP trial) compared the efficacy of ^{177}Lu-PSMA-617 with cabazitaxel in patients with mCRPC [185]. The study results showed that ^{177}Lu-PSMA-617 treatment compared to cabazitaxel led to a higher PSA response and fewer grade 3 or 4 adverse events.

The VISION trial (Funded by Endocyte, a Novartis company) evaluated the advantages of ^{177}Lu-PSMA-617 over best supportive care in improving the overall survival (OS) and image-based progression-free survival (PFS) in patients with progressive mCRPC [186, 187]. Five hundred and fifty-one patients were allotted to the ^{177}Lu-PSMA-617 group (who received 7.4 GBq of ^{177}Lu-PSMA-617 every 6 weeks in 4–6 cycles), while 280 patients were in the standard of care (SOC) group. The results of the study report that the median PFS was significantly longer among patients in the ^{177}Lu-PSMA-617 arm at 8.7 months compared with 3.4 months in patients in the SOC-

alone arm. There was a significant improvement in the OS in the patients who received ^{177}Lu-PSMA-617 compared to standard care alone (15.3 months vs. 11.3 months). Around 46% (vs. 7.1% in control group) of the patients had >50% reduction and >33% (vs. 2% in control group) patients had >80% reduction in the PSA levels (SOC). The FDA granted priority review to NDA for ^{177}Lu-PSMA-617 to treat patients with metastatic castration-resistant prostate cancer (mCRPC) who have previously received androgen receptor pathway and taxane-based chemotherapy.

In March 2022, the US FDA approved Lu 177 vipivotide tetraxetan for the treatment of patients with metastatic castration-resistant prostate cancer in the post-androgen receptor pathway inhibition, post-taxane-based chemotherapy setting.

22.6.3.2 ^{177}Lu-PSMA-I&T

As discussed in Sect. 22.4.7.3, PSMA-I&T was developed using DOTAGA chelator to facilitate labeling with ^{68}Ga or [177]Lu. Compared to DOTA, the DOTAGA chelator has one extra carboxylic acid group which improves the stability of the radiometal complex. Several clinical studies quickly demonstrated the therapeutic potential of ^{177}Lu-PSMA-I&T [188–190]. Subsequently, ^{177}Lu-PSMA-I&T was evaluated in PSMA-positive patients with mCRPC under a compassionate use protocol [191]. One hundred patients received ^{177}Lu dose (7.4 GBq/cycle) every 6–8 weeks up to six cycles. PSA decline of ≥50% was achieved in 38 patients, median clinical PFS was 4.1 months, and median OS was 12.9 months.

A phase III, Open-Label, randomized study evaluating mCRPC treatment using ^{177}Lu-PSMA-I&T (also known as [Lu-177]-PNT2002) was performed after second-line hormonal treatment (SPLASH) (NCT04647526) (sponsored by Point Biopharma). The primary objective of the study is to determine the efficacy of ^{177}Lu therapy vs. abiraterone or enzalutamide in delaying radiographic progression in patients with mCRPC. PSMA-positive patients ($n = 390$) will be randomized in a 2:1 ratio to receive either PNT2002 (Arm A), or enzalutamide or abiraterone (Arm B). All patients will be followed long-term for at least 5 years following the first therapeutic dose.

22.6.3.3 Dosimetry of ^{177}Lu-PSMA Ligands

Several studies reported radiation dosimetry results of ^{177}Lu-PSMA therapy with favorable outcomes [192]. Table 22.7 shows a summary of absorbed doses to several organs and tissues based on published data for both PSMA-617 and PSMA-I&T ligands. The studies used different dosimetry methods (whole body vs. SPECT/CT; MIRD (medical internal radiation dose) vs. voxel-based dosimetry) or molecules (PSMA-617 vs. I&T), which made the results heterogeneous. The usage of whole-body imaging for dosimetry could cause the overestimation of the absorbed organ doses, while studies based on SPECT/CT reported lower doses [192]. Based on the dosimetry data, the minimum and maximum organ doses from six cycles of [177]Lu (7.4 GBq/cycle) were estimated as shown in Table 22.7. Lacrimal glands may receive a minimum of 124 Gy and the general accepted limit is 40 Gy for lacrimal glands.

Table 22.7 Absorbed dose estimates for ^{177}Lu-labeled PSMA-617 and PSMA-I&T ligands

Organ/tissue	Absorbed radiation dose		Threshold dose[a] (Gy)
	Gy/GBq	Gy/44.4 GBq[b]	
Lacrimal glands	2.80–3.8	124–167	34
Salivary glands	0.44–1.4	19–62	20
Kidney	0.39–0.99	17–44	23
Liver	0.10–0.36	4.4–16	32
Spleen	0.06–0.10	2.6–4.4	
Bone marrow	0.002–0.11	0.09–4.8	2.0
Tumor	3.2–13.1	141–576	

[a] Current thresholds of absorbed organ doses were defined based on external beam radiotherapy (EBRT) literature
[b] The absorbed doses to several organs is from Sanli et al. [192]

22.6.3.4 ^{225}Ac-PSMA-617 and ^{225}Ac-PSMA-I&T

In order to increase DNA damage, the investigators from Heidelberg introduced ^{225}Ac-PSMA-617 for α-particle therapy with substantial therapeutic efficacy which has the potential to overcome resistance to therapy based on β^- emitting nuclides [182, 183, 193–196]]. In a preliminary study, in which patients with mCRPC were treated with ~8 MBq (0.1 MBq/kg) every 2 months showed highly promising results (Fig. 22.31), with a PSA decline of at least 50% in 63% of patients and any PSA response in 87% of patients. The median duration of tumor control was 9.0 months and 5 patients (13%) had enduring responses of >2 year following complete remission of PSA. Some of the patients experienced hematological grade 3/4 toxicities, while all patients experienced at least grade 1–2 xerostomia [193] Another study in chemotherapy-naïve mCRPC patients ($n = 17$) reported an overall PSA decline of at least 50% in 88% of patients, while maintaining low toxicity [195].

The first clinical results for PSMA-targeted α-therapy using ^{225}Ac-PSMA-I&T in advanced mCRPC patients ($n = 14$) showed a promising antitumor effect, highly comparable to the data with ^{225}Ac-PSMA-617 therapy [197]. In 14 patients, ^{225}Ac-PSMA-I&T dose (6–8.5 MBq) was given in 1–5 cycles and a total of 34 cycles was given. PSA decline of >50% was observed in 50% of patients and any PSA decline was observed in 78% of patients.

The limited clinical data with ^{225}Ac-labeled PSMA inhibitors indicate that alpha therapy of mCRPC is promising and that several potential clinical situations in early- and end-stage disease could potentially benefit from ^{225}Ac therapy. Further evaluation and clinical study design strategies, however, need to be optimized to minimize toxicity and improve efficacy.

22.7   Combination Therapy

A combination therapy strategy employing two or more distinct therapeutic approaches in cancer management is aimed at circumventing tumor
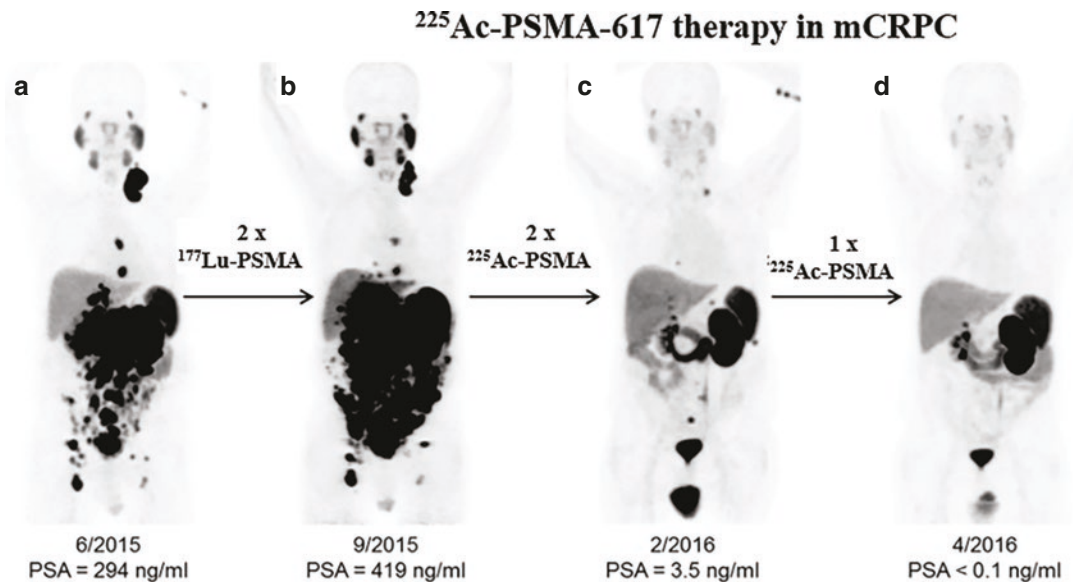
Fig. 22.31 ^{225}Ac-PSMA-617 therapy in a patient presented with peritoneal carcinomatosis and liver metastases that were progressive under ^{177}Lu-PSMA-617 therapy. The patient received 3 cycles of 6.4 MBq (100 kBq per kilogram of body weight) at bimonthly intervals. ^{68}Ga-PSMA-PET scans before (**a**, **b**) and after ^{225}Ac treatment (**c**, **d**) showed impressive response [182, 183]

resistance by simultaneously targeting compensatory signaling pathways or bypassing survival selection mutations acquired in response to individual monotherapies. Combination radionuclide therapy (CRT) is a newer application of the concept, utilizing a combination of radiolabeled molecular targeting agents with chemotherapy and beam radiation therapy for enhanced therapeutic index [198, 199].

The clinical studies based on PSMA-targeted radionuclide therapy based on both β^- and α emitting radionuclides have clearly documented that ~30% of patients, especially with bone metastasis, do not respond at all or develop resistance to TRT. The potential benefits of combining β^- and α emitting PSMA-targeted radiopharmaceuticals (also called tandem TRT) or combining targeted radiopharmaceuticals with chemotherapy or immunotherapy need to be explored to improve the efficacy of TRT and at the same time reducing the toxicity to normal organs.

The DLT with RIT is hematologic toxicity but, with small-molecule PSMA inhibitors, and the DLT is due to the absorbed dose to lacrimal glands and parotids. Combination of radiolabeled antibodies and peptides may be a practical strategy to enhance the tumor dose and reduce toxicity to normal organs. At Weill Cornell Medicine in New York, the combination of ^{225}Ac-J591 mAb with ^{177}Lu-PSMA-I&T is currently studied in a phase I/II protocol in patients with progressive mCRPC (NCT04886986). The two primary objectives of this trial are to determine the highest dose (MTD) of ^{225}Ac-J591 and ^{177}Lu-PSMA-I&T that can be administered together and to determine the effectiveness of the drug combination. The phase I component is a 3 + 3 dose escalation design, with maximum two cohorts. ^{177}Lu-PSMA-I&T will be given at a fixed dose of 6.8 GBq. ^{225}Ac-J591 will be given starting at 30 kBq/kg, with a subsequent dose escalation by an increment of 10–40 kBq/kg. The two drugs will be administered every 8 weeks, for two cycles. Once the maximum tolerated dose has been established, the phase II component of the trial will enroll up to 24 patients.

References

1. Siegel RL, Miller KD, Jemal A. Cancer statistics, 2021. CA Cancer J Clin. 2021;71:7–33.
2. Lilja H, Ulmert D, Vickers AJ. Prostate-specific antigen and prostate cancer: prediction, detection and monitoring. Nat Rev Cancer. 2008;8:268–78.
3. Logothetis C, Morris MJ, Den R, Coleman RE. Current perspectives on bone metastases in castrate-resistant prostate cancer. Cancer Metastasis Rev. 2018;37:189–96.
4. Augello MA, Den RB, Knudsen KE. AR function in promoting metastatic prostate cancer. Cancer Metastasis Rev. 2014;33:399–411.
5. Carver BS. Strategies for targeting the androgen receptor axis in prostate cancer. Drug Discov Today. 2014;19:1493–7.
6. Abou D, Benabdallah N, Jiang W, et al. Prostate cancer theranostics – an overview. Front Oncol. 2020;10:884.
7. Litwin MS, Tan H-J. The diagnosis and treatment of prostate cancer, a review. JAMA. 2017;317(24):2532–42.
8. Nuhn P, De Bono JS, Fizazi K, et al. Update on systemic prostate cancer therapies: management of metastatic castration-resistant prostate cancer in the era of precision oncology. Eur Urol. 2019;75:88–99.
9. Boettcher AN, Usman A, Morgans A, et al. Past, current, and future of immunotherapies for prostate cancer. Front Oncol. 2019;9:884.
10. Cattrini C, Castro E, Lozano R, et al. Current treatment options for metastatic hormone-sensitive prostate cancer. Cancers. 2019;11:1355.
11. Moreira DM, Howard LE, Sourbeer KN, et al. Predicting time from metastasis to overall survival in castration-resistant prostate cancer: results from SEARCH. Clin Genitourin Cancer. 2016;15:60–66. e2.
12. Czerwinska M, Bilewicz A, Kruszewski M, et al. Targeted radionuclide therapy of prostate cancer—from basic research to clinical perspectives. Molecules. 2020;25:1743–75.
13. Neels OC, Kopka K, Liolios C, Afshar-Oromieh A. Radiolabeled PSMA inhibitors. Cancers. 2021;2021(13):6255.
14. Piron S, Verhoeven J, Vanhove C, et al. Recent advancements in [^{18}F]F-labeled PSMA targeting PET radiopharmaceuticals. Nucl Med Biol. 2022;106–107:29–51.
15. Sandhu S, Guo C, Hofman MS. Radionuclide therapy in prostate cancer: from standalone to combination PSMA theranostics. J Nucl Med. 2021;62:1660.
16. Savit-Baruch B, Werner RA, Towe SP, Schuster DM. PET imaging for prostate cancer. Radiol Clin N Am. 2021;59(5):801–11.
17. Vallabhajosula S, Polack BD, Babich JW. Molecular imaging of prostate cancer: radiopharmaceuticals for positron emission tomography (PET) and single-

photon emission computed tomography (SPECT). In: Precision molecular pathology of prostate cancer. Berlin: Springer; 2018. p. 475–501.

18. Zhang H, Koumna S, Pouliot F, Beauregard JM, Kolinsky M. PSMA theranostics: current landscape and future outlook. Cancers. 2021;13:23.

19. Handkiewicz-Junak D, Poeppel TD, Bodei L, et al. EANM guidelines for radionuclide therapy of bone metastases with beta-emitting radionuclides. Eur J Nucl Med Mol Imaging. 2018;45:846–59.

20. Pandit-Taskar N, Batraki M, Divgi CR. Radiopharmaceutical therapy for palliation of bone pain from osseous metastases. J Nucl Med. 2004;45:1358–65.

21. Manafi-Farid R, Masoumi F, Divband G, et al. Targeted palliative radionuclide therapy for metastatic bone pain. J Clin Med. 2020;9:2622. https://doi.org/10.3390/jcm9082622.

22. Messner EA, Steele TM, Tsamouri MM, et al. The androgen receptor in prostate cancer: effect of structure, ligands and spliced variants on therapy. Biomedicine. 2020;8:422.

23. Shafi AA, Yen AE, Weigel NL. Androgen receptors in hormone-dependent and castration-resistant prostate cancer. Pharmacol Ther. 2013;140:223–38.

24. Fox JJ, Gavane SC, Blanc-Autran E, et al. Positron emission tomography/computed tomography–based assessments of androgen receptor expression and glycolytic activity as a prognostic biomarker for metastatic castration-resistant prostate cancer. JAMA Oncol. 2018;4(2):217–24.

25. Larimer BM, Dubois F, Bloch E, et al. Specific 18F-FDHT accumulation in human prostate cancer xenograft murine models is facilitated by prebinding to sex hormone-binding globulin. J Nucl Med. 2018;59:1538–43.

26. Larson SM, Morris M, Gunther I, et al. Tumor localization of 16beta-18F-fluoro-5alpha-dihydrotestosterone versus 18F-FDG in patients with progressive, metastatic prostate cancer. J Nucl Med. 2004;45(3):366–73.

27. Boers J, Venema CM, de Vries EFJ, et al. Serial [18F]-FDHT-PET to predict bicalutamide efficacy in patients with androgen receptor positive metastatic breast cancer. Eur J Cancer. 2021;144:151–61.

28. Katzenellenbogen JA. PET imaging agents (FES, FFNP, and FDHT) for estrogen, androgen, and progesterone receptors to improve management of breast and prostate cancers by functional imaging. Cancers. 2021;12:2020. https://doi.org/10.3390/cancers12082020.

29. O'Keefe DS, Su SL, Bacich DJ, et al. Mapping, genomic organization and promoter analysis of the human prostate-specific membrane antigen gene. Biochim Biophys Acta. 1998;1443:113–27.

30. Evans JC, Malhotra M, Cryan JF, O'Driscoll CM. The therapeutic and diagnostic potential of the prostate specific membrane antigen/glutamate carboxypeptidase II(PSMA/GCPII) in cancer and neurological disease. Br J Pharmacol. 2016;2016:1733041–307.

31. Bařinka C, Rojas C, Slusher B, Pomper M. Glutamate carboxypeptidase II in diagnosis and treatment of neurologic disorders and prostate cancer. Curr Med Chem. 2012;19:856.

32. Israeli RS, Powell CT, Fair WR, Heston WD. Molecular cloning of a complementary DNA encoding a prostate specific membrane antigen. Cancer Res. 1993;53:227–30.

33. Evans MJ, Smith-Jones PM, Wongvipat J, et al. Noninvasive measurement of androgen receptor signaling with a positron-emitting radiopharmaceutical that targets prostate-specific membrane antigen. Proc Natl Acad Sci U S A. 2011;108:9578–82.

34. Wright GL, Grob BM, Haley C, et al. Upregulation of prostate-specific membrane antigen after androgen-deprivation therapy. Urology. 1996;48:326–34.

35. Horoszewicz JS, Kawinski E, Murphy GP. Monoclonal antibodies to a new antigenic marker in epithelial prostatic cells and serum of prostatic cancer patients. Anticancer Res. 1987;7:927–35.

36. Israeli RS, Powell CT, Corr JG, Fair WR, Heston WD. Expression of the prostate-specific membrane antigen. Cancer Res. 1994;54:1807–11.

37. Wright GL Jr, Haley C, Beckett ML, Schellhammer PF. Expression of prostate-specific membrane antigen (PSMA) in normal, benign and malignant prostate tissues. Urol Oncol. 1995;1:18–28.

38. Wright GL, Grob B, Haley C, et al. Upregulation of prostate-specific membrane antigen after androgen-deprivation therapy. Urology. 1998;48:326–34.

39. Troyer JK, Beckett ML, Wright GL. Location of prostate-specific membrane antigen in the LNCaP prostate carcinoma cell line. Prostate. 1997;1997(30):232–42.

40. Liu H, Rajasekaran AK, Moy P, et al. Constitutive and antibody-induced internalization of prostate-specific membrane antigen. Cancer Res. 1998;58:4055–60.

41. Liu H, Moy P, Kim S, et al. Monoclonal antibodies to the extracellular domain of prostate-specific membrane antigen also react with tumor vascular endothelium. Cancer Res. 1997;57:3629–34.

42. Smith-Jones PM, Vallabahajosula S, Goldsmith SJ, et al. In vitro characterization of radiolabeled monoclonal antibodies specific for the extracellular domain of prostate-specific membrane antigen. Cancer Res. 2000;60:5237–43.

43. Pastorino S, Riondato M, Uccelli L, et al. Toward the discovery and development of PSMA targeted inhibitors for nuclear medicine applications. Curr Radiopharm. 2020;13:63–79.

44. Kozikowski AP, Nan F, Conti P, et al. Design of remarkably simple, yet potent urea-based inhibitors of glutamate carboxypeptidase II (NAALADase). J Med Chem. 2001;44:298–301.

45. Schroeder RPJ, van Weerden WM, Krenning EP, et al. Gastrin-releasing peptide receptor-based targeting

using bombesin analogues is superior to metabolism-based targeting using choline for in vivo imaging of human prostate cancer xenografts. Eur J Nucl Med Mol Imaging. 2011;38:1257–66.

46. Körner M, Waser B, Rehmann R, Reubi JC. Early over-expression of GRP receptors in prostatic carcinogenesis. Prostate. 2014;74:217–24.

47. Ischia J, Patel O, Bolton D, Shulkes A, Baldwin GS. Expression and function of gastrin-releasing peptide (GRP) in normal and cancerous urological tissues. BJU Int. 2014;113:40–7.

48. Aprikian AG, Tremblay L, Han K, Chevalier S. Bombesin stimulates the motility of human prostate-carcinoma cells through tyrosine phosphorylation of focal adhesion kinase and of integrin-associated proteins. Int J Cancer. 1997;72:498–504.

49. Baratto L, Jadvar H, Iagaru A. Prostate cancer theranostics targeting gastrin-releasing peptide receptors. Mol Imaging Biol. 2018;20:501–9.

50. Filippi L, Frantellizzi V, Chiaravalloti A, et al. Prognostic and theranostic applications of positron emission tomography for a personalized approach to metastatic castration-resistant prostate cancer. Int J Mol Sci. 2021;22:3036.

51. O'Donoghue JA, Bardiés M, Wheldon TE. Relationships between tumor size and curability for uniformly targeted therapy with beta-emitting radionuclides. J Nuci Med. 1995;36:1902–9.

52. Hall EJ. Radiation, the two-edged sword: cancer risks at high and low doses. Cancer J. 2000;6:343–50.

53. Hall EJ. Molecular biology in radiation therapy: the potential impact of recombinant technology on clinical practice. Int J Radiat Oncol Biol Phys. 1994;30:1019–28.

54. Subramanian G, McAfee JG, Thomas FD, et al. New diphosphonate compounds for skeletal imaging: comparison with methylene diphosphonate. Radiology. 1983;149(3):823–8.

55. Wong KK, Piert M. Dynamic bone imaging with ^{99m}Tc-labeled diphosphonates and ^{18}F-NaF: mechanisms and applications. J Nucl Med. 2013;54:590–9.

56. Helyar V, Mohan HK, Barwick T, et al. The added value of multi-slice SPECT/CT in patients with equivocal bony metastasis from carcinoma of the prostate. Eur J Nucl Med Mol Imaging. 2010;37(4):706–13.

57. Dennis ER, Jia X, Mezheritskiy IS, et al. Bone scan index: a quantitative treatment response biomarker for castration-resistant metastatic prostate cancer. J Clin Oncol. 2012;30(5):519–24.

58. Fernandez R, Eppard E, Lehnert W, et al. Evaluation of safety and dosimetry of ^{177}Lu-DOTA-ZOL for therapy of bone metastases. J Nucl Med. 2021;62:1126–32.

59. Khawar A, Eppard E, Roesch F, et al. Preliminary results of biodistribution and dosimetric analysis of [68Ga]Ga-DOTAZOL: a new zoledronate-based bisphosphonate for PET/CT diagnosis of bone diseases. Ann Nucl Med. 2019;33:404–13.

60. Khawar A, Eppard E, Roesch F, et al. Biodistribution and post-therapy dosimetric analysis of [177Lu]Lu-DOTA ZOL in patients with osteoblastic metastases: first results. EJNMMI Res. 2019;9:102.

61. Even-Sapir E, Metser U, Mishani E, et al. The detection of bone metastases in patients with high-risk prostate cancer: ^{99m}Tc-MDP planar bone scintigraphy, single- and multi-field-of-view SPECT, ^{18}F-fluoride PET, and ^{18}F-fluoride PET/CT. J Nucl Med. 2006;47(2):287–97.

62. Macheda ML, Rogers S, Bets JD. Molecular and cellular regulation of glucose transport (GLUT) proteins in cancer. J Cell Physiol. 2005;202:654–62.

63. Smith TA. Mammalian hexokinases and their abnormal expression in cancer. Br J Biomed Sci. 2000;57:170–8.

64. Stewardt GD, Gray K, Pennington CJ, et al. Analysis of hypoxia-associated gene expression in prostate cancer: lysyl oxidase and glucose transporter 1 expression correlate with Gleason score. Oncol Rep. 2008;20:1561.

65. Fox JJ, Schoder H, Larson SM. Molecular imaging of prostate cancer. Curr Opin Urol. 2012;22(4):320–7.

66. Meirelles GS, Schoder H, Ravizzini GC, et al. Prognostic value of baseline [18F] fluorodeoxyglucose positron emission tomography and ^{99m}Tc-MDP bone scan in progressing metastatic prostate cancer. Clin Cancer. 2010;16(24):6093–9.

67. Schoder H, Herrmann K, Gonen M, et al. 2-[18F]fluoro-2-deoxyglucose positron emission tomography for the detection of disease in patients with prostate-specific antigen relapse after radical prostatectomy. Clin Cancer Res. 2005;11(13):4761–9.

68. Jadvar H. Is there use for FDG-PET in prostate cancer? Semin Nucl Med. 2016;46(6):502–6.

69. Shen K, Liu B, Zhou X, et al. The evolving role of ^{18}F-FDG PET/CT in diagnosis and prognosis prediction in progressive prostate cancer. Front Oncol. 2021;11:683793. https://doi.org/10.3389/fonc.2021.683793.

70. Podo F. Tumor phospholipid metabolism. NMR Biomed. 1999;12:413–39.

71. Hara T, Kosaka N, Shinoura N, et al. PET imaging of brain tumor with [methyl-^{11}C] choline. J Nucl Med. 1997;38:842–7.

72. Umbehr MH, Muntener M, Hany T, et al. The role of ^{11}C-choline and ^{18}F-fluorocholine positron emission tomography (PET) and PET/CT in prostate cancer: a systematic review and meta-analysis. Eur Urol. 2013;64(1):106–17.

73. Evangelista L, Zattoni F, Guttilla A, et al. Choline PET or PET/CT and biochemical relapse of prostate cancer: a systematic review and meta-analysis. Clin Nucl Med. 2013;38(5):305–14.

74. Souvatzoglou M, Krause BJ, Purschel A, et al. Influence of [^{11}C]choline PET/CT on the treatment planning for salvage radiation therapy in patients

with biochemical recurrence of prostate cancer. Radiother Oncol. 2011;99(2):193–200.

75. Castellucci P, Picchio M. ^{11}C-Choline PET/CT and PSA kinetics. Eur J Nucl Med Mol Imaging. 2013;40(Suppl 1):S36–40.

76. Fanti S, Minozzi S, Castellucci P, et al. PET/CT with ^{11}C-choline for evaluation of prostate cancer patients with biochemical recurrence: meta-analysis and critical review of available data. Eur J Nucl Med Mol Imaging. 2016;43:55–69.

77. Paymani Z, Rohringer T, Vali R, et al. Diagnostic performance of [18F]Fluorocholine and [68Ga] Ga-PSMA PET/CT in prostate cancer: a comparative study. J Clin Med. 2020;9:2308. https://doi.org/10.3390/jcm9072308.

78. Virgolini I, Decristoforo C, Haug A, et al. Current status of theranostics in prostate cancer. Eur J Nucl Med Mol Imaging. 2018;45:471–95.

79. Parent EE, Schuster DM. Update on ^{18}F-fluciclovine PET for prostate cancer imaging. J Nucl Med. 2018;59:733–9.

80. Segawa A, Nagamori S, Kanai Y, et al. L-type amino acid transporter 1 expression is highly correlated with Gleason score in prostate cancer. Mol Clin Oncol. 2013;1:274–80.

81. Shiiba M, Ishihara K, Kimura G, et al. Evaluation of primary prostate cancer using ^{11}C-methionine-PET/CT and ^{18}F-FDG-PET/CT. Ann Nucl Med. 2012;26(2):138–45.

82. Okudaira H, Shikano N, Nishii R, et al. Putative transport mechanism and intracellular fate of trans-1-amino-3-^{18}F-fluorocyclobutanecarboxylic acid in human prostate cancer. J Nucl Med. 2011;52:822–9.

83. Schuster DM, Nanni C, Fanti S, et al. Anti-1-amino-3-^{18}F-fluorocyclobutane-1-carboxylic acid: physiologic uptake patterns, incidental findings, and variants that may simulate disease. J Nucl Med. 2014;55(12):1986–92.

84. Schuster DM, Votaw JR, Nieh PT, et al. Initial experience with the radiotracer anti-1-amino-3-[18F] fluorocyclobutane-1-carboxylic acid with PET/CT in prostate carcinoma. J Nucl Med. 2007;48(1):56–63.

85. Calais J, Czernin J, Cao M, et al. ^{68}Ga-PSMA-11 PET/CT mapping of prostate cancer biochemical recurrence after radical prostatectomy in 270 patients with a PSA level of less than 1.0 ng/mL: impact on salvage radiotherapy planning. J Nucl Med. 2018;59(2):230–7.

86. Tan N, Oyoyo U, Bavadian N, et al. PSMA-targeted radiotracers versus ^{18}F fluciclovine for the detection of prostate cancer biochemical recurrence after definitive therapy: a systematic review and meta-analysis. Radiology. 2020;296:44–55.

87. Bin X, Yong S, Kong Q-F, et al. Diagnostic performance of PET/CT using ^{18}F-FACBC in prostate cancer: a meta-analysis. Front Oncol. 2020;9:1438.

88. Scher HI, Beer TM, Higano CS, et al. Anti-tumour activity of MDV3100 in castration-resistant prostate cancer: a phase 1-2 study. Lancet. 2010;375(9724):1437–46.

89. Dehdashti F, Picus J, Michalski JM, et al. Positron tomographic assessment of androgen receptors in prostatic carcinoma. Eur J Nucl Med Mol Imaging. 2005;32(3):344–50.

90. Hoving H, Palthe S, Vallinga M, et al. Early ^{18}F-FDHT PET/CT as a predictor of treatment response in mCRPC treated with enzalutamide. J Clin Oncol. 2019;37(7s):232.

91. Fox JJ, Morris MJ, Larson SM, et al. Developing imaging strategies for castration resistant prostate cancer. Acta Oncol. 2011;50(Suppl 1):39–48.

92. Staniszewska M, Costa PF, Eiber M, et al. Enzalutamide enhances PSMA expression of PSMA-low prostate cancer. Int J Mol Sci. 2021;22:7431.

93. Beattie BJ, Smith-Jones PM, Jhanwar YS, et al. Pharmacokinetic assessment of the uptake of 16β-^{18}F-fluoro-5α-dihydrotestosterone (FDHT) in prostate tumors as measured by PET. J Nucl Med. 2010;51(2):183–92.

94. Antunes IF, Dost RJ, Hoving HD, et al. Synthesis and evaluation of ^{18}F-enzalutamide, a new radioligand for PET imaging of androgen receptors: a comparison with 16β-^{18}F-Fluoro-5α-dihydrotestosterone. J Nucl Med. 2021;62:1140–5.

95. Rosenthal SA, Haseman MK, Polascik TJ. Utility of capromab pendetide (ProstaScint) imaging in the management of prostate cancer. Tech Urol. 2001;7(1):27–37.

96. Hinkle GH, Burgers JK, Neal CE, et al. Multi center radioimmunoscintigraphic evaluation of patients with prostate carcinoma using indium-111 capromab pendetide. Cancer. 1998;83(4):739–47.

97. Wilkinson S, Chodak G. The role of [111]indium-capromab pendetide imaging for assessing biochemical failure after radical prostatectomy. J Urol. 2004;172(1):133–6.

98. Smith-Jones PM, Vallabhajosula S, Navarro V, et al. Radiolabeled monoclonal antibodies specific to the extracellular domain of prostate-specific membrane antigen: preclinical studies in nude mice bearing LNCaP human prostate tumor. J Nucl Med. 2003;44:610–7.

99. Smith-Jones PM, Vallabhajosula S, St. Omer S, et al. ^{177}Lu-DOTA-HuJ591: a new radiolabeled monoclonal antibody (mAb) for targeted therapy of prostate cancer. J Label Compds Radiopharm. 2001;44:90–2.

100. Bander NH, Trabulsi EJ, Kostakoglu L, Yao D, Vallabhajosula S, et al. Targeting metastatic prostate cancer with radiolabeled monoclonal antibody J591 to the extracellular domain of prostate specific membrane antigen. J Urol. 2003;170:171.

101. Bander NH, Milowsky MI, Nanus DM, Kostakoglu L, Vallabhajosula S, Goldsmith SJ. Phase I trial of [177]lutetium labeled J591, a monoclonal antibody to prostate-specific membrane antigen, in patients with androgen-independent prostate cancer. J Clin Oncol. 2005;23:4591–601.

102. Vallabhajosula S, Goldsmith SJ, Kostakoglu L, et al. Radioimmunotherapy of prostate cancer using [90]Y- and ^{177}Lu-labeled J591 monoclonal antibodies: effect

of multiple treatments on myelotoxicity. Clin Cancer Res. 2005;11:7195s–200s.

103. Vallabhajosula S, Goldsmith SJ, Hamacher KA, et al. Prediction of myelotoxicity based on bone marrow radiation-absorbed dose: radioimmunotherapy studies using ^{90}Y- and ^{177}Lu-labeled J591 antibodies specific for prostate-specific membrane antigen. J Nucl Med. 2005;46:850–8.

104. Vallabhajosula S, Kuji I, Hamacher A, et al. Pharmacokinetics and biodistribution of ^{111}In- and ^{177}Lu-labeled J591 antibody specific for prostate-specific membrane antigen: prediction of ^{90}Y-J591 radiation dosimetry based on ^{111}In or ^{177}Lu? J Nucl Med. 2005;46:634–41.

105. Yoon J-K, Park B-N, Ryu E-K, et al. Current perspectives on ^{89}Zr-PET imaging. Int J Mol Sci. 2020;21:4309. https://doi.org/10.3390/ijms21124309.

106. Osborne JR, Green DA, Spratt DE, et al. A prospective pilot study of ^{89}Zr-J591/prostate specific membrane antigen positron emission tomography in men with localized prostate cancer undergoing radical prostatectomy. J Urol. 2014;191:1439–45.

107. Pandit-Taskar N, O'Donoghue JA, Durack JC, et al. A phase I/II study for analytic validation of ^{89}Zr-J591 immunoPET as a molecular imaging agent for metastatic prostate cancer. Clin Cancer Res. 2015;21:5277–85.

108. Pandit-Taskar N, O'Donoghue JA, Beylergil V, et al. ^{89}Zr-huJ591 immuno-PET imaging in patients with advanced metastatic prostate cancer. Eur J Nucl Med Mol Imaging. 2014;41:2093–105.

109. Viola-Villegas NT, Sevak KK, Carlin, et al. Noninvasive imaging of PSMA in prostate tumors with (89)Zr-labeled huJ591 engineered antibody fragments: the faster alternatives. Mol Pharm. 2014;11:3965–73.

110. Joraku A, Hatano K, Kawai K, et al. Phase I/IIa PET imaging study with (89)zirconium labeled anti-PSMA minibody for urological malignancies. Ann Nucl Med. 2019;33:119–27.

111. Pandit-Taskar N, O'Donoghue JA, Ruan S, et al. First-in-human imaging with ^{89}Zr-Df-IAB2M anti-PSMA Minibody in patients with metastatic prostate cancer: pharmacokinetics, biodistribution, dosimetry, and lesion uptake. J Nucl Med. 2016;57:1858–64.

112. Gomes I, Maia C, Santos CRA. STEAP proteins: from structure to applications in cancer therapy. Mol Cancer Res. 2012;10:573–87.

113. O'Donoghue JA, Danila DC, Pandit-Taskar N, et al. Pharmacokinetics and biodistribution of [^{89}Zr]Zr-DFO-MSTP2109A anti-STEAP1 antibody in metastatic castration resistant prostate cancer patients. Mol Pharm. 2019;16(7):3083–90.

114. Pomper MG, Musachio JL, Zhang J, et al. ^{11}C-MCG: synthesis, uptake selectivity, and primate PET of a probe for glutamate carboxypeptidase II (NAALADase), Mol Imaging. 2002;2:96–101.

115. Pillai MRA, Nanabala R, Joy A, et al. Radiolabeled enzyme inhibitors and binding agents targeting PSMA: effective theranostic tools for imaging and therapy of prostate cancer. Nucl Med Biol. 2016;43:692–720.

116. Mease RC, Dusich CL, Foss CA, et al. N-[N-[(S)-1,3-Dicarboxypropyl]Carbamoyl]-4-[^{18}F]fluorobenzyl-L-cysteine, [^{18}F]DCFBC: a new imaging probe for prostate cancer. Clin Cancer Res. 2008;14(10):3036–43.

117. Mena E, Lindenberg ML, Shih JH, et al. Clinical impact of PSMA-based ^{18}F-DCFBC PET/CT imaging in patients with biochemically recurrent prostate cancer after primary local therapy. Eur J Nucl Med Mol Imaging. 2018;45(1):4–11.

118. Chen Y, Pullambhatla M, Foss CA, et al. 2-(3-{1-carboxy-5-[(6-[^{18}F]fluoro-pyridine3-carbonyl)-amino]-pentyl}-ureido)-pentanedioic acid, [^{18}F]DCFPyL, a PSMA based PET imaging agent for prostate cancer. Clin Cancer Res. 2011;17:7645–53.

119. Dietlein F, Kobe C, Neubauer S, et al. PSA-stratified performance of ^{18}F- and ^{68}Ga-PSMA PET in patients with biochemical recurrence of prostate cancer. J Nucl Med. 2017;58:947–52.

120. Giesel FL, Will L, Lawal T, et al. Intraindividual comparison of ^{18}F-PSMA-1007 and ^{18}FDCFPyL PET/CT in the prospective evaluation of patients with newly diagnosed prostate carcinoma: a pilot study. J Nucl Med. 2018;59:1076–80.

121. Morris MJ, Rowe SP, Gorin MA, et al. Diagnostic performance of ^{18}F-DCFPyL-PET/CT in men with biochemically recurrent prostate cancer: results from the CONDOR phase III, multicenter study. Clin Cancer Res. 2021;27(13):3674–82.

122. Maresca KP, Hillier SM, Femia FJ, et al. A series of halogenated heterodimeric inhibitors of prostate-specific membrane antigen (PSMA) as radiolabeled probes for targeting prostate cancer. J Med Chem. 2009;52:347–57.

123. Barrett JA, Coleman RE, Goldsmith SJ, et al. First-in-man evaluation of two high-affinity PSMA-avid small molecules for imaging prostate cancer. J Nucl Med. 2013;54:1–8.

124. Zechmann CM, Afshar-Oromieh A, Armor T, et al. Radiation dosimetry and first therapy results with a ^{124}I/^{131}I-labeled small molecule (MIP-1095) targeting PSMA for prostate cancer therapy. Eur J Nucl Med Mol Imaging. 2014;41:1280–92.

125. Maresca KP, Hillier SM, Lu G, Marquis JC, Zimmerman CN, Eckelman WC, Joyal JL, Babich JW. Small molecule inhibitors of PSMA incorporating technetium-99m for imaging prostate cancer: effects of chelate design on pharmacokinetics. Inorganica Chimica Acta. 2012;389:168–75.

126. Vallabhajosula S, Smith-Jones PM, Navarro V, et al. Radioimmunotherapy of prostate cancer in human xenografts using monoclonal antibodies specific to prostate specific membrane antigen: studies in nude mice. Prostate. 2004;58:145–55.

127. Vallabhajosula S, Smith-Jones PM, Navarro V, Goldsmith SJ, Bander NH. Radioimmunotherapy of prostate cancer in human xenografts using

monoclonal antibodies specific to prostate specific membrane antigen: studies in nude mice. Prostate. 2004;58:145–55.

128. Vallabhajosula S, Polack JW, Babich JW. Molecular imaging of prostate cancer: radiopharmaceuticals for positron emission tomography (PET) and single-photon emission computed tomography (SPECT). In: Robinson B, Mosquera J, Ro J, Divatia M, editors. Precision molecular pathology of prostate cancer. Springer; 2017. p. 475–501.

129. Schmidkonz C, Gotz TI, Atzinger A, et al. ^{99m}Tc-MIP-1404 SPECT/CT for assessment of whole-body tumor burden and treatment response in patients with biochemical recurrence of prostate cancer. Clin Nucl Med. 2020;45(8):e349–57.

130. Eder M, Schäfer M, Bauder-Wust U, et al. ^{68}Ga-complex lipophilicity and the targeting property of a urea-based PSMA inhibitor for PET imaging. Bioconjug Chem. 2012;23:688–97.

131. Afshar-Oromieh A, Haberkorn U, Eder M, et al. [^{68}Ga]Gallium labelled PSMA ligand as superior PET tracer for the diagnosis of prostate cancer: comparison with ^{18}F-FECH. Eur J Nucl Med Mol Imaging. 2012;39:1085–6.

132. Bois F, Noirot C, Dietemann S, et al. [^{68}Ga]Ga-PSMA-11 in prostate cancer: a comprehensive review. Am J Nucl Med Mol Imaging. 2020;10(6):349–74.

133. Carlucci G, Ippisch R, Slavik R, et al. ^{68}Ga-PSMA-11 NDA approval: a novel and successful academic partnership. J Nucl Med. 2021;62:149–55.

134. Weineisen M, Schottelius M, Simecek J, et al. ^{68}Ga- and ^{177}Lu-labeled PSMA I&T: optimization of a PSMA-targeted theranostic concept and first proof-of-concept human studies. J Nucl Med. 2015;56:1169–76.

135. Weineisen M, Simecek J, Schottelius M, et al. Synthesis and preclinical evaluation of DOTAGA-conjugated PSMA ligands for functional imaging and endoradiotherapy of prostate cancer. EJNMMI Res. 2014;4:63.

136. Benešová M, Schäfer M, Bauder-Wüst U, et al. Preclinical evaluation of a tailor-made DOTA-conjugated PSMA inhibitor with optimized linker moiety for imaging and endoradiotherapy of prostate cancer. J Nucl Med. 2015;56(6):914–20.

137. Giesel FL, Cardinale J, Schäfer M, et al. [^{18}F]-Labelled PSMA-1007 shows similarity in structure, biodistribution and tumour uptake to the theragnostic compound PSMA-617. Eur J Nucl Med Mol Imaging. 2016;43:1929–30.

138. Cardinale J, Schäfer M, Benesova M, et al. Preclinical evaluation of ^{18}F-PSMA-1007, a new prostate-specific membrane antigen ligand for prostate cancer imaging. J Nucl Med. 2017;58:425–31.

139. Wurzer A, Di Carlo D, Schmidt A, et al. Radiohybrid ligands: a novel tracer concept exemplified by ^{18}F- or ^{68}Ga-labeled rhPSMA inhibitors. J Nucl Med. 2020;61:735–42.

140. Wurzer A, Parzinger M, Konrad M. Preclinical comparison of four [(18)F, (nat)Ga]rhPSMA-7 isomers: influence of the stereo configuration on pharmacokinetics. EJNMMI Res. 2020;10(1):149.

141. Eiber M, Kroenke M, Wurzer A, Ulbrich L, Jooß L, Maurer T, et al. (18)F-rhPSMA-7 PET for the detection of biochemical recurrence of prostate cancer after radical prostatectomy. J Nucl Med. 2020;61(5):696–701.

142. Langbein T, Wang H, Rauscher I, et al. Utility of ^{18}F-rhPSMA-7.3 positron emission tomography for imaging of primary prostate cancer and pre-operative efficacy in N-staging of unfavorable intermediate to very high-risk patients validated by histopathology. J Nucl Med. 2022;63:1334. https://doi.org/10.2967/jnumed.121.263440.

143. Yusufi N, Wurzer A, Herz M, et al. Comparative preclinical biodistribution, dosimetry and endoradiotherapy in mCRPC using ^{19}F/^{177}Lu-rhPSMA-7.3 and ^{177}Lu-PSMA I&T. J Nucl Med. 2021;62:1106–11.

144. Liu Z, Chen X. Simple bioconjugate chemistry serves great clinical advances: albumin as a versatile platform for diagnosis and precision therapy. Chem Soc Rev. 2016;45:1432–56.

145. Zorzi A, Linciano S, Angelini A, et al. Non-covalent albumin-binding ligands for extending the circulating half-life of small biotherapeutics. Medchemcomm. 2019;10(7):1068–81.

146. Gharibkandi NA, Conlon JM, Hosseinimehr SJ. Strategies for improving stability and pharmacokinetic characteristics of radiolabeled peptides for imaging and therapy. Peptides. 2020;133(12):170385.

147. Dumelin CE, Trussel S, Buller F, et al. A portable albumin binder from a DNA-encoded chemical library. Angew Chem Int Ed Engl. 2008;47:3196–201.

148. Müller C, Struthers H, Winiger C, et al. DOTA conjugate with an albumin-binding entity enables the first folic acid–targeted 177Lu-radionuclide tumor therapy in mice. J Nucl Med. 2013;54:124–31.

149. Kelly JM, Amor-Coarasa A, Ponnala S, et al. Albumin-binding PSMA ligands: implications for expanding the therapeutic window. J Nucl Med. 2019;60(5):656–63.

150. Umbricht CA, Benešová M, Schibli R, Müller C. Preclinical development of novel PSMA-targeting radioligands: modulation of albumin-binding properties to improve prostate cancer therapy. Mol Pharm. 2018;15:2297–306.

151. Deberle LM, Benešová M, Umbricht CA, et al. Development of a new class of PSMA radioligands comprising ibuprofen as an albumin-binding entity. Theranostics. 2020;10(4):1678–93.

152. Kuo H-T, Lin K-S, Zhang Z, et al. ^{177}Lu-labeled albumin-binder–conjugated PSMA-targeting agents with extremely high tumor uptake and enhanced tumor-to-kidney absorbed dose ratio. J Nucl Med. 2021;62:521–7.

153. Mansi R, Nock BA, Dalm SU, et al. Radiolabeled bombesin analogs. Cancers. 2021;13:5766.

154. Li X, Cai H, Wu X, et al. New frontiers in molecular imaging using peptide-based radiopharmaceuticals for prostate cancer. Front Chem. 2020;8:583309. https://doi.org/10.3389/fchem.2020.583309.

155. Zhang J, et al. PET using a GRPR antagonist ^{68}Ga-RM26 in healthy volunteers and prostate cancer patients. J Nucl Med. 2018;59:922.

156. Fassbender TF, Schiller F, Zamboglou C, et al. Voxel-based comparison of [^{68}Ga]Ga-RM2- PET/CT and [^{68}Ga]Ga-PSMA-11-PET/CT with histopathology for diagnosis of primary prostate cancer. EJNMMI Res. 2020;10:62.

157. Wieser G, Popp I, Christian Rischke H, et al. Diagnosis of recurrent prostate cancer with PET/CT imaging using the gastrin-releasing peptide receptor antagonist ^{68}Ga-RM2: preliminary results in patients with negative or inconclusive [^{18}F]fluoro-ethylcholine-PET/CT. Eur J Nucl Med Mol Imaging. 2017;44(9):1463–72.

158. Kurth J, Krause BJ, Schwarzenböck SM, et al. First-in-human dosimetry of gastrin releasing peptide receptor antagonist [^{177}Lu]Lu-RM2: a radiopharmaceutical for the treatment of metastatic castration-resistant prostate cancer. Eur J Nucl Med Mol Imaging. 2020;47:123–35.

159. Baratto L, Duan H, Laudicella R, et al. Physiological ^{68}Ga-RM2 uptake in patients with biochemically recurrent prostate cancer: an atlas of semi-quantitative measurements. Eur J Nucl Med Mol Imaging. 2020;47(1):115–22.

160. Baratto L, Song H, Duan H, et al. PSMA- and GRPR-targeted PET: results from 50 patients with biochemically recurrent prostate cancer. J Nucl Med. 2021;62(11):1545–9.

161. Nock BA, Kaloudi A, Lymperis E, et al. Theranostic perspectives in prostate cancer with the gastrin-releasing peptide receptor antagonist NeoBOMB1: preclinical and first clinical results. J Nucl Med. 2017;58:75–80.

162. Das T, Banerjee S. Radiopharmaceuticals for metastatic bone pain palliation: available options in the clinical domain and their comparisons. Clin Exp Metastasis. 2017;34(1):1–10.

163. Liepe K, Murray I, Flux G. Dosimetry of bone seeking beta emitters for bone pain palliation metastases. Semin Nucl Med. 2021;52:178.

164. Pecher C. Biological investigation with radioactive calcium and strontium: preliminary report on the use of radioactive strontium in treatment of metastatic bone cancer. Pharmacology. 1942;11:117–49.

165. Turner JH, Claringbold PG, Hetherington EL, et al. (1989) a phase I study of samarium-153 ethylenediaminetetra-methylene phosphonate therapy for disseminated skeletal metastases. J Clin Oncol. 1989;7:1926–31.

166. Askari E, Harsini S, Vahidfar N, et al. ^{177}Lu-EDTMP for metastatic bone pain palliation: a systematic review and meta-analysis. Cancer Biother Radiopharm. 2021;36(5):383–90.

167. Larsen RH, Henriksen G, Bruland O. Preparation and use of radium-223 to target calcified tissues for pain palliation, bone cancer therapy, and bone surface conditioning. Google Patents; 2003.

168. Parker C, Finkelstein SE, Michalski JM, et al. Efficacy and safety of radium-223 dichloride in symptomatic castration-resistant prostate cancer patients with or without baseline opioid use from the phase 3 ALSYMPCA trial. Eur Urol. 2016;70(5):875–83.

169. Sartor O, Coleman R, Nilsson S, et al. Effect of radium-223 dichloride on symptomatic skeletal events in patients with castration resistant prostate cancer and bone metastases: results from a phase 3, double-blind, randomised trial. Lancet Oncol. 2014;15:738–46.

170. Milowsky MI, Nanus DM, Kostakoglu L, Vallabhajosula S, Goldsmith SJ, Bander NH. Phase I trial of ^{90}Y-labeled anti-prostate specific membrane antigen monoclonal antibody J591 for androgen-independent prostate cancer. J Clin Oncol. 2004;22:2522–31.

171. Vallabhajosula S, Nikolopoulou A, Jhanwar YS, et al. Radioimmunotherapy of metastatic prostate cancer with ^{177}Lu-DOTA-huJ591 anti prostate specific membrane antigen specific monoclonal antibody. Curr Radiopharm. 2016;9:44–53.

172. Tagawa ST, Milowsky MI, Morris M, Vallabhajosula S, et al. Phase II study of lutetium-177-labeled anti-prostate-specific membrane antigen monoclonal antibody J591 for mCRPC. Clin Cancer Res. 2013;19:5182–91.

173. Tagawa ST, Akhtar NH, Nikolopoulou A, et al. Bone marrow recovery and subsequent chemotherapy following radiolabeled anti-prostate-specific membrane antigen monoclonal antibody J591 in men with mCRPC. Front Oncol. 2013;3:1–6.

174. O'Donoghue JA, Sgouros G, Divgi CR, Humm JL. Single-dose versus fractionated radioimmunotherapy: model comparisons for uniform tumor dosimetry. J Nucl Med. 2000;41:538–47.

175. Tagawa ST, Osborne JR, Hackett A, et al. Preliminary results of a phase I/II dose-escalation study of fractionated dose ^{177}Lu-PSMA-617 for progressive metastatic castration resistant prostate cancer (mCRPC). Ann Oncol. 2019;30(Suppl_5):v325–55. https://doi.org/10.1093/annonc/mdz248.

176. Tagawa ST, Vallabhajosula S, Christos PJ, et al. Phase 1/2 study of fractionated dose lutetium-177-labeled anti-prostate-specific membrane antigen monoclonal antibody J591 (^{177}Lu-J591) for mCRPC. Cancer. 2019;125:2561–9.

177. Batra JS, Niaz MJ, Whang YE, et al. Phase I trial of docetaxel plus lutetium-177-labeled anti–prostate-specific membrane antigen monoclonal antibody J591 (^{177}Lu-J591) for metastatic castration-resistant prostate cancer. Urol Oncol. 2020;38(11):848.e9–848.

178. Niaz MJ, Bastra JS, Walsh RD, Ramirez-Fort MK, Vallabhajosula S, et al. Pilot study of hyperfraction-

ated dosing of lutetium-177 labeled antiprostate-spe-cific membrane antigen monoclonal antibody J591 (^{177}Lu-J591) for metastatic castration-resistant pros-tate cancer. Oncologist. 2020;25(6):477–e895.

179. Li Y, Tian Z, Rizvi SM, Bander NH, Allen BJ. In vitro and preclinical targeted alpha therapy of human prostate cancer with Bi-213 labeled J591 antibody against the prostate specific membrane antigen. Prostate Cancer Prostatic Dis. 2002;5:36–46.

180. Tagawa ST, Osborne J, Fernandez E, et al. Phase I dose-escalation study of PSMA-targeted alpha emit-ter [225]Ac-J591 in men with metastatic castration-resistant prostate cancer (mCRPC). J Clin Oncol. 2020;38(Suppl 15):5560.

181. Tagawa ST, Sun M, Sartor AO, et al. Phase I study of [225]Ac-J591 for men with metastatic castration-resistant prostate cancer (mCRPC). J Clin Oncol. 2021;39(Suppl 15):abstr 5015.

182. Kratochwil C, Bruchertseifer F, Giesel FL, et al. [225]Ac-PSMA-617 for PSMA-targeted alpha-radiation therapy of metastatic castration-resistant prostate cancer. J Nucl Med. 2016;57:1941–4.

183. Kratochwil C, Giesel FL, Stefanova M, et al. PSMA-targeted radionuclide therapy of metastatic castra-tion-resistant prostate cancer with ^{177}Lu-labeled PSMA-617. J Nucl Med. 2016;57:1170–6.

184. Hofman MS, Violet J, Hicks RJ, et al. [^{177}Lu]-PSMA-617 radionuclide treatment in patients with metastatic castration-resistant prostate cancer (LuPSMA trial): a single-center, single-arm, phase 2 study. Lancet Oncol. 2018;19:825–33.

185. Hofman MS, Emmett L, Sandhu S, et al. [^{177}Lu]Lu-PSMA-617 versus cabazitaxel in patients with meta-static castration-resistant prostate cancer (TheraP): a randomized, open-label, phase 2 trial. Lancet. 2021;397(10276):797–804.

186. Sartor O, de Bono J, Chi KN, Fizazi K, Herrmann K, Rahbar K, et al. Lutetium-177-PSMA-617 for meta-static castration-resistant prostate cancer. N Engl J Med. 2021;385:1091–103.

187. Yadav MP, Ballal S, Bal C, Sahoo RK, et al. Efficacy and safety of ^{177}Lu-PSMA-617 radioligand therapy in metastatic castration-resistant prostate cancer patients. Clin Nucl Med. 2020;45:19–31.

188. Baum RP, Kulkarni HR, Schuchardt C, et al. ^{177}Lu-labeled prostate-specific membrane antigen radioligand therapy of metastatic castration-resistant prostate cancer: safety and efficacy. J Nucl Med. 2016;57:1006–13.

189. Heck MM, Retz M, D'Alessandria C, et al. Systemic radioligand therapy with ^{177}Lu-PSMA-I&T in patients with metastatic castration-resistant prostate cancer. J Urol. 2016;196:382–91.

190. Okamoto S, Thieme A, Allmann J, et al. Radiation dosimetry for ^{177}Lu-PSMA I&T in metastatic cas-tration-resistant prostate cancer: absorbed dose in Normal organs and tumor lesions. J Nucl Med. 2016;58:445–50.

191. Heck MM, Tauber R, Schwaiger S, et al. Treatment outcome, toxicity, and predictive factors for radio-ligand therapy with ^{177}Lu-PSMA-I&T in meta-static castration-resistant prostate cancer. Eur Urol. 2019;75(6):920–6.

192. Sanli YR, Simsek DH, Sanli O, et al. ^{177}Lu-PSMA therapy in metastatic castration-resistant prostate cancer. Biomedicine. 2021;9:430.

193. Kratochwil C, Bruchertseifer F, Rathke H, et al. Targeted alpha-therapy of metastatic castration-resistant prostate cancer with 225Ac-PSMA-617: swimmer-plot analysis suggests efficacy regard-ing duration of tumor control. J Nucl Med. 2018;59:795–802.

194. Kratochwil C, Haberkorn U, Giesel FL. (225) Ac-PSMA-617 for therapy of prostate cancer. Semin Nucl Med. 2020;50:133–40.

195. Sathekge M, Bruchertseifer F, Knoesen O, et al. [225]Ac-PSMA-617 in chemotherapy-naive patients with advanced prostate cancer: a pilot study. Eur J Nucl Med Mol Imaging. 2019;46:129–38.

196. Yadav MP, Ballal S, Sahoo RK, et al. Efficacy and safety of (225)Ac-PSMA-617 targeted alpha therapy in metastatic castration-resistant prostate cancer patients. Theranostics. 2020;10:9364–77.

197. Zacherl MJ, Gildehaus FJ, Mittlmeier L, et al. First clinical results for PSMA-targeted a-therapy using [225]Ac-PSMA-I&T in advanced-mCRPC patients. J Nucl Med. 2021;62:669–74.

198. Suman SK, Subramanian S, Mukherjee A. Combination radionuclide therapy: a new para-digm. Nucl Med Biol. 2021;98:40–58.

199. Khreish F, Ebert N, Ries M, et al. (225)AcPSMA-617/ (177)Lu-PSMA-617 tandem therapy of metastatic castration-resistant prostate cancer: pilot experience. Eur J Nucl Med Mol Imaging. 2020;47:721–8.